

Revista Română de Inginerie Civilă

Indexată în bazele de date internaționale (BDI)

ProQuest, IET INSPEC, EBSCO, GOOGLE SCHOLAR, CROSSREF,
TDNET, DIMENSIONS, DRJI, J-GATE, INDEX COPERNICUS,
ULRICH'S, JOURNALSEEK, RESEARCH GATE,
SEMANTIC SCHOLAR, ERIHPLUS, WORLDCAT

Volumul 16 (2025), Numărul 3

Study regarding adaptive envelopes based on origami
Studiu privind fațadele adaptabile inspirate de origami 237-248
Carmen Mârza, Ana-Maria Graur, Georgiana Corsiuc

Characterization of fiber reinforced concrete for classification based on strength and ductility
Caracterizarea betonului armat dispers în vederea clasificării pe baza rezistenței și ductilității 249-261
Muheeb Altaleb, Andrei Gîrboveanu, Dan Georgescu

Tracking the performance of an air-to-water heat pump over time for a residential house located in a hilly area with low outdoor temperature
Urmărirea comportării în timp a pompei de căldură aer-apă pentru o casă de locuit situată într-o zonă deluroasă cu temperatură exterioară scăzută 262-269
Alexandru Dorca, Adriana Tokar, Marius Adam, Danut Tokar, Daniel Muntean, Daniel Bisorca, Calin Sebarchievici

Porous geopolymeric material for insulation applications
Material geopolimeric poros pentru aplicații în izolații 270-279
Lucian Paunescu, Sorin Mircea Axinte, Enikő Volceanov

Considerations regarding the operational reliability of equipment in the structure of water supply systems
Conșiderații privind fiabilitatea operațională a echipamentelor din structura sistemelor de alimentare cu apă 280-291
Gheorghe – Constantin Ionescu, George – Lucian Ionescu, Dragoș-Vasile Ilie

A general review on night ventilation systems used to reduce energy consumption in buildings
Recenzie generală a sistemelor de ventilare pe timp de noapte utilizate pentru reducerea consumului de energie în clădiri 292-298
Marius Adam, Adriana Tokar, Alexandru Dorca, Dănuț Tokar, Alexandru Filipovici

The role of ventilation systems on indoor air quality. Analysis and Solutions for a Healthy Environment

Rolul sistemelor de ventilare asupra calității aerului interior. Analiză și soluții pentru un mediu sănătos 299-304

Cristian Pacurar, Adriana Tokar, Marius Adam

Experimental Analysis of Thermo-Mechanical Effects on Geothermal Piles

Analiză experimentală a efectelor termo-mecanice asupra piloților geotermici 305-315

Bahadır Kivanç, Florescu Virgil

Numerical modeling of thermal transfer through a refrigeration room wall - thermal bridge phenomenon highlighting

Simulare numerică transfer termic prin perete camera frigorifică – evidențierea fenomenului de punte termică 316-325

Mirela Tomoșoiu, Grațiana Maria Țârlea

Retrofit of refrigeration installations with low GWP refrigerants

Modernizarea instalațiilor frigorifice cu agenți frigorifici cu GWP scăzut 326-339

Mihai Adrian, Tokar Adriana

Fine porosity-cellular glass obtained by microwaveassisted heat treatment using the expansion ability of glycerol together with water glass

Sticlă celulară cu porozitate fină obținută prin tratament termic asistat de microunde folosind capacitatea de expansiune a glicerolului împreună cu apă de sticlă 340-351

Sorin Mircea Axinte, Lucian Paunescu

MATRIX ROM
3 Politehnicii Street, Bucharest, Romania
Tel. +4021.4113617, +40733882137
e-mail: office@matrixrom.ro
www.matrixrom.ro

EDITORIAL BOARD

Ph.D. Harish Chandra ARORA - *CSIR-Central Building Research Institute, Roorkee, India*
Ph.D. Assoc. Prof. Arch. Eur. Ing. Lino BIANCO, *University of Malta, Malta*
Ph.D.Prof.Eng. Ioan BOIAN, *Transilvania University of Brasov, Romania*
Ph.D. Ilhem BORCHENI, *Institut International Technologie, Sfax, Tunisie*
Ph.D.Prof.Eng. Ioan BORZA, *Polytechnic University of Timisoara, Romania*
Ph.D.Assoc.Prof.Eng. Vasilică CIOCAN, *Gh. Asachi Technical University of Iași, Romania*
Ph.D.Prof. Stefano CORGNATI, *Politecnico di Torino, Italy*
Ph.D.Assoc.Prof.Eng. Andrei DAMIAN, *Technical University of Constructions Bucharest, Romania*
Ph.D.Prof. Yves FAUTRELLE, *Grenoble Institute of Technology, France*
Ph.D.Prof.Eng. Carlos Infante FERREIRA, *Delft University of Technology, The Netherlands*
Ph.D.Prof. Manuel GAMEIRO da SILVA, *University of Coimbra, Portugal*
Ph.D.Prof.Eng. Dragoș HERA, *Technical University of Constructions Bucharest, Romania, honorary member*
Ph.D. Jaap HOGELING, *Dutch Building Services Knowledge Centre, The Netherlands*
Ph.D.Lawyer Cristina Vasilica ICOCIU, *Polytechnic University of Bucharest, Romania*
Ph.D.Prof.Eng. Anica ILIE, *Technical University of Constructions Bucharest, Romania*
Ph.D.Prof.Eng. Gheorghe Constantin IONESCU, *Oradea University, Romania*
Ph.D.Prof.Eng. Florin IORDACHE, *Technical University of Constructions Bucharest, Romania – editorial director*
Ph.D.Prof.Eng. Vlad IORDACHE, *Technical University of Constructions Bucharest, Romania*
Ph.D.Prof.Eng. Karel KABELE, *Czech Technical University, Prague, Czech Republic*
Ph.D.Prof. Birol KILKIS, *Baskent University, Ankara, Turkey*
Ph.D.habil. Assoc.Prof. Zoltan MAGYAR, *Budapest University of Technology and Economics, Hungary*
Ph.D.Assoc.Prof.Eng. Carmen MĂRZA, *Technical University of Cluj Napoca, Romania*
Ph.D.Prof.Eng. Ioan MOGA, *Technical University of Cluj Napoca, Romania*
Ph.D.Assoc.Prof.Eng. Gilles NOTTON, *Pascal Paoli University of Corsica, France*
Ph.D.Prof.Eng. Daniela PREDA, *Technical University of Constructions Bucharest, Romania*
Ph.D.Prof.Eng. Adrian RETEZAN, *Polytechnic University of Timisoara, Romania*
Ph.D.Prof. Emeritus Aleksandar SEDMAK, *University of Belgrad, Serbia*
Ph.D. Boukarta SOUFIANE, *Institute of Architecture and Urban Planning, BLIDA1, Algeria*
Ph.D.Assoc.Prof.Eng. Daniel STOICA, *Technical University of Constructions Bucharest, Romania*
Ph.D.Prof. Branislav TODOROVIĆ, *Belgrad University, Serbia*
Ph.D.Prof. Marija S. TODOROVIĆ, *Academy of Engineering Sciences of Serbia*
Ph.D.Eng. Ionuț-Ovidiu TOMA, *Gh. Asachi Technical University of Iași, Romania*
Ph.D.Prof.Eng. Ioan TUNS, *Transilvania University of Brasov, Romania*
Ph.D.Assoc.Prof.Eng. Constantin ȚULEANU, *Technical University of Moldova Chisinau, Republic of Moldova*
Ph.D.Prof.Eng. Ioannis VAYAS, *National Technical University of Athens, Greece*
Ph.D.Assoc.Prof.Eng. Eugen VITAN, *Technical University of Cluj Napoca, Romania*

**Romanian Journal of Civil Engineering is founded, published and funded by
publishing house MATRIX ROM
Executive Director: mat. Iancu ILIE**

Online edition ISSN 2559-7485

Print edition ISSN 2068-3987; ISSN-L 2068-3987

Study regarding adaptive envelopes based on origami

Studiu privind fațadele adaptabile inspirate de origami

Carmen Mârza¹, Ana-Maria Graur², Georgiana Corsiuc³.

¹Universitatea Tehnică din Cluj-Napoca, Facultatea de Inginerie a Instalațiilor
B-dul 21 Decembrie 1989, nr. 128-130, Cluj Napoca, România
E-mail: carmen.marza@insta.utcluj.ro

²Universitatea Tehnică din Cluj-Napoca, Facultatea de Arhitectură și Urbanism
Str. Observatorului, nr 34-36, Cluj Napoca, România
E-mail: anamaria.graur@arch.utcluj.ro

³Universitatea Tehnică din Cluj-Napoca, Facultatea de Inginerie a Instalațiilor
B-dul 21 Decembrie 1989, nr. 128-130, Cluj Napoca, România
E-mail: georgiana.corsiuc@gmail.com

DOI: 10.37789/rjce.2025.16.3.1

Abstract. *This paper explores the integration of adaptive façade systems in curtain wall buildings as a means to enhance energy efficiency, thermal performance, and visual comfort. Starting from the geometric versatility of the hexagon and drawing inspiration from origami folding principles, the study proposes a kinetic external shading system capable of responding dynamically to variations in solar radiation. The design is inspired by principles of biomimicry and aims to contribute both aesthetically and functionally to the building envelope.*

Key words: sustainable design, adaptive envelope, hexagon tessellation, ventilated façades, wellbeing.

Rezumat. *Această lucrare analizează integrarea sistemelor de fațade adaptabile în clădirile cu pereți cortină, având ca obiectiv îmbunătățirea eficienței energetice, a performanței termice și a confortului vizual. Având ca punct de plecare versatilitatea geometrică a hexagonului și fiind inspirat de principiile de pliere din origami, studiul propune un sistem de umbrire exterioară cu mecanism cinetic, capabil să reacționeze în mod dinamic la schimbările radiației solare. Designul este ghidat de principii de biomimetism și urmărește să contribuie atât estetic, cât și funcțional la anvelopa clădirii.*

Cuvinte cheie: design sustenabil, anvelopă adaptabilă, teselare hexagonală, fațade ventilate, stare de bine.

1. Introduction

In the context of growing global efforts to reduce energy demand and mitigate greenhouse gas emissions, the construction industry emerges as a key contributor, responsible for nearly 40% of worldwide energy consumption. Nonetheless, such reduction strategies must ensure that occupant comfort and overall well-being are not affected.

The building envelope plays a fundamental role in separating the interior environment of a structure from external conditions. It typically comprises structural construction elements and operable components such as doors and windows. A comprehensive definition [1] describes the building envelope as the physical barrier that separates the heated volume of the building from: the outdoor air; the ground (in the case of floors in direct contact with the soil, whether located above or below the finished ground level, as well as walls in contact with the soil); adjacent unheated or minimally heated spaces within the building, such as storage areas, technical basements, cellars, attics, enclosed balconies, and loggias, which are thermally insulated from the heated volume; internal spaces with different functions (e.g., commercial spaces at the ground floor of residential buildings, office areas); and neighboring buildings, provided that they are separated by expansion joints. In the current context, where minimizing energy consumption is a major priority, the performance and quality of the building envelope are of critical importance.

The building envelope serves multiple functions, including:

- thermal insulation of the building,
- regulation of indoor air humidity,
- protection against wind and weather conditions,
- acoustic insulation,
- fire protection,
- admission of natural light,
- and, not least, contributing to the architectural identity of the building through aesthetically designed solutions.

Traditionally, building envelopes were regarded as static components, albeit incorporating operable elements. Maintaining indoor comfort required constant attention and manual intervention from occupants. However, in the late 20th century, and increasingly in the early 21st century, a new approach to façades emerged: the concept of the adaptive façade, also referred to as responsive or dynamic façade [2].

This concept refers to the ability of building envelopes to change their form and functions in response to external environmental changes, such as seasonal variations or the time of day. This adaptability can be achieved through the integration of layers or spaces equipped with systems that regulate airflows, enable ventilation, provide shading, or modulate natural lighting. These functions are typically managed by automated control systems that respond to external conditions and indoor microclimate requirements. In addition, photovoltaic systems for energy generation can be incorporated either within or on the surface of the envelope. A related approach is the

use of kinetic façades, which use mechanical systems to dynamically change their configuration in response to environmental conditions.

Another emerging concept in architecture, also observed in other fields, is the use of nature as a source of inspiration, a principle known as biomimicking or bioinspiration. In building design, analogies have been drawn between the function of the building envelope and the behavior of biological skin in humans and animals. Such observations have led to the development of innovative technical solutions and the discovery of new materials.

The design of adaptive façades, fully aligned with current energy efficiency and sustainability policies, requires the collaboration of multidisciplinary design teams composed of architects and engineers from various fields. This integrated approach is essential to address the complex challenges such systems present. Even though the concept of adaptive façades has been known for some time, its practical implementation is relatively recent, with several notable projects exemplifying its application, such as the Al Bahr Towers in Abu Dhabi (2012–) - Fig. 1.a, and the Council House CH2 in Melbourne (2004–2006) - Fig. 1.b [3].

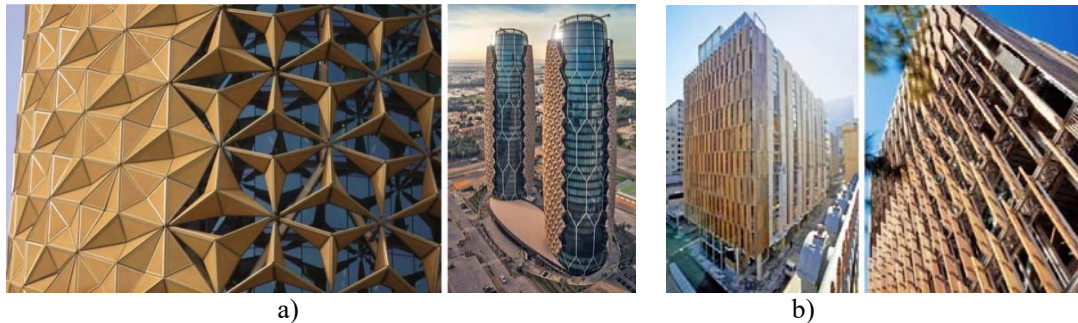


Fig.1. Adaptive envelope - exemples

2. Proposed solution

A comprehensive evaluation of a building's performance, considering all previously discussed aspects, requires large, multidisciplinary design teams and complex multi-criteria analyses. This is due to the fact that certain design measures may enhance specific performance parameters while potentially having a less favorable impact on others.

This paper aims to propose a shading system suitable for a building having glass wall façade, intended to enhance the performance of the building envelope from several perspectives:

- aesthetic enhancement, through the addition of a secondary layer applied over the curtain wall, which also contributes to improved energy performance;
- a study focused on improving thermal performance;
- analysis of airflow behavior within the newly created structure;
- ensuring visual comfort for building occupants.

2.1 Defining the Design of Adaptive Façade. Geometric exploration

As climate concerns have intensified in recent years, the field of responsive façades has gained increasing attention, as it enables buildings to adapt their exterior envelopes to fluctuations in outdoor temperature and variations in solar radiation intensity [4].

As a source of inspiration for the development of the proposed shading system the authors explored the folding techniques found in origami art, which allow for the creation of a wide variety of geometric forms. The primary objective was to design a planar structure composed of modules interconnected with adjacent units to form a continuous network. Based on this interconnected grid and utilizing Rhino 7 software, the hexagon was selected as the fundamental geometric shape.

The hexagon can be harmoniously subdivided due to its symmetrical structure. It is the only regular polygon whose side length is equal to its radius. Among the three well-known regular tessellations, triangular, square, and hexagon, the hexagonal grid yields the minimum perimeter for a given unit area. As a result, the hexagonal pattern also emerges naturally in structures shaped by physical forces, as exemplified by the honeycomb. The equal distribution of in-plane stresses, the tendency toward structural stability, and material efficiency all contribute to the formation of equally sized circular cells that are arranged in the most compact and isotropic configuration. Whether formed by internal growth or external compression, these conditions inherently lead to a hexagonal network.

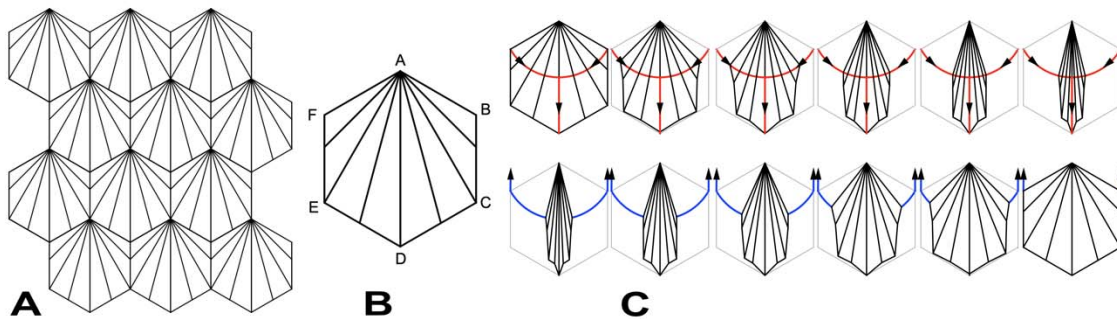


Fig.2. a. Hexagonal tessellation; b. Hexagonal symmetry; c. Opening/closing system of the shading system

Starting from the hexagonal shape and its interconnection with adjacent areas in a grid, tessellation was selected as the geometric strategy. In simple terms, surface tessellation refers to covering a surface with one or more polygonal shapes without overlaps or gaps. While numerous examples of tessellations on curved surfaces are known [5], this study focuses on a more straightforward case, tessellating a flat surface, specifically the planar façades of a building, as illustrated in Fig. 2.a.

In descriptive geometry, the tiling of a plane using regular polygons of equal side length and type is classified as regular or homogeneous tessellation. The admissible polygons include equilateral triangles, squares, regular hexagons, as well as semi-

regular polygons. There are eight known types of semi-regular tessellations with a single vertex type and fourteen types involving multiple vertex types. Such tessellations are only possible using regular polygons whose internal angles are exact divisors of 360 degrees.

Based on this principle, by applying symmetry to a regular hexagon ABCDEF along the diagonal AD and dividing the sides BC, CD, DE, and EF into two equal segments (Fig. 2.b), a mechanism can be implemented that allows for dynamic opening and closing, as shown in Fig. 2.c. In the following section, the geometric configurations of the proposed shading system and the folding motion of the façade based on origami principles are analyzed.

2.2 Dynamic characteristics of sun shading device

Architectural design involves, among other aspects, the study of how natural light enters in the space and how the surrounding environment is perceived factors that can be significantly enhanced through the proposed façade system [6]. The entire system becomes an integral part of the building envelope, influencing the overall architectural expression. A key design consideration lies in selecting actuation mechanisms that are both efficient and visually appealing. Consequently, parameters such as the number of actuating points, required displacements, and actuation forces must be carefully evaluated during the design phase to ensure the long-term sustainability of the system. The façade is designed to respond to specific levels of solar radiation. Functioning like an origami structure, it seamlessly integrates into the building envelope, with its primary role being the regulation of indoor light intensity. The geometric properties and symmetry of the hexagon enable its large-scale repetition across a planar surface. The actuation axis for the shading module's closing mechanism corresponds to the diagonal AD of the hexagon ABCDEF, as illustrated in Fig. 2. By pulling tension cables located at the lower edge of the façade along the direction of diagonal AD, indicated by red arrows in Fig. 2.c, the shading system rotates the vertices F and B around the fixed-point A, initiating the closing motion to allow sunlight to enter the interior space. Conversely, to activate the opening mechanism, represented by blue arrows in Fig. 2.c, tension cables located at the upper edge of the façade, aligned with edges EF and BC, are engaged. This movement causes vertices F and B to rotate around point A in the opposite direction, thereby deploying the shading elements and fully protecting the façade from direct solar radiation.

Through folding, the module creates new angles that reflect incoming solar radiation away from the façade. Fig. 3.a presents a top view of the shading device, illustrating a gradient transition from 100% opacity to 60%, and further to 30% opacity. The same assembly is shown in perspective view in Fig. 3.b.

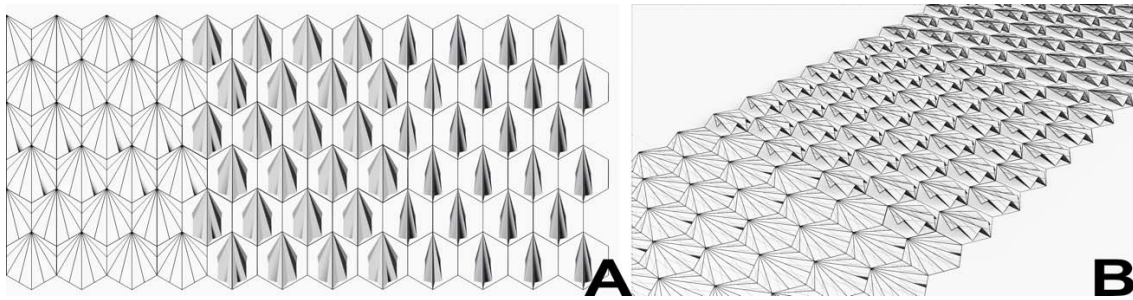


Fig.3. a. Plan view of the shading system with different opening; b. Perspective of the shading system with different opening.

During operation, the system generates animated patterns across the building façade, which are perceptible both from the exterior and the interior, as illustrated in Fig. 3 and Fig. 4.

The visual appearance of these movements can vary across the entire façade, creating a customized scenographic effect for the building's occupants. Due to the independent operation of individual modules, natural light can enter interior spaces without altering the overall geometry of the façade. Offering a high degree of flexibility and a wide range of configurations, the kinetic shading device can adapt effectively to varying solar intensities. The resulting hexagonal units form openings of different sizes, producing inventive dynamic compositions and generating a three-dimensional textured surface along the vertical axes of the façade. The responsive and vibrant envelope becomes dynamic through the formal attributes of its surface, modulating its appearance in accordance with light intensity, as demonstrated in Fig. 4.a (exterior view) and Fig. 4.b (interior view).

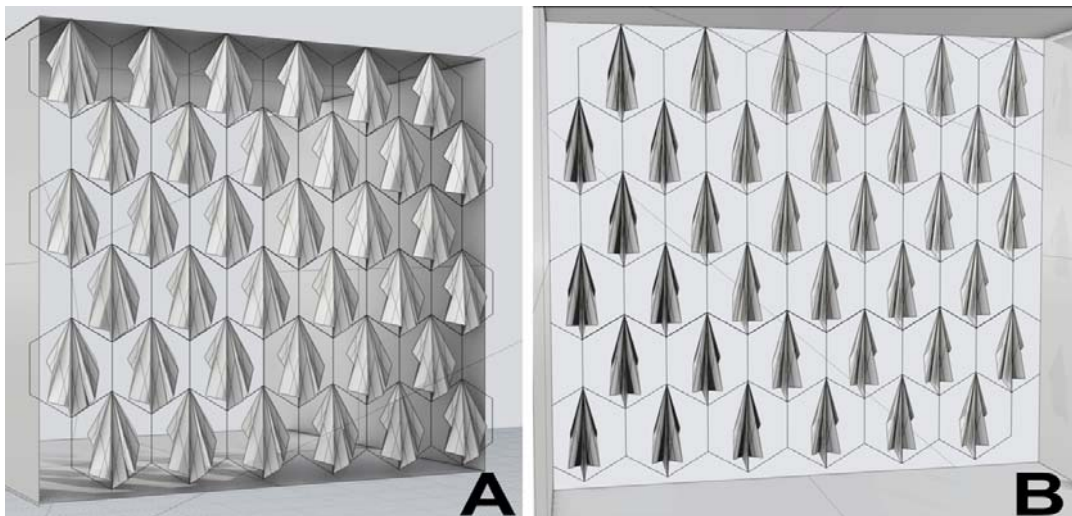


Fig.4 a. View of the shading system from the outside; b. View of the shading system from inside

As illustrated, the system can be fully closed (100%) to create complete shading and prevent direct sunlight from entering the interior when solar rays strike the façade

perpendicularly. As previously described, the shading system can be opened by applying force at the lower part of the façade along the vertical diagonal of the hexagon, while closing is achieved by applying force at the upper part of the façade along the vertical edges of the hexagon. The proposed shading design alters the façade's geometry through a kinetic structure that passively responds to variations in light intensity [7]. Future research, in collaboration with colleagues from the Faculties of Mechanical and Electrical Engineering, will enable a more in-depth investigation of the shading system's performance.

1.1. Energy efficiency and well-being

The concept of well-being encompasses the fulfillment of multiple criteria, which can be evaluated through both objective and subjective indicators. From an objective standpoint, well-being is closely linked to quantifiable physical parameters related to indoor environmental quality, including thermal comfort, visual comfort, acoustic performance, and indoor air quality. These factors can be measured using established engineering and environmental metrics. However, well-being also depends on subjective, psychological components, such as perceived comfort, emotional response to space, and a sense of control over the environment, which cannot be directly measured. Instead, these aspects require statistical evaluation, typically conducted through structured surveys and interviews with a significant number of building occupants [8].

1.2. Thermal comfort elements

In terms of the building envelope's contribution to achieving thermal comfort, several key parameters must be met, with recommended values provided by experts in the field [1, 11]:

- Indoor air temperature (t_i) and its spatial and temporal distribution within the occupied zone: These values should generally fall within the range of 19 - 23°C.
- Mean radiant temperature (θ_{mr}) and the solid angle under which an occupant perceives surrounding surfaces with varying temperatures: The difference between indoor air temperature and the mean temperature of enclosing surfaces should be minimal (not exceeding 3°C). Additionally, surface temperatures of enclosure elements must be no lower than 16°C.
- Air velocity within the occupied space, particularly in rooms with mechanical ventilation or air conditioning: The recommended range is 0.15 - 0.2 m/s to avoid drafts while ensuring proper air circulation.
- Indoor relative humidity (ϕ_i): Recommended values fall within the range of 35 - 70%, ensuring both comfort and indoor air quality.

Thermal transfer can be characterized using several physical parameters [1], among which the most relevant is:

- Thermal resistance (measured in $\text{m}^2\text{K/W}$): \rightarrow describes a material's ability to resist heat flow and is critical in assessing the insulating performance of building components. For a multilayer construction element composed of homogeneous materials, the total thermal resistance is calculated as the sum of the convective resistances of the adjacent fluid layers (typically air) and the conductive resistances of the solid layers. The overall thermal resistance can be expressed by the following equation:

$$R = R_{si} + \sum R_s + \sum R_a + R_{se} \quad (1)$$

or explicitly,

$$R = 1/\alpha_i + \sum d/\lambda + \sum R_a + 1/\alpha_e \quad (2)$$

where,

R_{si} , R_{se} represents superficial thermal resistances, calculated according to the direction and sense of the thermal flow (they are given in norms);

R_s represents the resistance of a homogeneous layer of a construction element;

R_a resistance of unventilated air layers;

$\alpha_{i,e}$ - coefficient of superficial surface heat transfer to the inside, respectively to the outside [$\text{W/m}^2\text{K}$];

d - finished thickness of the wall [m];

λ - the thermal conductivity of the material [W/mK].

- Heat transfer coefficient (or transmittance) [$\text{W/m}^2\text{K}$], frequently used both in thermotechnics calculations of construction and also in the catalogues of some companies that produce or sell construction materials, represents the reverse of the thermal resistance and is determined with the relationship:

$$U = 1/R \quad (3)$$

It reflects the heat transfer capacity, so the lower the U value is, the lower the transmission losses are.

According to current Romanian standards, conventional building envelopes for residential structures must meet a minimum thermal resistance of $R_{\min} = 1.8 \text{ m}^2\text{K/W}$ and a maximum thermal transmittance of $U_{\max} = 0.6 \text{ W/m}^2\text{K}$, as specified by MDRAPFE Order 2641 from 2017. Unfortunately, in the case of lightweight façade systems typically used for administrative and commercial buildings, the thermal performance often falls below these required thresholds. As a result, efforts are being made to identify alternative design solutions and advanced materials to enhance the energy performance of such façades.

In order to evaluate the effect of the shading system during the cold season, a comparative simulation was performed. The analysis focused on a building with aluminum frame envelope and triple-glazed glass. Ubakus software [9], a U -value calculator that evaluates wall components for insulation, moisture protection, and thermal performance, was used to calculate the Heat Transfer Coefficient of the wall, both with and without the shading system.

In the case of the wall without the shading system, a value of $R=1.43 \text{ m}^2\text{K/W}$ was obtained. In the case of the same glass wall with the application of the shading system, the thermal resistance increased to $R=1.523 \text{ m}^2\text{K/W}$, indicating a 6% improvement.

While the proposed solution has a limited impact on heating performance during the cold season, it significantly reduces cooling needs in the warm season, thus improving the building's overall energy efficiency.

Table 1

Analysis of the obtained results				
Layers (from inside to outside)	Without shading		With shading	
	Thickness [mm]	R [$\text{m}^2\text{K/W}$]	Thickness [mm]	R [$\text{m}^2\text{K/W}$]
Thermal contact resistance		0.130	-	0.130
Insulation glass, tripple glazed	36	1.263	36	1.263
Thermal contact resistance		0.040	-	0.130
Ventilated level	-		200	
Shading	-		2	
Whole component	36	1.433	238	1.523

2.3.2. Aspects Related to Air Quality. Airflow Along the Façade

To ensure an adequate level of indoor air quality, it is essential to provide controlled air exchange with the outdoor environment. This process compensates for oxygen consumption and facilitates the removal of excess pollutants, including metabolic byproducts, combustion residues, tobacco smoke, volatile organic compounds (VOCs), microorganisms, radioactive substances, settleable particulate matter, and other harmful agents generated by technological processes occurring within buildings.

This air exchange can occur either with or without the use of external energy. Air movement may result from the building's inherent physical properties or be assisted by mechanical systems. Accordingly, the following ventilation scenarios can be identified [10]:

- Natural ventilation
 - unorganized (passive infiltration and exfiltration)
 - organized (intentional airflow paths, such as operable windows or vents)
- Mechanical ventilation
 - basic (forced air supply or exhaust)
 - integrated with:
 - heating/cooling systems
 - humidification/dehumidification systems

- Mixed-mode ventilation
 - mechanical air supply combined with natural exhaust
 - natural air supply combined with mechanical exhaust
- Air conditioning
 - for thermal comfort
 - for technological or process-specific requirements

Technical literature provides methods for calculating air flow rates based on seasonal conditions (summer or winter) and depending on the selected ventilation or air conditioning system. In addition to air flow rate calculations derived from pollutant balance assessments, an approximate method is often used during the early design phases, as well as for validating classical calculation methods. Two key indicators are commonly defined in this context:

➤ Specific air flow rate:

$$L_s = \frac{L}{N} \quad [\text{m}^3/\text{h}, \text{object}] \quad (4)$$

➤ Air exchange rate:

$$n = \frac{L}{V} \quad [\text{h}^{-1}] \quad (5)$$

where:

L = air flow rate $[\text{m}^3/\text{h}]$

N = number of occupants, equipment, or sanitary fixtures

V = room volume $[\text{m}^3]$

These indicators have recommended values established by technical standards, depending on the intended use of the indoor spaces, and are employed for preliminary estimations of air flow rates. It is important to note that for rooms without significant emissions of harmful substances, the air flow rate can be determined based solely on these indicators, without the need for detailed pollutant balance calculations. While both indicators are used depending on the application, the air exchange rate is more commonly referenced in practice. In the specific case of the analyzed building, which accommodates office activities, current regulations recommend an air exchange rate of $n = 3 - 6 [\text{h}^{-1}]$.

When implementing external shading devices, it is essential to consider the airflow dynamics along the façade. The ventilated cavity between the shading system and the façade promotes natural convection, enabling continuous air circulation that dissipates heat effectively – Fig. 5.

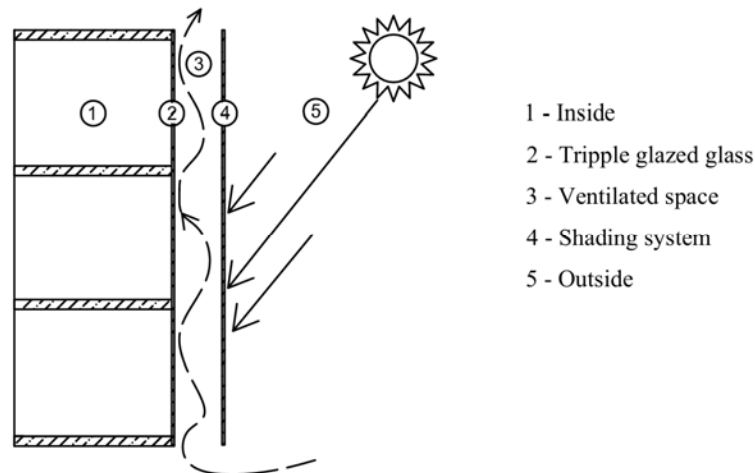


Fig. 5. Air circulation on the facade

2.3.3. Visual Comfort Elements. The Importance of Applying Shading Devices.

The building envelope also plays a crucial role in ensuring access to natural daylight. Glass façades have become a defining feature of contemporary architecture due to their ability to provide consistent natural illumination. However, to optimize energy efficiency, it is essential to strike a careful balance between the amount of daylight admitted into the interior and its thermal impact on the indoor environment.

An important point of view in achieving this balance is adjusting illumination levels according to the function of the space and the nature of activities performed within. In office environments, for instance, current standards recommend an illuminance level of 300–500 lux, with a maximum permissible value of 750 lux, in order to support both visual comfort and occupant productivity.

Visual comfort is a fundamental aspect in the design of office spaces, having a significant impact on user productivity and well-being [12]. It extends beyond mere illumination levels and encompasses a range of qualitative parameters that must be met to ensure an optimal visual environment, as specified in the SR EN 12464 standard, some of which are summarized below.

For instance, the lighting uniformity level should exceed 0.6 to ensure an even distribution of light, thereby avoiding discomfort caused by overly bright or insufficiently lit areas. Additionally, the unified glare rating (UGR) must be equal to or less than 19, in order to minimize visual disturbances caused by glare and reflections, which can negatively affect concentration.

Another important parameter is the Color Rendering Index (CRI), which ranges from 0 to 100. In office environments, the CRI should exceed 80 to ensure accurate color representation and maintain a natural visual atmosphere. In addition, the Correlated Color Temperature (CCT) is also critical. For office spaces, a recommended CCT value is 4000 K, on a scale typically ranging from 2700 K to 6500 K, corresponding to a neutral white light that supports concentration and reduces visual fatigue.

Incorporating these parameters into the design of lighting systems, whether natural or artificial, plays a key role in ensuring that workspaces are both comfortable and high-performing. By aligning with ergonomic standards and sustainability goals, this design strategy emphasizes the value of integrated solutions and thoughtful planning in enhancing the functionality and quality of office environments.

3. Conclusions

Natural daylight helps reduce the reliance on artificial lighting. However, when solar radiation is too intense, it can lead to increased indoor temperatures and greater energy demand for cooling. Therefore, adaptable shading systems enable the reduction of unwanted heat gains while still maintaining high-quality natural illumination.

Building façades can no longer be regarded only as barriers between interior and exterior spaces. They are evolving into intelligent interfaces between humans and the environment, playing a crucial role in energy performance, occupant comfort, and architectural expression. Their design must be approached as a complex engineering challenge, multidisciplinary in nature and guided by the principles and demands of sustainability.

References

- [1] Mârza, C., Abrudan, A., Elemente de termotehnica construcțiilor, Ed. UT Press, Cluj-Napoca, 2012.
- [2] Sandak, A., Sandak, J., Marcin, B., Kutnar, A., State of the Art in Building Façades, <https://www.researchgate.net/publication/331516581>, 2019.
- [3] Alotaibi, F., The Role of Kinetic Envelopes to Improve Energy Performance in Buildings, Journal of Architectural Engineering Technology, 2015.
- [4] Mârza, C., Graur, A.M., Corsiuc, G., Adaptive Shading Envelope – a Challenge for Architects and Engineers, 10th Jubilee International Conference on Geometry and Graphics -Mongeometrija 2025, 5-6 june, Belgrade, Serbia.
- [5] Fioravanti, A., Cursi, S., Elahmar, S., Gargaro, S., Loffreda, G., Novembri, G., Trento, A., Square tessellation patterns on curved surfaces: In search of a parametric design method, ShoCK! - Sharing Computational Knowledge! - Proceedings of the 35th eCAADe Conference - Volume 2, Sapienza University of Rome, Rome, Italy, 20-22 September 2017, pp. 371-378, doi <https://doi.org/10.52842/conf.ecaade.2017.2.371>.
- [6] Graur, A.M., Design of adaptive solar shading system based on the Cuboctahedron, Revista Română de Inginerie Civilă, vol. 13, no.2, pp.182-191.
- [7] Graur, A.M., Mârza, C., Corsiuc, G., Adaptive shading envelope inspired by the geometry of nature, Journal of Industrial Design and Engineering Graphics, vol. 19 no. 1, 2024, pp. 203-206.
- [8] Boon Lay Ong, Beyond environmental comfort, Ed. by Routledge Taylor and francis Group, London and New York, 2013.
- [9] <https://www.ubakus.de/u-wert-rechner>.
- [10] Mârza, C., Corsiuc, G., Despre relația confort ambiental-calitate a aerului-permeabilitate la aer a construcțiilor. Revista Română de Inginerie Civilă, 2017, vol. 8, no.3, pp. 167-172.
- [11] C107-2005 Normativ privind calculul termotehnic al elementelor de construcție ale clădirilor.
- [12] Albu, H., Beu, D., Rus, T., Moldovan, R., Domnita, F., Vilcekova, S., Life cycle assessment of LED luminaire and impact on lighting installation –A case study, Alexandria Engineering Journal, Vol. 80, 2023, pp. 282-293, <https://doi.org/10.1016/j.aej.2023.08.068>.

Characterization of fiber reinforced concrete for classification based on strength and ductility

Caracterizarea betonului armat dispers în vederea clasificării pe baza rezistenței și ductilității

Muheeb Altaieb¹, Andrei Gîrboveanu¹, Dan Georgescu¹

¹Technical University of Civil Engineering of Bucharest
121-126 Bvd Lacul Tei, Bucharest, Sector 2, Romania
E-mail: andrei-sorin.girboveanu@phd.utcb.ro

DOI: 10.37789/rjce.2025.16.3.2

Abstract. *Fiber reinforced concrete is a solution whereby some of the conventional steel reinforcement can be replaced by adding fibers to the concrete mass. Steel fiber reinforced concrete is classified based on strength and ductility. Depending on the amount of fiber, the behavior can be softening or hardening. In the present paper, individual results show a specific hardening behavior. However, this fiber reinforced concrete is classified into a class with weakening behavior due to the variability of experimental results.*

Key words: *fiber reinforced concrete, softening, hardening, strength, ductility*

Rezumat. *Betonul armat dispers reprezintă o soluție prin care se pot înlocui o parte din armăturile convenționale din oțel prin adăugarea de fibre în masa betonului. Betoanele armate dispers cu fibre de oțel sunt clasificate pe baza rezistenței și a ductilității. În funcție de cantitatea de fibre, comportarea poate fi de slăbire sau întărire. În articolul de față, rezultatele individuale arată o comportare specifică de întărire. Cu toate acestea, betonul armat dispers este încadrat într-o clasă cu comportament de slăbire, din cauza variabilității rezultatelor experimentale.*

Cuvinte cheie: beton armat dispers, slăbire, întărire, rezistență, ductilitate

1. Introduction

Fiber reinforced concrete is the result of incorporating a variable amount of discontinuous fibers into the concrete mass. Fiber reinforced concrete is defined as "the material obtained by mixing cement, aggregates, fibers, additives, mineral additions and water during preparation, in predetermined proportions, whose properties develop through the hydration and hardening of the cement and the interaction between the fibers and the matrix".

Fiber reinforced concrete cannot completely replace conventional reinforced concrete. However, there are scopes of use in which fiber-reinforced concrete can be used as an alternative or in addition to conventional reinforced concrete, offering technical and economic advantages. It has been found that fibers, of any nature, improve the properties of plain concrete. The basic requirements of fibers, when it is necessary to improve the mechanical resistance of concrete and delay the cracking process, are: high tensile strength and adequate modulus of elasticity, increased adhesion to the matrix, chemical stability.

The improvement of the properties of steel fibers influences the increase in the tensile strength of concrete reinforced with such fibers. In practice, the increase in the bending strength of the concrete element reinforced with steel fibers is observed, due to the fact that the distribution of stresses in the tension area is almost constant.

After cracking occurs, if the fibers are perpendicular to the direction of crack propagation, they act as bridges between the crack walls, limiting its development. The preferred areas of use are elements with limited thicknesses (or cast in successive layers of limited thickness). For these types of elements, it is possible to obtain an orientation of the fibers perpendicular to the cracks, and an increased effectiveness of them. The main applications are: floors and slabs for industrial buildings, prefabricated beams, foundation piles, continuous foundations, bridge decks, tunnel linings, explosion-proof structures, facade elements, etc.

2. Fresh properties of fiber concrete

The rheological properties of fiber reinforced concrete depend on the consistency of the matrix as well as the fiber nature, dosage and geometry. The use of fiber contents typical for structural applications, reduces the workability of the mix, especially for fibers with a complex shape and large aspect ratios. Appropriate modifications of the mix composition may be carried out where necessary:

- by increasing the fine aggregate fraction and/or by reducing the maximum aggregate size;
- by using an appropriate type and amount of superplasticizer.

Fiber distribution in the mix should be uniform. In order to achieve this condition, particular attention must be paid to avoid fiber agglomeration (balling). Even though the amount of these agglomerations is limited, their presence can cause some obstructions and make pumping difficult. The more diffused the regions with heterogeneous distributions of fibers, the more diverse the properties of the fiber reinforced concrete are from the nominal ones.

The addition of fibers to concrete may reduce the slump and/or increase the cohesiveness of the mix. This has to be compensated either by using plasticizers or by adjusting the mix proportions.

Pumping fiber concrete does not require special equipment. However, it is useful to have a vibrator on the grid of the pump. Concrete containing short fibers of any type will not cause problems. However, longer steel fibers with an aspect ratio of more than about 60 may require careful attention to mix design, particularly at high dosages

(typically, more than 25 kg/m³ of steel fibers. This is very much dependent on the type of fiber being used and the fiber supplier should be able to advise on these aspects. It is recommended that the diameter of the pump pipeline should not be less than one and a half times the length of the fibers used, as they exhibit some flexibility in the pipeline.

It is recognized that plastic shrinkage and cracking are related to bleeding and/or autogenous/chemical shrinkage. Polymer micro-fibers may therefore have beneficial effects, while steel and macro-polymer fibers have little influence. This is one of the main reasons for the use of polymer micro-fibers, particularly in horizontal elements. If fibers of this type are used for this purpose, typical addition rates range between 600 g/m³ and 900 g/m³.

3. Hardened properties of fiber concrete

Fibers are mainly added to influence the hardened concrete properties. Many of the hardened properties which are affected are rarely specified, and are unlikely to be familiar to ready-mixed concrete producers. Fibers significantly affect hardened properties in the following ways:

- increasing post-crack flexural tensile strength;
- increasing shear strength;
- increasing impact resistance;
- reducing crack widths (Design in Serviceability Limit State);
- increasing fatigue resistance.

3.1. Tensile strength

The ability of fibers to transfer stresses across cracks is one of the most important properties of fibers in concrete. This allows a fiber reinforced element to take on a substantial load even after the first crack appears. Fiber reinforced concrete exhibits a specific behavior in axial tension. The fibers improve the tensile stress behavior (tensile strength) of the cracked matrix.

The post-cracking strength may be defined on the basis of point values, f_i , corresponding to specified nominal value of crack opening, or on mean values, f_{eqi} , calculated for assigned intervals of crack opening. When a notched specimen is considered, the crack opening may be conventionally assumed equal to the displacement between two points at the notch tip, $CTOD$ (Fig. 1) .

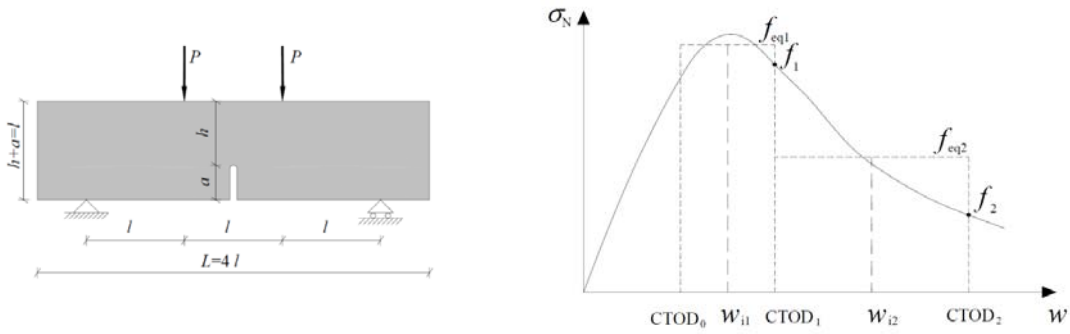


Fig. 1 Definition of point and mean residual strength depending on crack opening values [1]

3.2. Compressive strength

The addition of fibers usually does not affect compressive strength except where the air content is increased, for example by the fiber coating. Fibers generally reduce the brittleness of the matrix, but they do not have significant effect on the compressive behavior. In practice, the constitutive law of fiber reinforced concrete can be assumed equal to that of ordinary concrete.

3.3 Fire resistance

The fire resistance of concrete structures is generally considered not to be influenced by the addition of steel fibers, though the fibers may reduce the degree of spalling somewhat by bridging areas of spalled concrete.

3.4. Impact resistance

Impact resistance, ductility and toughness are generally increased by the addition of any fibers. When impact resistance is required, design is usually determined by testing and then the concrete is specified by type and fiber content.

3.5. Shear strength

The addition of steel fibers to concrete will enhance the shear strength of structural elements. A ductile failure mode is induced, in the same way as by the use of reinforcement stirrups.

3.6. Durability

While steel fibers may reduce the risk of spalling due to corrosion of reinforcement, they do not reduce the rate of corrosion or the rate of loss of cross section. Corrosion of steel fibers themselves at the surface does not cause any spalling.

3.7. Fiber orientation

Orientation of individual steel fibers immersed in fiber reinforced concrete origins from a combination of several basic phenomena of which the most important ones are the so-called wall effect, shear induced orientation and tension stress induced orientation.

The wall effect is caused by the interaction of the immersed steel fibers with the surrounding rigid obstacles such as the formwork. It is geometrically impossible to have a rigid fiber located normal to the formwork at a distance less than half-length of the fiber (red rectangle). Hence, the rigid fiber tends to orientate according to the surrounding flow with a restriction imposed by the wall (blue rectangle).

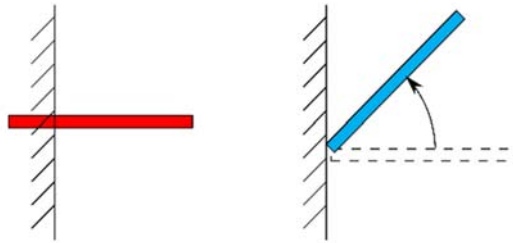


Fig. 2 Wall effect: Blue and red bars represent the possible and impossible orientation of the rigid fiber [2]

4. Mechanical behavior of hardened fiber reinforced concrete

The mechanical behavior of hardened fiber reinforced concrete, the main peculiarity is its tensile behavior. Depending on the tensile strength in the cracked state, fiber reinforced concrete can be classified into concrete with softening or hardening behavior. For low fiber content (with volume fractions approximatively lower than 2%), the behavior is softening. For high fiber content (with volume fractions higher than 2%), the strength can be higher than the matrix one, since a hardening behavior related to multi-cracking phenomenon may occur (Fig. 3).

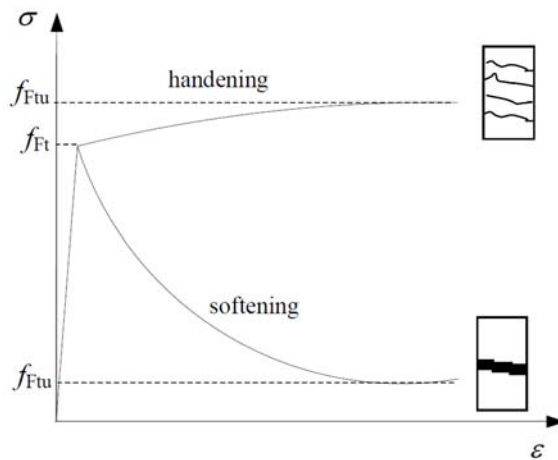


Fig. 3 Fiber reinforced concrete behavior in uniaxial tension depending on fiber content [1]

The properties of the fibers have a direct effect on the behavior of the fiber reinforced concrete. One of these properties is the aspect ratio, defined as the ratio of the total length of the fiber to its "diameter". The aspect ratio has an important effect on the tensile strength of cracked concrete. The tensile strength is higher in concrete containing fibers with a high aspect ratio (Fig. 4).

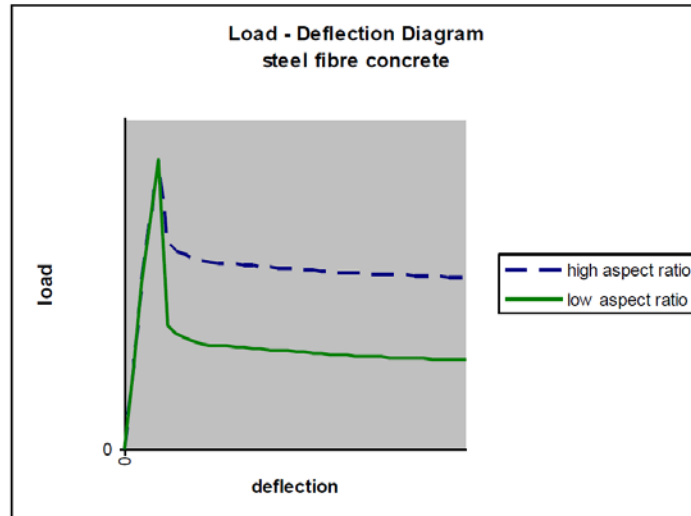


Fig. 4 Post-crack flexural tensile strength of concrete with fibers of different aspect ratios, the same length and the same fiber content (kg/m^3) [3]

Correct fiber tensile strength and bond to the concrete matrix are important to obtain a proper pull-out response. Steel fibers usually have hooked ends or other means to transmit stresses from the matrix to the fiber. The anchorage of the fiber must be good enough to attract enough stress to give a high performance while not so high that it results in fiber rupture. In an ideal situation the fiber is slowly deformed and pulled-out from the concrete matrix (Fig. 5).

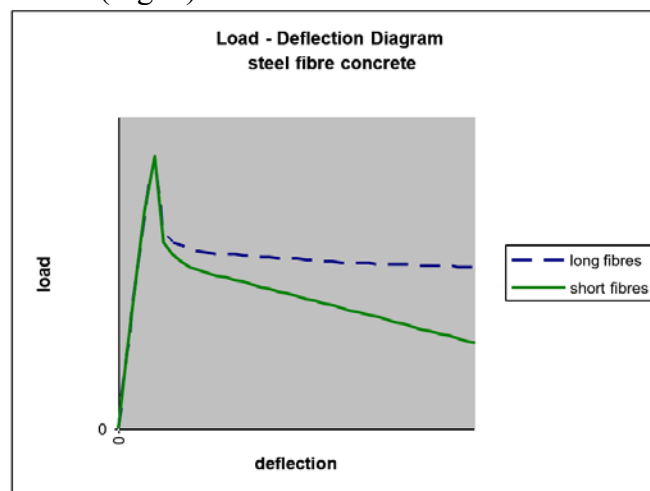


Fig. 5 Post-crack flexural tensile strength of concrete with fibers of different length, the same aspect ratio and the same fiber content. [3]

In addition to the characteristics of the fibers presented above, their shape can also generate different behaviors of fiber reinforced concrete. In Fig. 6, the characteristic load/deflection curves for bending of two concretes with similar compositions, but with different fiber shapes, are presented. If in the case of fiber reinforced concrete with waved fibers, consolidation can be observed after the appearance of cracking, in the case of hooked-end fibers, this phenomenon does not occur, but the ductility is higher and the decrease in strength is slower.

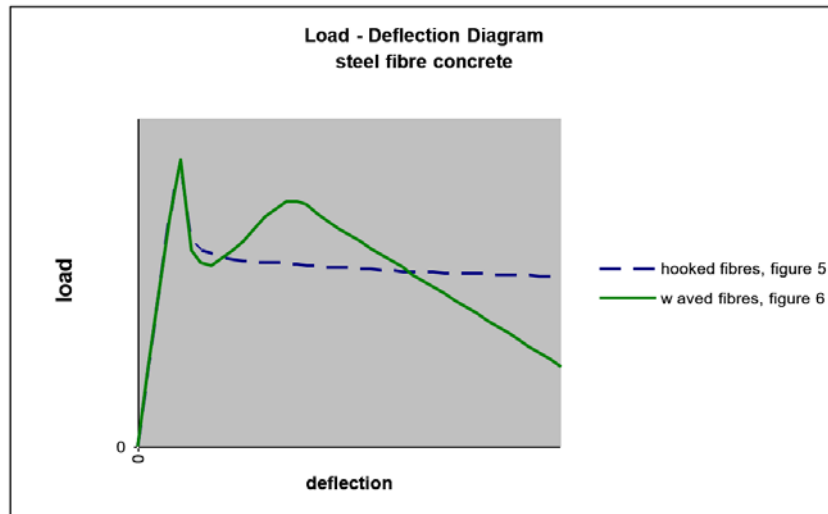


Fig. 6 Post-crack flexural tensile strength of concrete with fibers of different designs and same fiber content [3]

5. Test method for fiber reinforced concrete in tension

This European Standard specifies a method of measuring the flexural tensile strength of metallic fibered concrete on molded test specimen. The method provides for the determination of the limit of proportionality (*LOP*) and of a set of residual flexural tensile strength values.

This testing method is intended for metallic fibers no longer than 60 mm. The method can also be used for a combination of metallic fibers and, a combination of metallic fibers with other fibers.

The tensile behavior of metallic fiber concrete is evaluated in terms of residual flexural tensile strength values determined from the load - Crack Mouth Opening Displacement (CMOD) curve (Fig. 7) or load-deflection curve obtained by applying a center-point load on a simply supported notched prism. (Fig. 8)

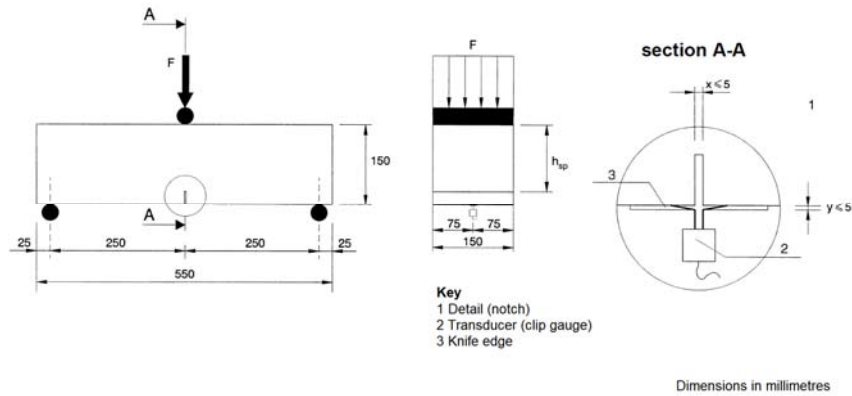


Fig. 7 Typical arrangement for measuring CMOD [4]

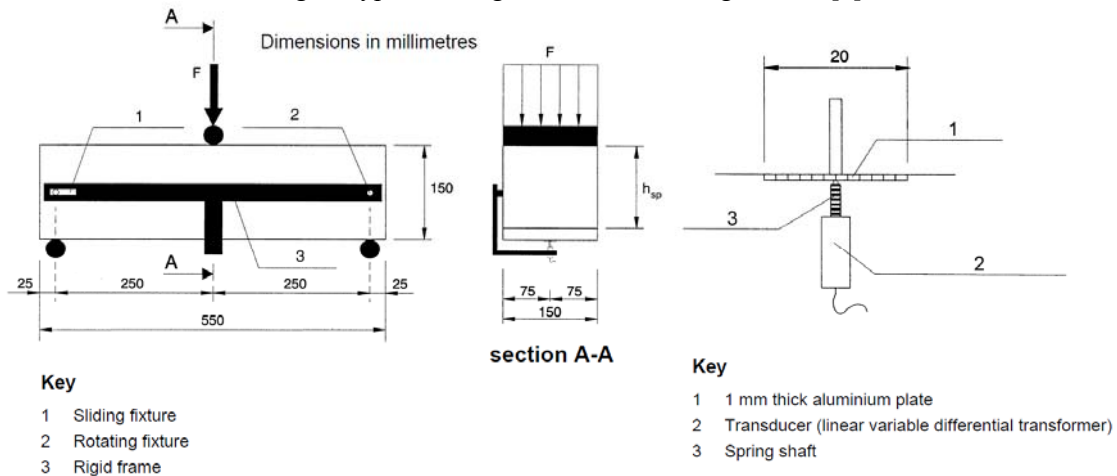


Fig. 8 Typical arrangement for measuring deflection [4]

5.1. Test procedure

In the test procedure for measuring CMOD (Fig. 77) the following terms and definitions apply:

- crack mouth opening displacement - linear displacement measured by a transducer installed on a prism subjected to a center-point load F (Fig.7);
- deflection - linear displacement measured by a transducer installed on a prism subjected to a center-point load F (Fig. 8);
- limit of proportionality - stress at the tip of the notch which is assumed to act in an untracked mid-span section, with linear stress distribution, of a prism subjected to the center-point load F_L ;
- residual flexural tensile strength - fictitious stress at the tip of the notch which is assumed to act in an untracked mid-span section, with linear stress distribution, of a prism subjected to the center-point load

F_j corresponding to $CMOD_j$ where $CMOD_j > CMOD_{FL}$ or to δ_j where $\delta_j > \delta_{FL}$ ($j = 1,2,3,4$).

The experimental device used to construct the stress/CMOD curve, necessary for classifying dispersed reinforced concrete is schematically shown in Fig. 7. The following relations are used for the stress f_{ctL}^f at LOP and for the residual strengths $f_{R,j}$:

$$f_{ctL}^f = \frac{3F_L l}{2bh_{sp}^2} \quad (1)$$

$$f_{ctL}^f = \frac{3F_L l}{2bh_{sp}^2} \quad (2)$$

where

f_{ctL}^f is the LOP , in N/mm^2 ;

F_L is the load corresponding to the LOP , in N ;

l is the span length, in mm ;

b is the width of the specimen, in mm ;

h_{sp} is the distance between the tip of the notch and the top of the specimen, in mm .

$$f_{R,j} = \frac{3F_j l}{2bh_{sp}^2} \quad (2)$$

where

$f_{R,j}$ is the residual flexural tensile strength corresponding with $CMOD = CMOD_j$ or $\delta = \delta_j$ ($j = 1,2,3,4$), in N/mm^2 ;

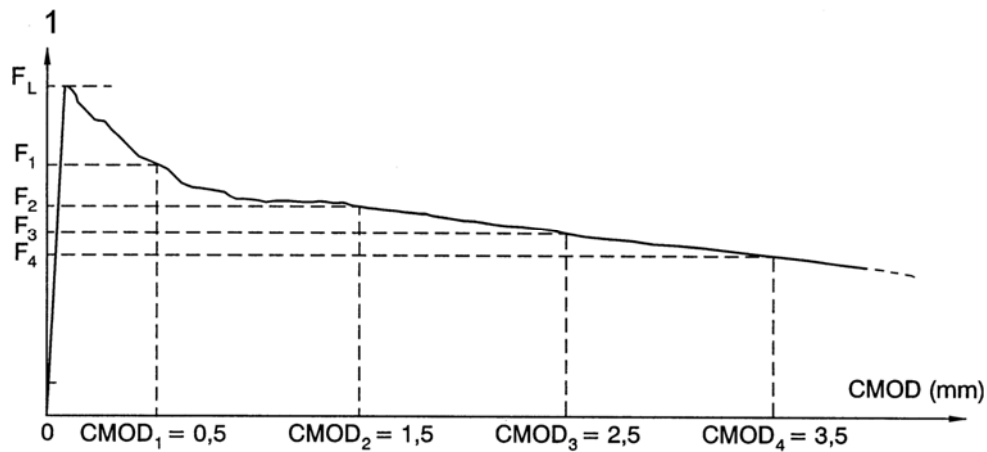
F_j is the load corresponding with $CMOD = CMOD_j$ or $\delta = \delta_j$ ($j = 1,2,3,4$), in N ;

l is the span length, in mm ;

b is the width of the specimen, in mm ;

h_{sp} is the distance between the tip of the notch and the top of the specimen, in mm .

The material class is obtained from two distinct points of the $\sigma_N - CMOD$ curve (Fig.9) that refer, respectively, to the Service Limit State (SLS; $w = 0.5 mm$; $f_{r1,k}$) and Ultimate Limit State (ULS, $w = 2.5 mm$; $f_{r3,k}$). The material class is defined by a numerical value between 1 and 8, obtained from the characteristic value of $f_{r1,k}$, followed by a letter of the Roman alphabet, from “a” to “e”. The letter determines FRC behaviour in the post-cracking phase (hardening or softening) from the ratio f_{r3k} / f_{r1k} , as shown in Table 1.

Fig. 8 Load – CMOD diagram and F_j ($j = 1, 2, 3, 4$) [4]

Fiber reinforced concrete is classified according to its strength and ductility according to Tab. 1. Ductility classes a, b, c, correspond to softening behavior, and classes d and e correspond to hardening behavior.

Table 1

Strength and ductility classes of fiber reinforced concrete [5]

Ductility classes	Characteristic residual flexural strength $f_{R,1k}$												Analytical formulae
	1.0	1.5	2.0	2.5	3.0	3.5	4.0	4.5	5.0	6.0	7.0	8.0	
a	0.5	0.8	1.0	1.3	1.5	1.8	2.0	2.3	2.5	3.0	3.5	4.0	$f_{R,3k}=0.5f_{R,1k}$
b	0.7	1.1	1.4	1.8	2.1	2.5	2.8	3.2	3.5	4.2	4.9	5.6	$f_{R,3k}=0.7f_{R,1k}$
c	0.9	1.4	1.8	2.3	2.7	3.2	3.6	4.1	4.5	5.4	6.3	7.2	$f_{R,3k}=0.9f_{R,1k}$
d	1.1	1.7	2.2	2.8	3.3	3.9	4.4	5.0	5.5	6.6	7.7	8.8	$f_{R,3k}=1.1f_{R,1k}$
e	1.3	2.0	2.6	3.3	3.9	4.6	5.2	5.9	6.5	7.8	9.1	10.4	$f_{R,3k}=1.3f_{R,1k}$

6. Experimental tests on fiber reinforced concrete prisms

Based on the test procedure and the classification into strength and ductility classes, an experimental study was carried out at the TUCEB (Technical University of Construction Bucharest) in which 6 notched prisms were tested. The experimental device is illustrated in Fig. 10. To plot the curves, the applied force and CMOD were measured.



Fig. 9 Experimental device used for 3-point bending test

The failure mode of these specimens after the test is illustrated in Fig. 11. This figure shows an irregular crack propagation, which although has a direction induced by the type and configuration of the load, also follows the defects of the material. For this reason, there is also a significant variability in the results, both in terms of the failure mode and the experimental curves. In the bottom view, the presence of fibers crossing the crack is also observed, generating the bridging effect, ensuring resistance in the cracked area. As can be seen, their arrangement is random. Some of them break before failure, or are torn off, but it is observed that some of them remain anchored on both sides of the crack.

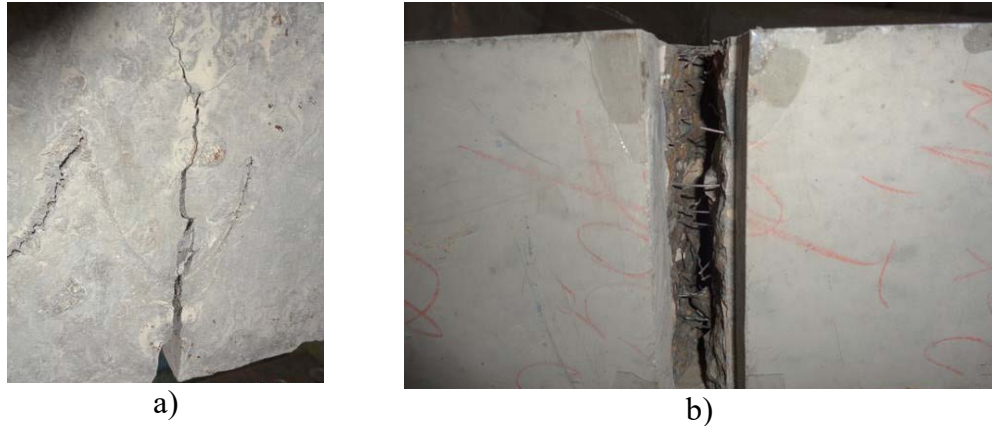


Fig. 10 Failure mode of the specimen. Side view (a) and bottom view (b)

7. Processing the results and determining the class of fiber reinforced concrete

The experimental Force/CMOD curves are presented in Fig. 11. In these diagrams, which present the 6 tests, a significant dispersion of the results is observed, especially in the cracked area. A significant increase in strength is observed, even after the appearance of the crack, but the differences between the stresses that occur in this area are large, compared to the stress values. From these curves, the values F_L and F_j are extracted, based on which the limit of proportionality f_{ctL}^f and the residual strengths $f_{R,j}$ can be determined.

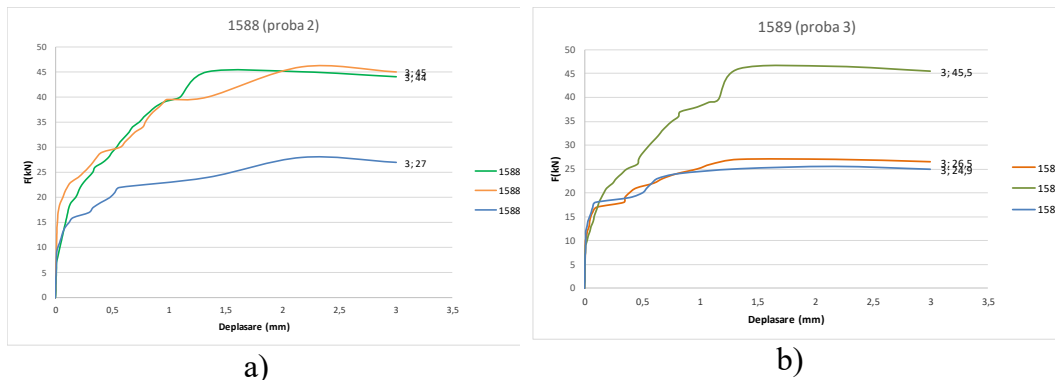


Fig. 11 Experimental Force/CMOD plots obtained through 3-point bending tests

The experimental results for the limit of proportionality f_{ctL}^f and the residual strengths $f_{R,j}$ are presented in Tab. 2. For each of the 5 strengths, the average and the coefficient of variation were calculated. An increasing dispersion of the results is observed, with the increase of CMOD, which reaches approximately 30% for $f_{R,4}$. Such behavior is specific to this type of material.

Table 2

Three-point bending test results

Residual strength	Specimen						Mean	Coefficient of variation
	1	2	3	4	5	6		
f_{ctL}^f	4.5	6.7	4.5	4.5	4.5	5.6	5.0	18.6%
$f_{R,1}$	9.0	9.6	6.7	6.7	8.6	6.4	7.8	17.7%
$f_{R,2}$	14.4	12.8	7.7	8.6	14.7	8.0	11.0	29.8%
$f_{R,3}$	14.4	14.7	9.0	8.6	14.9	8.2	11.6	28.7%
$f_{R,4}$	14.1	14.4	8.6	8.5	14.6	8.0	11.4	29.0%

Based on these results, to determine the characteristic values X_k of the resistances, the following relationship is used, according to Eurocode 0 [6].

$$X_k = X_m \cdot (1 - K_m \cdot V_X) \quad (4)$$

where X_k is the characteristic value of the generic property, X_m is the mean stress, K_m is a parameter dependent on the number of specimens tested and the previously knowledge of V_X , and V_X is the coefficient of variation. The value of the parameter K_m for 6 specimens tested and inexistent previous knowledge is 2,18.

Thus, the values $f_{R,1k} = 4,82MPa$ și $f_{R,3k} = 4,35MPa$. strength class for $f_{R,1}$ is 4,5 and the ratio of $f_{R,3k}/f_{R,1,k} = 0,9$ the fiber reinforced concrete goes into class of 4,5. It is observed that the ductility class c is specific to a softening behavior, even if individually, the specimens show hardening behaviors, fact also highlighted by the higher average value for $f_{R,3}$ than for $f_{R,1}$. The result is justified by the fact that the greater dispersion of the results for $f_{R,3}$ than for $f_{R,1}$ led to lower characteristic values.

8. Conclusions

This study presents the main influencing factors and properties necessary to ensure the final properties. To exemplify their behavior, a case study was carried out to determine the strength and ductility class according to current standards.

Fiber reinforced concrete is classified by its tensile behavior in a cracked state, following a three-points bending test, its behavior being either softening or hardening, depending on the amount of fibers added to the mix.

The random nature of the position and orientation of the fibers causes the experimental values of the residual strengths in the cracked state to present an increasingly greater dispersion of the results as the crack mouth opening increases.

In the case of the present experimental study, even if the experimental curves present a typical hardening behavior, the strength and ductility class is specific to a

softening behavior. This result is justified by the fact that the high dispersion led to a lower characteristic value for a larger crack mouth opening.

9. References

- [1] L. Ascione, V.P. Berardi, L. Feo, others, Technical Document CNR-DT 204/2006, Guide for the Design and Construction of Fiber-Reinforced Concrete Structures, (2007).
- [2] L.N. Thrane, Guideline for execution of steel fibre reinforced SCC, Dansk Technological Institute, 2013.
- [3] O. Aßbrock, J. Carlswärd, R. Dietze, P. Guirguis, W. Hemrich, A. Lambrechts, I. Löfgren, M. Schulz, J. Troy, J. Gibbs, others, Guidance to fibre concrete, Prop. Specif. Pract. Eur. Eur. Ready Mix. Concr. Organ. (2012).
- [4] European Standards, Test method for metallic fibered concrete - Measuring the flexural tensile strength (limit of proportionality (LOP), residual), Eur. Stand. CEN. (2005) 1–17.
- [5] SR EN 1992-1-1 Eurocod 2 Proiectarea structurilor din beton Partea 1-1: Reguli generale și reguli pentru clădiri, poduri și structuri de inginerie civilă, (2024).
- [6] EN 1990. Eurocode: Basis of Structural Design, (2002).

Tracking the performance of an air-to-water heat pump over time for a residential house located in a hilly area with low outdoor temperature

Urmărirea comportării în timp a pompei de căldură aer-apă pentru o casa de locuit situata într-o zonă deluroasă cu temperatură exterioară scăzută

Alexandru Dorca¹, Adriana Tokar¹, Marius Adam¹, Danut Tokar¹, Daniel Muntean¹, Daniel Bisorca¹, Calin Sebarchievici¹.

¹ University Politehnica Timisoara

Victory Square, No. 2

300006 Timisoara, Timiș County, Romania

E-mail: alexandru.dorca@upt.ro, adriana.tokar@upt.ro, marius.adam@upt.ro, danut.tokar@upt.ro, daniel-beniamin.muntean@upt.ro, daniel.bisorca@upt.ro, calin.sebarchievici@upt.ro

DOI: 10.37789/rjce.2025.16.3.3

Abstract. *The paper analyzes the performance of an air-to-water heat pump installed in a single-family home in the hilly area of Romania, during the cold season. Based on in situ measurements and simulations, COP values between 2.90–3.54 for heating and 1.71–2.62 for DHW were obtained. The results confirm the efficiency of the system in low temperature conditions and reveal the importance of correct sizing and intelligent control. The study supports the use of heat pumps as a sustainable solution for residential buildings in cold climates.*

Keywords: heat pump, heating, energy efficiency, renewable energy

1. Introduction

Energy efficiency is essential for the building sector, as heating systems are energy consumers worldwide, with implications for economic sustainability and environmental performance for society [1,2].

Air-to-water heat pumps are increasingly becoming sustainable and energy-efficient solutions for modern heating, cooling and domestic hot water systems. For homes located in hilly areas, characterized by cold winters and significant thermal amplitudes, the selection of a heat pump must take into account the system's performance at negative outdoor temperatures, as well as the national technical regulations in force.[3]

According to the Methodology for calculating the energy performance of buildings – Mc 001/2022, the calculation external temperature for hilly areas in Romania can reach up to -18°C [4], which imposes high requirements on the operating capacity

of air-to-water heat pumps in unfavorable conditions. In this context, SCOP (Seasonal Coefficient of Performance) and low temperature capacity become determining factors in equipment selection.[5]

In addition, Regulation (EU) No 813/2013 sets minimum ecodesign requirements for heating equipment, including the obligation to achieve minimum seasonal efficiency values ($\geq 115\%$ for electric heat pumps in low temperature mode, in average climate zones). In Romania, according to the cold climate zone established by European legislation, these requirements are even more stringent.

At the same time, normative I 13/2015 [6] regulates the technical conditions for the integration of heat pumps into indoor installation systems, including aspects such as: use of thermal reserves, hydraulic balancing, intelligent control and adaptation to intermittent or cascade operation.

Also, through programs such as "Green House" or "Energy-efficient House", the authorities support investments in renewable equipment, provided that the requirements for energy efficiency, ErP certification and performance in climatic conditions specific to the region are met.

The main purpose of this research is to obtain information based on in situ measurements and data processing on the behavior of the air-to-water heat pump used in a single-family house located in a hilly area, which provides both heating and DHW, given the increasingly frequent use of these systems. In addition to improving energy efficiency and reducing CO₂ emissions, this study aims to disseminate the information obtained to better understand the relevant systems among specialists.

2. Methodology

The method used in this study consists of examining through in situ investigations the operation of the air-to-water heat pump located in a heating-dominated climate in Curtea de Arges, Romania, on the energy efficiency and environmental performance of the radiant floor heating system interconnected to an ASHP. The conventional heating season runs from October 1 to April 30, corresponding to 212 days.

2.1 Description of the examined building

To correctly size an air-to-water heat pump, it is essential to define the thermal and construction characteristics of the building as precisely as possible. In this example, we analyze a single-family home located in a hilly area, at an altitude of approximately 450 m, in a temperate-continental climate with mountain influences, characterized by cold winters and moderate summers.

2.1.1 General data

- Building type: Single-family house, ground floor + attic;
- Usable area: 220 m²;
- Heated interior volume: approximately 550 m³;

Tracking the performance of an air-to-water heat pump over time for a residential house located in a hilly area with low outdoor temperature

- Estimated energy class:A (according to the energy performance certificate);

2.1.2 Tire characteristics

- Exterior walls:BCA masonry 30 cm + EPS thermal system 15 cm ($\lambda = 0.037$ W/m K);
- Attic ceiling:mineral wool: 30 cm;
- Plate on the ground:extruded polystyrene: 10 cm;
- Windows:PVC joinery with triple glazing, $U_w = 0.9$ W/m²K;
- Airtightness:good, with Blower-Door test under 2.5 h^{-1} at 50 Pa.

2.1.3 Facilities

- Interior heating:underfloor heating system throughout the house;
- Domestic hot water: 300 liter storage tank;
- Ventilation:decentralized system with heat recovery.

2.1.4 Thermal requirements

Based on calculations according to the Global Performance Index, for this configuration we have:

- Thermal requirement for heating: 10.2 kW at an outdoor temperature of -18°C ;
- Required for DHW: 2.5–3 kWh/day/family.

2.1.5 Air-to-water heat pump parameters

The parameters air-to-water heat pump is presented in Table 1.

Table 1

Main parameters of the air-to-water heat pump	
Parameters	Value
Heating thermal power	11.2 kW at A7/W35, 11.2 kW at A2/W35
COP (coefficient of performance)	4.22 at A7/W35, 3.35 at A2/W35
Cooling thermal power	9.8 kW at A35/W7
EER (energy efficiency ratio)	2.15 on A35/W7, 4.21 on A35/W18
Maximum heating agent temperature	60°C
Outdoor temperature range	-28°C to $+46^\circ\text{C}$
Refrigerant	R410A
Power supply	400 V / 3 phases / 50 Hz
Outdoor unit weight	110 kg
Outdoor unit dimensions	1350 x 950 x 330 mm

The heat pump model used, Zubadan 11.2 kW, is ideal for homes located in hilly areas, where winters are cold and can reach temperatures of -20°C or even lower. Its consistent performance at low temperatures makes this model a good choice for a monovalent heating regime, without the need for auxiliary heating sources.

2.2 Technical parameter formulas

2.2.1 Coefficient of Performance (COP) equation:

The coefficient of performance (COP) is an indicator of the efficiency of the heat pump, expressing the ratio between the heat supplied and the energy consumed. It is a measure of energy efficiency. The higher the COP, the more efficient the heat pump is [7]. The calculation relationship is:

$$COP = \frac{Q_{hot}}{W_{input}} \quad (1)$$

where: Q_{hot} is the heat delivered in (kW); W_{input} is the energy consumed by the compressor in (kW)

For an air-to-water heat pump system, the COP is an essential parameter to evaluate efficiency at low outdoor temperatures [6].

2.2.2 SCOP equation (Seasonal Coefficient of Performance):

SCOP represents the average efficiency of the heat pump over the entire heating season. The formula is:

$$SCOP = \frac{\int Q_{hot}(t) \cdot dt}{\int W_{input}(t) \cdot dt} \quad (2)$$

where: $Q_{hot}(t)$ is the heat delivered at a given time t in (kW); $W_{input}(t)$ is the energy consumed by the compressor at time t in (kW); t represents the entire duration of the heating season.

2.2.3 Equation for available thermal power (Power at the outlet of the outdoor unit):

The thermal power Q_{hot} of the heat pump is influenced by external conditions, and this power can be calculated using the formula:

$$Q_{hot} = m \cdot c_p \cdot (T_{out} - T_{in}) \quad (3)$$

where: m is the mass flow rate of the heat carrier (kg/s); c_p is the specific heat capacity of the heat carrier (kJ/kg·K); T_{out} is the outlet temperature of the heat carrier in (°C); T_{in} is the inlet coolant temperature (°C)

Tracking the performance of an air-to-water heat pump over time for a residential house located in a hilly area with low outdoor temperature

2.2.4. Equation for electrical power consumed:

The electrical power W_{input} consumed by the heat pump depends on the compressor performance and the losses in the distribution system. The calculation relationship is:

$$W_{input} = \frac{Q_{hot}}{COP} \quad (4)$$

where: W_{input} is the electrical power consumed in (kW); COP is the coefficient of performance at those conditions.

It is a weighted average value that expresses the total efficiency of a heat pump over the entire heating season, taking into account: variable external temperatures (not just a fixed temperature of $+7^{\circ}\text{C}$ as in COP), on-off cycles, auxiliary consumption (e.g. fan, pumps, defrost), partial operation mode (at 30–50–70% of capacity) and the effective duration of each external temperature.

3. In-situ investigations and numerical simulations

A conventional ASHP feeds the heating system was analyzed insitu. Sets of measurements were performed for heating, hot water preparation and electricity consumption. The building's ASHP underfloor heating system was monitored during October 1, 2023 and April 30, 2024, respectively. The outside air temperature varied between -7°C and $+10^{\circ}\text{C}$.

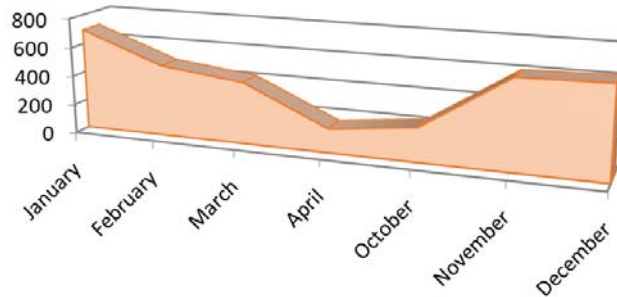


Fig. 1. Electrical power consumed for the heating and domestic hot water system

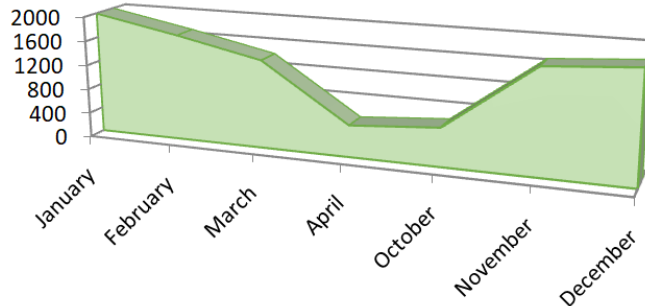


Fig. 2. Thermal power produced for the heating and domestic hot water system

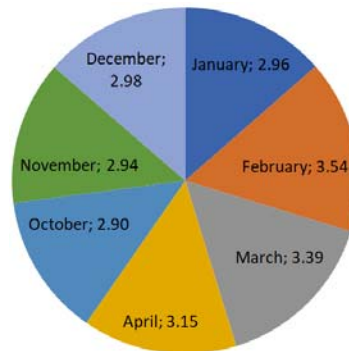


Fig. 3. Coefficient of performance for the heating and domestic hot water system

The maximum efficiency was recorded in February ($\text{COP} = 3.54$), which can be explained by relatively mild outdoor temperatures and the efficient operation of the pump in stable mode.

The minimum COP values occur in October (2.90) and November (2.94), months in which frequent starts and stops, variable temperatures, and operation at partial load affect performance.

The winter season (December–January) shows a constant and decent COP, around 2.96–2.98, which reflects average efficiency in low temperature conditions.

In spring (March–April), the COP increases again towards better values (3.15–3.39), indicating better performance in milder conditions.

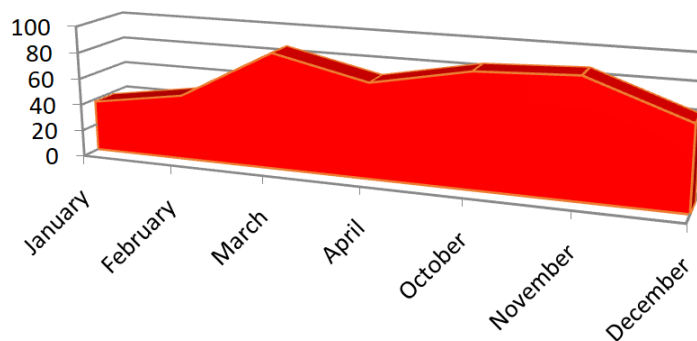


Fig. 4. Electrical power consumed for the preparation of domestic hot water

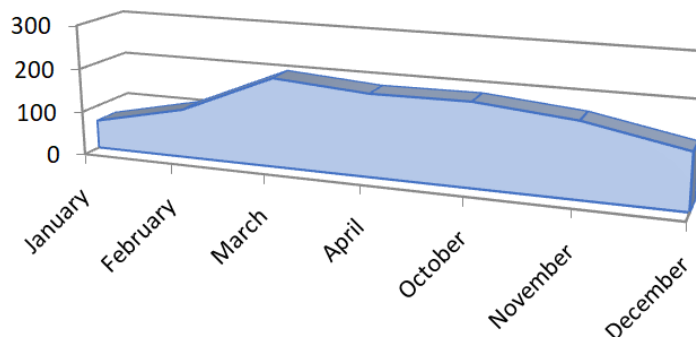


Fig. 5. Thermal power produced for the preparation of domestic hot water

Tracking the performance of an air-to-water heat pump over time for a residential house located in a hilly area with low outdoor temperature

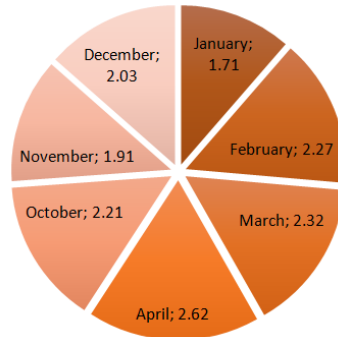


Fig. 6. Thermal power produced for the preparation of domestic hot water

The COP values for DHW range between 1.7 and 2.6, reflecting typical behavior for a heat pump in DHW preparation mode, where the efficiency is lower than in heating. Peak efficiency – April (2.62) suggests ideal conditions: higher outdoor temperature and more stable and efficient operation of the compressor.

Decrease in winter – January (1.71), the lowest COP indicates: very low outdoor temperatures, reduced evaporator efficiency and increased specific electricity consumption.

For the intermediate months (October, November, December) COP values between 1.9–2.2 are normal, but indicate an area for optimization – it can be improved by: intelligent programming (operation during warm periods of the day), lowering the temperature of the stored water (ex: from 55°C to 50°C) and finer adjustments in the thermal controller.

4. Conclusions

The analysis of monthly COP values shows that the heat pump operates efficiently and in a balanced manner both in heating mode and for domestic hot water preparation, with normal seasonal variations dictated by the outdoor air temperature and operating mode.

The COP for heating remains within an optimal range of 2.90–3.54, indicating a correctly sized system, with good integration into the installation.

The COP for DHW is predictably lower, ranging between 1.71 and 2.62, due to the higher preparation temperature and short operating cycles.

The average difference between the heating COP and that for DHW is approximately 1, reflecting the technological particularities of hot water preparation: punctual thermal requirements, standby losses and low efficiency in intermittent mode.

References

- [1] EC.New energy technologies, innovation and clean coal:Mapping and analyzes of the current and future (2020-2030) heating/cooling fuel deployment.European Commission, Brussels, Belgium;2016.

- [2] Cao J, Hong X, Zheng Z, Asim M, Hu M, Wang Q, Pei G, Leung MKH. Performance characteristics of variable conductance loop thermosyphon for energy-efficient building thermal control. *Applied Energy* 2020.
- [3] Sarbu I, Sebarchievici C. General review of ground-source heat pump systems for heating and cooling of buildings. *Energy and Buildings* 2014;70(2):454-467.
- [4] Mc 001-2022, Methodology for calculating the energy performance of buildings, Bucharest
- [5] Maffei L, Ciervo A, Perrotta A, Masullo M, Rosato A. Innovative energy-efficient prefabricated movable 722 buildings for smart/co-working: Performance assessment upon varying building configurations. *Sustainability* 723 2023;15:9581
- [6] I13/2015 with amendments and additions from 2022, Norm for the design, execution and operation of central heating installations
- [7] Sarbu I, Sebarchievici C. *Ground-Source Heat Pumps: Fundamentals, Experiments and Applications*. Elsevier, Oxford, UK; 2016.

Porous geopolymetric material for insulation applications

Material geopolimeric poros pentru aplicații în izolații

Lucian Paunescu¹, Sorin Mircea Axinte^{2,3}, Enikö Volceanov^{4,5}

¹Daily Sourcing & Research SRL
95-97 Calea Grivitei, sector 1, Bucharest 010705, Romania
E-mail: lucianpaunescu16@gmail.com

²National University of Science and Technology „Politehnica”, Faculty of Applied Chemistry and Materials Science
1-7 Gh. Polizu street, sector 1, Bucharest 011016, Romania
E-mail: sorinaxinte@yahoo.com

³Daily Sourcing & Research SRL
95-97 Calea Grivitei, sector 1, Bucharest 010705, Romania
E-mail: sorinaxinte@yahoo.com

⁴National University of Science and Technology „Politehnica”, Faculty of Engineering in Foreign Language
313 Independence Splai, Sector 6, Bucharest 060541, Romania
E-mail: evolceanov@yahoo.com

⁵Metallurgical Research Institute SA
39 Mehadia street, sector 6, Bucharest 060541, Romania
E-mail: evolceanov@yahoo.com

DOI: 10.37789/rjce.2025.16.3.4

Abstract. Cellular fly ash-based geopolymer with suitable physico-thermal and mechanical strength characteristics was prepared using sodium perborate as an expanding agent, palm oil as a surfactant for stabilization of the froth, montmorillonite as a nanoclay for growing the strength of geopolymer, and an alkaline activator composed of potassium hydroxide and silicate solutions. Results showed excellent thermal insulation properties (density between 438-502 kg·m⁻³ and heat conductivity in the range of 0.077-0.103 W·m⁻¹·K⁻¹) as well as adequate compression and flexural strength up to 5.4 and 4.1 MPa respectively, being interesting the excellent strength values obtained at early age only 7 days.

Key words: geopolymer, porosity, insulation, expanding agent, foam.

Rezumat. Geopolimer celular pe bază de cenușă zburătoare cu caracteristici adecvate fizico-termice și de rezistență mecanică a fost preparat utilizând perborat de sodiu ca agent de expansiune, ulei de palmier ca surfactant pentru stabilizarea spumei,

montmorillonit ca o nanoargilă pentru creșterea rezistenței geopolimerului și un activator alcalin compus din soluții de hidroxid și silicat de potasiu. Rezultatele au arătat excelente proprietăți termoizolante (densitate între 438-502 kg·m⁻³ și conductivitate termică în intervalul 0,077-0,103 W·m⁻¹·K⁻¹), precum și rezistență la compresiune și încovoiere până la 5,4 și respectiv, 4,1 MPa, fiind interesante excelentele valori ale rezistențelor obținute timpuriu, după numai 7 zile.

Cuvinte cheie: geopolimer, porozitate, izolație, agent de expansiune, spumă.

1. Introduction

The new type of inorganic cementitious material, named geopolimer, has offered a huge interest for world specialists since the last decade of 20th century and in present. The amorphous alkali alumina-silicate gel, as the major binding phase generated into geopolimer, clearly distinguishes this material for the traditional Portland cement [1]. The geopolimer is mainly composed of calcium silicate hydrate (C-S-H) gel phase [2]. Main abilities of geopolimers are rapid reaching of early strength [3], high bonding resistance [4], fire-resistance [5], high durability [6], and very low carbon footprint [7]. The strength of geopolimers used as thermal or acoustic insulating board coming in direct contact with external factors is exhibited by its high resistance to bacteria, insects or rodents [8].

The pore structure represents an important key in reaching the qualitative performances of geopolimer. Higher porosity can contribute to improving some of its properties such as strength, heat conductivity, permeability depending on the porous structure [9]. Pores have a major role in sorption, capillary condensation, and determine the heat insulation level of the geopolimer [10, 11].

Several pore-generating methods are recently known. Thus, impregnating the polymer matrix with a ceramic suspension, introducing froth-forming additives, direct expanding, the use of templates for porous materials, adding lightweight fillers into a ceramic mix, utilizing additives for suspension generation [12] are possible methods.

Among the methods for producing porous geopolimer, the main procedure is that of direct expanding, which is based on the release of gaseous products by chemically dissolving additives acting as expanding agents in the suspension generated in the alkaline environment.

More expanding agent variants (aluminum powder, zinc powder, and hydrogen peroxide-H₂O₂) were tested in [13]. The use of aluminum powder aimed to determine its effect on the geopolimerization reaction at early age, while the other agents were involved in evaluating the effect of geopolimerization for longer times up to 28 days. The research results showed that the expanding agent type strongly influences the generation and composition of N-A-S-H gel. Aluminum powder proved to be the most suitable for gel formation. The duration of the geopolimerization reaction influences the proportion of fly ash content reduction in the geopolimer compared to the initial one. The mentioned experiment [13] used an extremely low CaO content (0.82 %). 12M NaOH and sodium silicate composed the alkaline activator. Aluminum powder

(0.1 wt. %) contributed to obtaining a porous and interconnected void material. Zinc powder (0.1 wt. %) showed an unfavourable influence on the geopolymerization reaction. H_2O_2 (1 wt. %) showed the best abilities for an excellent control of froth density and pore size.

In the work [14], aluminum powder was used as an expanding agent for preparing porous fly ash-geopolymer. Results indicated that substituting 5 % fly ash with aluminum powder into a mixture characterized by alkali activator/fly ash ratio of 0.35 and $\text{Na}_2\text{SiO}_3/\text{NaOH}$ weight ratio of 2.5 favours making a lowest density-product. Corresponding compression strength dropped to 0.9 MPa.

The production of cellular geopolymer requires proper stabilization of the created porous structure. For this purpose, some authors have used sodium dodecyl sulfate, which has experimentally proven this capacity. Also, sodium, potassium or calcium chlorides (NaCl , KCl , CaCl_2) have been used due to the increase in surface activity and their beneficial influence on the structural stability of the porous matrix, which, however, can decrease the foaming ability of sodium dodecyl sulfate [15].

Metakaolin-based geopolymer was manufactured through the direct expansion procedure and the use of surfactants to protect the formed porous structure [16]. The chosen expanding agent was hydrogen peroxide added to the alumina-silicate mix and the favourable effect of the alkaline environment led to developing the geopolymerization reaction and turning the mixture into a porous geopolymer material.

Porous fly ash-based geopolymer was produced using also hydrogen peroxide [17]. Results revealed that the H_2O_2 content has the ability to control the main properties of the geopolymer (porosity, heat conductivity, and mechanical strength). The porous geopolymer has adequate properties for thermal insulation applications. Heat conductivity lower than $0.107 \text{ W}\cdot\text{m}^{-1}\cdot\text{K}^{-1}$ and density of $0.56 \text{ g}\cdot\text{cm}^{-3}$ were obtained. The study promoted the valorization of alumina-silicate waste, fly ash being such an example.

The French geopolymer inventor J. Davidovits designed and experimentally tested a porous geopolymer using H_2O_2 and sodium perborate (NaH_2BO_4) as expanding agents [18]. The products had density in the range of $0.2\text{-}0.8 \text{ g}\cdot\text{cm}^{-3}$, heat conductivity of around $0.037 \text{ W}\cdot\text{m}^{-1}\cdot\text{K}^{-1}$, and high heat resistance at 1200°C .

Cellular fly ash-based geopolymer using sodium borate monohydrate as a foaming agent was made in [19]. Sodium dodecyl sulfate as a foam-stabilizing agent was also introduced in the mix. The product was examined both at ambient temperature and after keeping at high temperature (1000°C). The density decreased from 1.2 to $0.3 \text{ g}\cdot\text{cm}^{-3}$ depending on the fly ash content. The compression strength increased between $1\text{-}6 \text{ MPa}$. The use of sodium borate allowed to obtain the heat resistance similar to the case of using H_2O_2 .

In another work from the literature [20], results of making cellular geopolymer based on fly ash using sodium perborate as a foaming agent and washing liquid as a surfactant with role in foam stabilizing are presented. The paper was mainly focused on the content effect of the surfactant on heat and mechanical features of the geopolymer samples. By using this surfactant type within the limits of $0.1\text{-}0.5 \text{ wt. \%}$,

porosity became finer, compression strength after 28 days of curing had values in the range of 4.2-4.8 MPa, increasing depending on the surfactant ratio, and heat conductivity was between 0.27-0.32 W·m⁻¹·K⁻¹. Also, the fire-resistant of the cellular geopolymer proved to be excellent.

Different variants of surfactants usable for stabilizing foams formed through cellular geopolymer manufacturing processes are highlighted in the work [21]. It is known that vegetable oils extracted from many plants (olive oil, palm oil, rapeseed oil, sunflower oil, cottonseed oil, corn oil, etc.) can be used in industrial applications such as polymer synthesis. According to [21], palm oil is extracted from the oil palm tree and is used in several applications such as oleochemicals, ingredients of several foods, health products, household products, biodiesel, etc. The fractionated products of palm oil and fatty acids (palm olein and palm stearin) are used as renewable raw materials for polymer making.

The current work brought as main novelties in the making recipe of cellular geopolymer the use of palm oil as a surfactant of vegetable origin [22] with the role of foam stabilizer as well as the combination KOH/K₂SiO₃ representing the composition of the alkaline activator chosen by the authors, unlike the frequently used combination NaOH/Na₂SiO₃. Both sodium and potassium were recommended and claimed by the inventor of the alkaline-geopolymerization process (J. Davidovits), but most researchers in this domain prefer sodium hydroxide and silicate.

2. Methods and materials

Production mechanism of cellular geopolymer requires forming the gas bubbles and then stabilizing the cellular structure. In this experiment, the direct expanding procedure was chosen that is based on the chemical reaction of releasing gaseous products inside the softened mass of raw materials. The experiment has promoted the use of sodium perborate (NaH₂BO₄) as an blowing agent considered more stable and easy handling compared to hydrogen peroxide (H₂O₂) large-scale used by researchers that investigate the cellular geopolymer producing [19, 20]. Avoiding the bubbles coalescence becomes a required operation and is performed through stabilizing the foamed mass. This is possible by diminishing the surface tension of gas bubbles adding the surfactant. In this case, the surfactant was palm oil (of vegetable origin). On the other hand, the use of a nanomaterial from the nanoclay category (montmorillonite) had the role of improving the cellular geopolymer strength. An important stage of the making method flux of cellular fly ash-based geopolymer was mixing in an electrically operated device (with 750 rpm for 12 min) until the paste is formed. Then, the paste was poured into SiC-moulds (made in China) and introduced into a laboratory electrical oven. The thermal process temperature was 65 °C for 24 hours. During the maintaining process at the mentioned temperature, alumina-silicate precursor materials polycondense forming a three-dimensional network of bonded molecules. Gas bubbles remain trapped into this network generating the cellular structure. The curing process for 7 and 28 days respectively, in which specimens were

removed from the moulds, allowed hardening the geopolymer samples before their determining physical, heat, mechanical, and microstructural features.

The fabrication of cellular fly ash-geopolymer required the following materials: class F-fly ash as the basic alumina-silicate raw material, montmorillonite as a nanoclay, sodium perborate as an expanding agent, palm oil as a surfactant, potassium hydroxide solution, and potassium silicate solution.

Class F-fly ash was purchased almost ten years ago from the Romanian Paroseni-Thermal power plant. The material had a particle size below 250 μm and required additional mechanical processing to lower the maximum granulation level below 70 μm . The oxide composition of fly ash included: 54.4 % SiO_2 , 26.5 % Al_2O_3 , 4.3 % Fe_2O_3 , 3.5 % CaO , 2.5 % MgO , 1.5 % TiO_2 , 0.4 % Na_2O , 0.6 % K_2O , and 1.7 % SO_3 .

Montmorillonite ($\text{Al}_2\text{H}_2\text{O}_{12}\text{Si}_4$) a versatile mineral nanomaterial is found in natural bentonite deposits of volcanic origine. Its use advantages in making polymer composite are: high surface area, high adsorption capacity, high contribution as a reinforcing agent growing the mechanical strength of composites. The particle size of this powder is on the order of microns. Its chemical composition contains 43.0 % SiO_2 , 16.8 % Al_2O_3 , 3.6 % Fe_2O_3 , 2.0 % MgO , 0.2 % Na_2O , 0.11 % CaO , 0.19 % Cl , and 34.0 % LOS .

Water-soluble sodium perborate (NaH_2BO_4) was chosen as an expanding agent. Through decomposition, this releases hydrogen perborate (H_2O_2), that decomposes in turn into water vapour and oxygen. Sodium perborate is available in high purity (up to 99 %) on the market, the product being made in China. Its particle size is very fine (under 24 μm). According to the date in the literature [23], the optimal proportion of sodium perborate into the mix is between 0.5-2.0 % of the total alumina-silicate precursor quantity.

Palm oil has been used in its commercially available form as a cooking product. It contains 50 % saturated, 40 % monounsaturated, and 10 % polyunsaturated fatty acids. The level of palmitic acid is high representing about 44 % of fatty acids [24].

Potassium hydroxide solution as a component of the alkaline activator used in this experiment was prepared using commercially available KOH pellets dissolved in distilled water to form an aqueous solution with 10 M molarity.

Potassium silicate solution as the other component of the alkaline activator adopted in this experiment was purchased from the market as an aqueous solution with 38 % concentration.

Methods of investigating physical, thermal, mechanical, and microstructural features of cellular geopolymer samples were generally those known and applied in cases of this kind. Density was measured using Archimedes' principle in conformity with the ASTM C373 standard and ISO 18754:2020 was applied for identifying the porosity. The compression strength of geopolymer specimens was determined with a hydraulically operated compression testing machine with a pressing capacity of 1000 tons-force (about 107 MPa) according to the ASTM C133-97 (2015) standard. Three-point bending tests to measure the flexural strength of samples required a multi-operational apparatus for testing (Instron type) at a crosshead speed of 1.2 $\text{mm}\cdot\text{min}^{-1}$ at

23 °C, in accordance with ASTM D790-17. The water uptake of specimens was determined in accordance with ASTM C373-18 standard by their immersion under water. Microstructural aspect of samples was examined with ASONa 100X Zoom Smartphone Microscope.

In conformity with the above-mentioned materials used in this experiment, four making recipe variants were adopted including the quantities shown in Table 1.

Table 1

Composition of experimental variants

Composition	Variant 1 (kg·m ⁻³)	Variant 2 (kg·m ⁻³)	Variant 3 (kg·m ⁻³)	Variant 4 (kg·m ⁻³)
Class F-fly ash	290	290	290	290
Montmorillonite	2.7	3.4	4.0	4.7
Palm oil	0.4	0.4	0.3	0.2
Sodium perborate	6.1	6.5	6.9	7.3
10M KOH solution	48	48	48	48
K ₂ SiO ₃ solution	114	114	114	114
Distilled water addition	80	80	80	80

According to the data in Table 1, it was exhibited the tendency to increase the porosity of samples and to decrease its fineness by growing the sodium perborate content between 6.1-7.3 kg·m⁻³ and decreasing the amount of palm oil from 0.4 to 0.2 kg·m⁻³. Also, by increasing the amount of montmorillonite from 2.7 to 4.7 kg·m⁻³, it was desired to improve the mechanical strength of the final cellular products. Using the constant K₂SiO₃/KOH ratio of 2.38, it has ensured an optimal ratio between the two components of the alkaline activator capable to initiate and to develop the geopolymerization reaction, thus leading to obtaining the designed geopolymer.

3. Results and discussion

As stated above, determining the compressive and flexural strength was performed both at early age after 7 days and at the end of the curing process after 28 days. Measuring results regarding features of cellular geopolymer specimens are presented in Table 2.

Table 2

Features of cellular geopolymer specimens

Feature	Variant 1	Variant 2	Variant 3	Variant 4
Apparent density (kg·m ⁻³)	502	480	459	438
Porosity (%)	73.5	75.0	77.4	80.9
Heat conductivity (W·m ⁻¹ ·K ⁻¹)	0.103	0.094	0.086	0.077
Compression strength				

Feature	Variant 1	Variant 2	Variant 3	Variant 4
- at early age (7 days)	4.3	4.7	5.0	5.3
- at 28 days	4.6	4.9	5.2	5.4
Flexural strength				
- at early age (7 days)	3.0	3.3	3.6	3.9
- at 28 days	3.1	3.5	3.9	4.1
Water uptake (vol. %)	5.1	6.3	7.4	8.4
Pore size (mm)	0.1-0.3	0.1-0.4	0.2-0.5	0.4-1.0

In general, physico-thermal characteristics of fly ash-based cellular geopolymer were influenced not very much by the increase of the amount of expanding agent (sodium perborate) and by the slight decrease of the already low amount of palm oil as a froth stabilizer. The apparent density decreased in value from $502 \text{ kg}\cdot\text{m}^{-3}$ (variant 1) to $438 \text{ kg}\cdot\text{m}^{-3}$ (variant 4). By default, the porosity increased slightly between 73.5-80.9 %, while the heat conductivity decreased from $0.103 \text{ W}\cdot\text{m}^{-1}\cdot\text{K}^{-1}$ to values very suitable for thermal insulation in construction ($0.077 \text{ W}\cdot\text{m}^{-1}\cdot\text{K}^{-1}$ in the case of variant 4 and also $0.086 \text{ W}\cdot\text{m}^{-1}\cdot\text{K}^{-1}$ in the case of variant 3). In terms of mechanical strength, rapid increase in compression and flexural strength values during the curing process was observed, so that at early age (after only 7 days), values close to the level obtained after 28 days of curing were reached. Thus, the compression strength of the specimen produced in variant 4 was 5.3 MPa after 7 days and 5.4 MPa after 28 days. Also, the flexural strength reached 3.9 MPa after 7 days and 4.1 MPa at the end of the curing process. Water uptake measured after immersion of cellular geopolymer samples under water showed an increase between 5.1-8.4 vol. % between specimens corresponding to variants 1-4, but the level is considered normal for this type of material. Appearances of specimen surfaces corresponding to the four preparing variants are shown in Fig. 1.

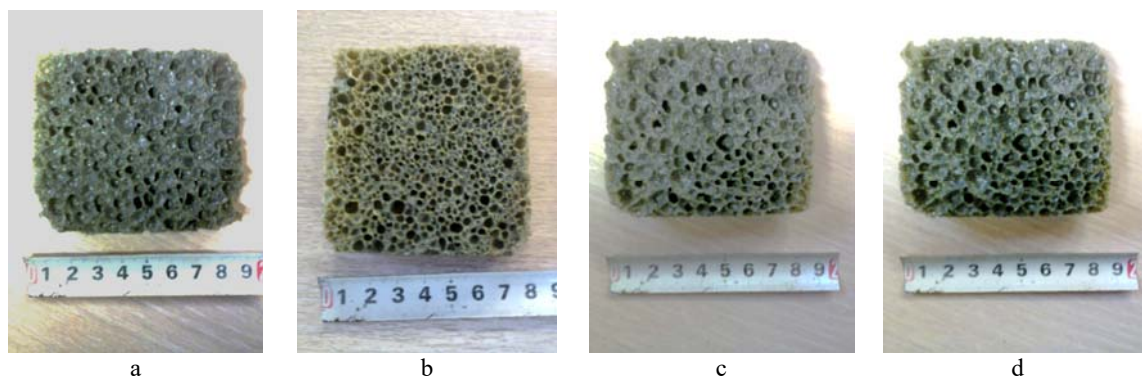


Fig.1. Appearance of specimen surfaces corresponding to the four preparing variants
a – variant 1; b – variant 2; c – variant 3; d – variant 4.

According to Fig. 1, the macrostructural dimension of specimens is increasing from the preparing variant 1 to variant 4. Images of the microstructural configuration of cellular geopolymer are shown in Fig. 2.

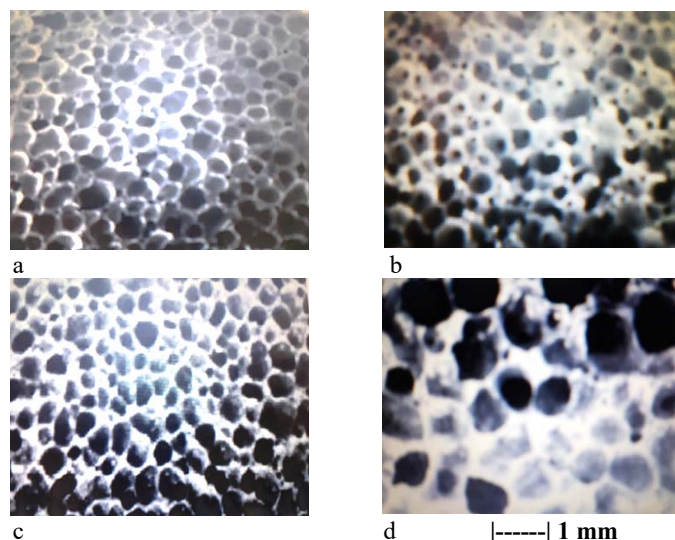


Fig. 2. Microstructural configuration of cellular geopolymer samples
a – variant 1; b – variant 2; c – variant 3; d – variant 4.

According to pictures in Fig. 2, the microstructural homogeneity of specimens is remarkable. Images (a)-(c) are characterized by very close dimensions, the dimensional ranges of the cells being shown in Table 2. These ranges are 0.1-0.3 mm (variant 1), 0.1-0.4 mm (variant 2), and 0.2-0.5 mm (variant 3). In the case of variant 4, the cell dimensions are slightly larger, being within the limits of 0.4-1.0 mm.

The experimental results provided some observations regarding the particularities of the geopolymer foaming process using sodium perborate. The maximum amount of sodium perborate in variant 4 of $7.3 \text{ kg} \cdot \text{m}^{-3}$ represented 2.5 % of the amount of alumina-silicate waste (fly ash). According to the literature [23], the recommended weight proportion of sodium perborate is around 2 %, because higher proportions can affect the foaming effect of this agent. The results obtained in this experiment proved that a proportion of 2.5 % did not affect the expanding process in any way.

The strength increasing of the cellular fly ash-geopolymer was possible through the use of a nanomaterial from nanoclay category (montmorillonite). This procedure constituted one of the original solutions. Also, the choice of palm oil as a less demanding surfactant from the group of vegetable oils is an original decision. Unlike most technical solutions adopted in the world for creating the alkaline activator including sodium hydroxide and silicate, in this experiment the combination of potassium hydroxide and potassium silicate was adopted. The combination of all these material choices, which are usually little used in cellular geopolymer manufacturing processes, allowed to obtain a set of specimens with excellent properties at the level of the most appreciated materials of this type.

4. Conclusions

The work aimed at the production of a cellular fly ash-based geopolymer using sodium perborate as an expanding agent. The experiment involved applying additive material types less frequently used in similar processes such as: montmorillonite as a nanomaterial, palm oil as a surfactant as well as potassium hydroxide and potassium silicate as components of the alkaline activator. Cellular geopolymer specimens had excellent heat insulation properties as well as compression and flexure strength, being applicable as insulation materials in building construction.

References

- [1] S. Chen, S. Ruan, Q. Zeng, Y. Liu, M. Zhang, Y. Tian, D. Yan, „Pore Structure of Geopolymer Materials and its Correlations to Engineering Properties: A Review”, in *Construction and Building Materials*, Elsevier, **vol. 328**, 2022. <https://doi.org/10.1016/j.conbuildmat.2022.127064>
- [2] V.Q. Lee, D.Q. Minh, D.H. Minh, H.T. Nguyen, „The Role of Active Silica and Alumina in Geopolymerization”, in *Ministry of Science and Technology Vietnam*, **vol. 60**, no. 2, 2018, pp. 16-23. [https://doi.org/10.31276/VJSTE.60\(2\).16](https://doi.org/10.31276/VJSTE.60(2).16)
- [3] L.M. Assi, E. Deaver, M.K. El Batanouny, P. Ziehl, „Investigation of Early Compressive Strength on Fly Ash-Based Geopolymer Concrete”, in *Construction and Building Materials*, Elsevier, **vol. 112**, 2016, pp. 807-815. <https://doi.org/10.1016/j.conbuildmat.2016.03.008>
- [4] H.Y. Zhang, V. Kadur, B. Wu, J. Yan, Z.S. Yuan, „Effect of Temperature on Bond Characteristics of Geopolymer Concrete”, in *Construction and Building Materials*, Elsevier, **vol. 163**, 2018, pp. 277-285. <https://doi.org/10.1016/j.conbuildmat.2017.12.043>
- [5] M. Lahoti, K.H. Tan, E-H. Yang, „A Critical Review of Geopolymer Properties for Structural Fire-Resistance Applications”, in *Construction and Building Materials*, Elsevier, **vol. 221**, 2019, pp. 514-526. <https://doi.org/10.1016/j.conbuildmat.2019.06.076>
- [6] L.S. Wong, „Durability Performance of Geopolymer Concrete: A Review”, in *Polymers*, MDPI, **vol. 14**, no. 5, 2022. <https://doi.org/10.3390/polym14050868>
- [7] S.A. Khan, N. Mir, A. Kul, O. Sahin, M. Sahmaran, M. Koç, „Renewable Energy for Carbon Footprint Reduction of Green Geopolymers Materials”, in *Energy Reports*, Elsevier, **vol. 8**, Supplement 13, 2022, pp. 852-858. <https://doi.org/10.1016/j.egyr.2022.08.104>
- [8] T. Kovarik, J. Hajek, „Porous Geopolymers: Processing Routes and Properties”, *IOP Conference Series: Materials Science and Engineering*, IOP Publishing, **vol. 613**, 2019. <https://doi.org/10.1088/1757-99X/613/1/012048>
- [9] Y. Ma, J. Hu, G. Ye, „The Pore Structure and Permeability of Alkali Activated Fly Ash”, in *Fuel*, Elsevier, **vol. 104**, 2013, pp. 771-780. <https://doi.org/10.1016/j.fuel.2012.05.034>
- [10] Z. Zhu, W. Huo, H. Sun, B. Ma, L. Yang, „Correlation between Unconfined Compressive Strength, Sorptivity and Pore Structures for Geopolymer Based on SEM and MIP Measurements”, in *Journal of Building Engineering*, Elsevier, **vol. 67**, 2023. <https://doi.org/10.1016/j.jobbe.2023.106011>
- [11] C. Lu, Z. Zhang, C. Shi, N. Li, D. Jiao, Q. Yuan, „Rheology of Alkali-Activated Materials: A Review”, in *Cement and Concrete Composites*, Elsevier, **vol. 121**, 2021. <https://doi.org/10.1016/j.cemconcomp.2021.104061>
- [12] X. Zhang, C. Bai, Y. Qiao, X. Wang, D. Jia, H. Li, Colombo, P., „Porous Geopolymer Composites: A Review”, in *Composites Part A: Applied Science and Manufacturing*, Elsevier, **vol. 150**, 2021. <https://doi.org/10.1016/j.compositesa.2021.106629>

- [13] G. Moutaoukil, I. Sobrados, S. Alehyen, M. Taibi, „Monitoring the Geopolymerization Reaction of Geopolymer Foams Using Si and Al MAS NMR”, in *Minerals*, MDPI, E. Kearsley (ed.), **vol. 14**, no. 5, 2024. <https://doi.org/10.3390/min14050516>
- [14] J.G. Sanjayan, A. Nazari, L. Chen, G.N. Nguyen, „Physical and Mechanical Properties of Lightweight Aerated Geopolymer”, in *Construction and Building Materials*, Elsevier, **vol. 79**, 2015, pp. 236-244. <https://doi.org/10.1016/j.conbuildmat.2015.01.043>
- [15] N. Jiang, X. Yu, Y. Sheng, R. Zong, C. Li, S. Lu, „Role of salts in performance of foam stabilized with sodium dodecyl sulfate”, in *Chemical Engineering Science*, Elsevier, **vol. 216**, 2020. <https://doi.org/10.1016/j.ces.2020.115474>
- [16] Svetlana Petlitckaia, A. Poulesquen, „Design and Lightweight Metakaolin Based Geopolymer Foamed with Hydrogen Peroxide”, in *Ceramics International*, Elsevier, **vol. 45**, no. 1, 2019, pp. 1322-1330. <https://doi.org/10.1016/j.ceramint.2018.10.021>
- [17] R.M. Movais, L.H. Burubberi, G. Ascensão, M.P. Scabra, J.A. Labrincha, „Porous Biomass Fly Ash-Based Geopolymer with Tailored Thermal Conductivity”, in *Journal of Cleaner Production*, Elsevier, **vol. 119**, 2016, pp. 99-107. <https://doi.org/10.1016/j.jclepro.2016.01.083>
- [18] J. Davidovits, „Geopolymer Chemistry and Applications”, 5th edition, Geopolymer Institute Publishing, J. Davidovits (ed.), Saint Quentin, France, 2020, ISBN 9782954453118.
- [19] Lidija Korat, Vilma Ducman, „Characterization of Fly Ash Alkali Activated Foams Obtained Using Sodium Perborate Monohydrate as a Foaming Agent at Room and Elevated Temperatures”, in *Frontiers in Materials*, Section of Structural Materials, Jackueline A. Johnson (ed.), **vol. 7**, 2020. <https://doi.org/10.3389/fmats.2020.572347>
- [20] V. Phavangkham, S. Wattanasiriwech, T. Cheng, D. Wattanasiriwech, „Effects of Surfactant on Thermo-Mechanical Behavior of Geopolymer Foam Paste Made with Sodium Perborate Foaming Agent”, in *Construction and Building Materials*, Elsevier, **vol. 243**, 2020. <https://doi.org/10.1016/j.conbuildmat.2020.118282>
- [21] E. Stavila, F. Yuliati, A. Adharis, J.A. Laksmono, M. Iqbal, „Recent Advances in Synthesis of Polymers Based on Palm Oil and its Fatty Acids”, in *Royal Society of Chemistry Advances*, **vol. 13**, 2023, pp. 14747-14775. <https://doi.org/10.1039/D3RAO.1913>
- [22] V. Gibon, „Palm Oil and Palm Kernel Oil Refining and Fractionation Technology”, in *Palm Oil: Production, Processing, Characterization, and Uses*, American Oil Chemists Society Press, O.M. Lai, C.P. Tan, C.C. Akoh (eds.), 2012, pp. 329-375. https://www.researchgate.net/publication/291309283_Palm_Oil_Production_Processing_Characterization_and_Uses
- [23] S. Wattanarach, S. Sapothina, P. Thavorniti, „Preparation and properties of metakaolin-based porous geopolymer foamed with sodium perborate”, in *Journal of Asian Ceramic Society*, The Ceramic Society of Japan, **vol. 10**, no. 3, 2022, pp. 567-574. <https://doi.org/10.1080/21870764.2022.2088755>
- [24] A.A. Abd El-Khair, A.A. Abdallah, A.H. Ateteallah, N.A. Hassan, „Physical and Chemical Properties of Palm Oil and its Derivatives Compared to Butter Oil”, in *Journal of Sohag Agriscience*, **vol. 2019**, no. 1, 2019, pp. 73-84, ISSN: 2357-0725. <https://jsasblog.wordpress.com>

Considerations regarding the operational reliability of equipment in the structure of water supply systems

Considerații privind fiabilitatea operațională a echipamentelor din structura sistemelor de alimentare cu apă

Gheorghe – Constantin Ionescu¹, George – Lucian Ionescu²,

Dragoș-Vasile Ille³

¹ University of Oradea

4 Delavrancea Str., Oradea, Bihor, Romania

E-mail: gheionescu@gmail.com

² University of Oradea

4 Delavrancea Str., Oradea, Bihor, Romania

E-mail: lucian.ionescu1985@yahoo.com

³ University of Oradea

4 Delavrancea Str., Oradea, Bihor, Romania

PhD student, Energy Engineering Field

E-mail: illedragos@yahoo.com

DOI: 10.37789/rjce.2025.16.3.5

Abstract. *Regardless of the precision or complexity of the reliability analysis method used, the quantitative assessment of the reliability of a system requires knowledge of the values of the reliability indicators of the component elements. Obtaining realistic results for the reliability of the system is conditioned by the credibility of the values of the reliability indicators of the elements. Information on the reliability of the elements is useful both for beneficiaries (for the purpose of optimizing maintenance) and for manufacturers (for the purpose of applying corrections in design and manufacturing).*

Key words: water supply, systems, operational reliability

1. Introduction

To estimate the reliability indicators of the elements, two analysis methods are used, namely: Experimental Reliability and Operational Reliability.

Operational reliability, corresponding to the situation in which the reliability indicators are determined based on observations made in real operating conditions of the equipment. As research has shown, there are a number of equipment for which

reliability tests in laboratory conditions are uneconomical and the only source of information on reliability remains monitoring in operation [5].

The evaluation variant of reliability indicators is clearly advantageous from an economic point of view, in relation to experimental reliability, requiring minimal expenses for recording and processing statistical data. The disadvantage of this analysis method is the long duration of observations and the difficulties encountered in ensuring a minimum required number of observed elements.

Studies of operational reliability of equipment in the structure of water supply systems are indispensable to obtain statistical data of adequate volume and credibility, on the basis of which to establish the values of reliability indicators and an optimal maintenance policy. Unfortunately, these studies in the field of water supplies are at a pioneering stage, which is why they must be based on incident sheets and event records existing at the level of water pumping stations (key point in a water supply installation) and on analyses performed on water samples taken from different treatment phases.

The studies in question mainly highlight the following aspects:

- the number of incidents at the pumping station level and their distribution across subsystems (pump drive motors, pumps themselves);
- the cost of corrective maintenance work carried out following incidents;
- the energy unavailable as a result of incidents and the distribution across subsystems;
- the causes of incidents and damaged elements

The observations that can be made regarding these studies are the following:

- they are not sufficiently detailed and in-depth, as they are limited to a part of the subsystems of a water supply installation;
- they prove useful, as they provide a first impression of the condition of the equipment, its operating behavior and its maintenance management;
- the data obtained are not processed in all aspects and, as a result, not all possible information is exploited;
- despite all efforts made towards the correct declaration of incidents and their parameters, there may still be errors.

Through this study, we aimed to overcome these issues, on the one hand by monitoring the equipment more closely and in more detail, and on the other hand, by processing the obtained data more extensively and at an adequate scientific level, in order to obtain more useful information in the operation of hydraulic installations within the water supply systems of urban centers [4], [5].

Based on the statistical data obtained from monitoring the operation of the equipment, three random variables can be studied, namely:

- the good operation time (TBF), representing the operation time between two successive failures;

- the corrective maintenance time (TMC), representing the failure time;
- the annual number of failures (NC).

The first two random variables are continuous, and the third is discrete.

It is well known that performing operational reliability studies for a sample (lot) from a population of a product involves assuming a risk [4], [5]. When performing operational reliability studies, in order to ensure the premises of risk minimization, when the research results extend from the lot level to the population level, it is necessary to ensure compatible working hypotheses in the two cases. Given this objective, an operational reliability study with a certain degree of scientific rigor involves indicating the technical characteristics and factors that can influence reliability indicators, such as: the level of long-term demands, the level and frequency of overloads, environmental factors, maintenance conditions, etc. Without performing a complete characterization under the aforementioned aspects, I will specify, within the case study, most of the influencing factors.

The results obtained for the water supply system of Oradea municipality are presented synthetically in this chapter, the working methodology being valid for any other water supply system of urban centers.

2. Presentation of the water supply system of the Oradea Municipality

The drinking water supply of Oradea is provided by 5 pumping stations (SPO) located on both banks of the Crișul Repede River in the NE part of the city [6], [12].

For this purpose, both groundwater, captured from the groundwater table using drains, and surface water, captured from the Crișul Repede River, are used.

Table 1

Pumping station structure					
Station	Group no. x pump type	Group characteristics			Normal operating configuration
		Q [mc/h]	H [m]	P _i [kW]	
SP 1	6 x KSB	435	55	145	4 + 2
SP 2	1 x SIGMA	500	59	160	5 + 1 (NDS)
	2 x GAZ	300	50	145	
	3 x NDS	400	53	160	
SP 3	3 x 8 NDS	350	80	110	2 + 1
SP 4	6 x 12 NDS	300	50	250	5 + 1
	3 x 8 NDS	400	83	160	2 + 1
SP 5	3 x BRATEȘ 2200 (TR. I)	1200	12	90	2 + 1
	3 x BRATEȘ 350 (TR. II)	1400	11	75	2 + 1
	5 X 12 NDS (TR. III)	900	60	200	4 + 1

On the right bank, surface water is captured using two Φ 1000 mm pipes. After passing through two horizontal decaners, the water enters the 13 basins with the role of enriching the underground phreatic layer, located parallel (8 +5) to the Criş riverbed. Between the two rows of basins and Criş, 2 drains are located for capturing groundwater, with the purpose of supplying the pump station 1 (S.P. 1). To the extent that this quantity of water does not satisfy the need for S.P. 1, surface water from the enrichment basins is also used, filtered using the 10 slow filters. The filters are fed directly from the raw water captured, through a Φ 600 mm² pipe, when the turbidity is reduced in the Criş water and respectively from the last enrichment basin if the water in Criş has high turbidity.

Table 2

Global energy indicators of SPO (values in one year)

	SP 1	SP2	SP3	SP4	SP5	Total
Total pumped water	11.039.600	5.134.120	4.272.020	17.050.700	17.724.300	55.221.500
Surface water	10.847.800	5134.120	1.071.200	17.050.700	-	34.103.700
Groundwater	191.800	-	3.201.700	-	17.724.300	21.117.800
Installed power in pumping units (kW)	882	670	330	1850	1870	5602
Installed power in exploitation technology (kW)	950	680	330	2012	2340	6300
Electricity consumption (kWh)	4.243.830	1.690.770	1.022.220	4.647.620	4.106.460	17.470.020
Specific consumption kWh/m ³	0,384	0,329	0,445	0,272	0,281	0,316

Pumping station no. 3 (SP 3), is also located on the right bank and pumps water into the compensation tanks (total capacity 22012 mc).

Pumping station no. 2 (S.P. 2) is located on the right bank and pumps groundwater into the network on the left bank. The groundwater supply to the drain is supplied through two enrichment basins.

On the left bank, the captured water reaches gravity through two pipes (Φ 1200 mm - Φ 1000 mm) in the 8 enrichment basins located perpendicular to the Criş riverbed. Among these basins are located the secondary drains that supply the main drain, located between the Criş riverbed and the 8 basins, ensuring the entire water needed for S.P. 4.

S.P. 5 exclusively uses surface water decanted with the two radial decaners and filtered through the 8 rapid filters within the plant.

The S.P.O. structure was presented in table 4.1., and the values of significant indicators regarding the operation of the stations, in one year (2020), were mentioned in table 4.2.

3. Special features of pumping stations

In the exploitation activity, the following must be followed:

- periodic verification of the degree of clogging by reading the level difference between the raw water and the filtered water with a gauge;
- the captured flows must be constant (by draining);
- the operation of the decanters in parallel or in series, depending on the degree of turbidity, respectively on their clogging level;
- the correct operation of the Parshall flowmeter;
- the evacuation of deposits must be done periodically depending on the raw water load - once every 60 days;
- the inspection and maintenance of the maneuvering seals;
- washing the filter in order to form the biological membrane;
- emptying the decanter in order to wash the concrete foundation;
- maintaining a constant water level on the slow filters by adjusting the supply valve;
- emptying the clogged filter, respectively cleaning it by removing the 2-3 cm thick layer from the sand surface;
- disinfection of the sand with a solution of lime chloride in an amount of 0.5 kg/m²;
- periodic reading of the flows on the two trapezoidal flowmeters.

The defense of pumping stations in different phases and defense hypotheses is carried out according to the defense plan, as follows:

a) upon reaching the attention level communicated by the County Flood Defense Commission, the observation-alarming and surveillance activity of the defense dikes will be organized, checking the existence of the materials necessary for the interventions in stock;

b) upon reaching the flood level communicated by the County Flood Defense Commission, the local defense of the basic objectives will be organized with the help of intervention teams and equipment, as follows:

- the dams at the raw water intakes will be closed and strengthened;
- the materials stored in the area of the basic objectives and the dangerous ones will be transported;
- the defense of the pumping stations and slow filters will be organized by executing local dams using our own materials and means;
- small infiltrations through the defense dikes will be eliminated;
- additional jute bags and sand stocks will be provided to raise the defense dikes and drains to the danger level;
- the County Flood Defense Commission will be requested to allocate additional forces, materials and equipment, the entire capable workforce and its own equipment will be mobilized and organized for interventions, in the event of reaching the danger level or the appearance of breaches in the defense dikes.

c) upon reaching the danger level or the appearance of large local erosions in the defense dike, with the support of additional forces and means allocated by the County Flood Defense Commission, the following will be done:

- evacuation of the coagulant stock;
- raising the dikes with sandbags and strengthening the eroded areas;
- announcement by the County Flood Defense Commission of the units that are located in the area.

If the intervention works cannot prevent flooding of the water plant territory, the pumping stations will be de-energized, the electric pumps and chlorine cylinders will be dismantled and evacuated until the temporary local dams fail [7], [9].

The operation of the pumping stations depending on the seasons of the year is as follows:

- During periods of average flow

They operate in normal mode: 4 groups at S.P. 1, 2 groups at S.P. 3, 2 groups at S.P. 2, 3 groups at S.P. 4, 1 or 2 groups at S.P. 5, depending on the pressure in the network. The intakes are opened depending on the water level in the enrichment basins.

- During periods of high water

The water in Crișul Repede being dirty (high turbidity) the intakes are closed to avoid clogging of the basins. At S.P. 5, where surface water is used, the dose of aluminum sulfate is increased to accelerate the decantation of solid suspensions from the water.

- During periods of freezing (ice rinks, ice floes, ice bridge)

Shifts of 2 people are formed, who will permanently supervise the intakes and will act with specific tools to avoid freezing in the intake area and clogging of the pipes.

- During periods of low water (drought)

The intakes will be permanently open. The flow rate of pumped water will be reduced depending on the water level in the caisson.

The functional schemes of pumping stations no. 1 and 3 are presented in fig.4.9. and 4.10.

Since the structure of the stations S.P. 1 and S.P. 3 is more homogeneous, the monitoring of the operating behavior of these S.P. is more rigorous. Since the specific electricity consumption is higher, the operational reliability study focused on these stations. The conclusions of the study are valid, for the most part, for the other SPs.

Considerations regarding the operational reliability of equipment in the structure of water supply systems

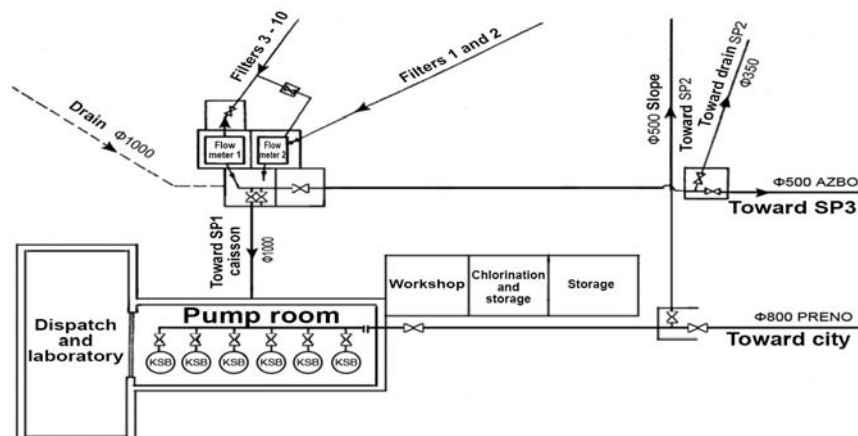


Fig. 3.1. – Functional diagram of Pumping Station no. 1 – ORADEA

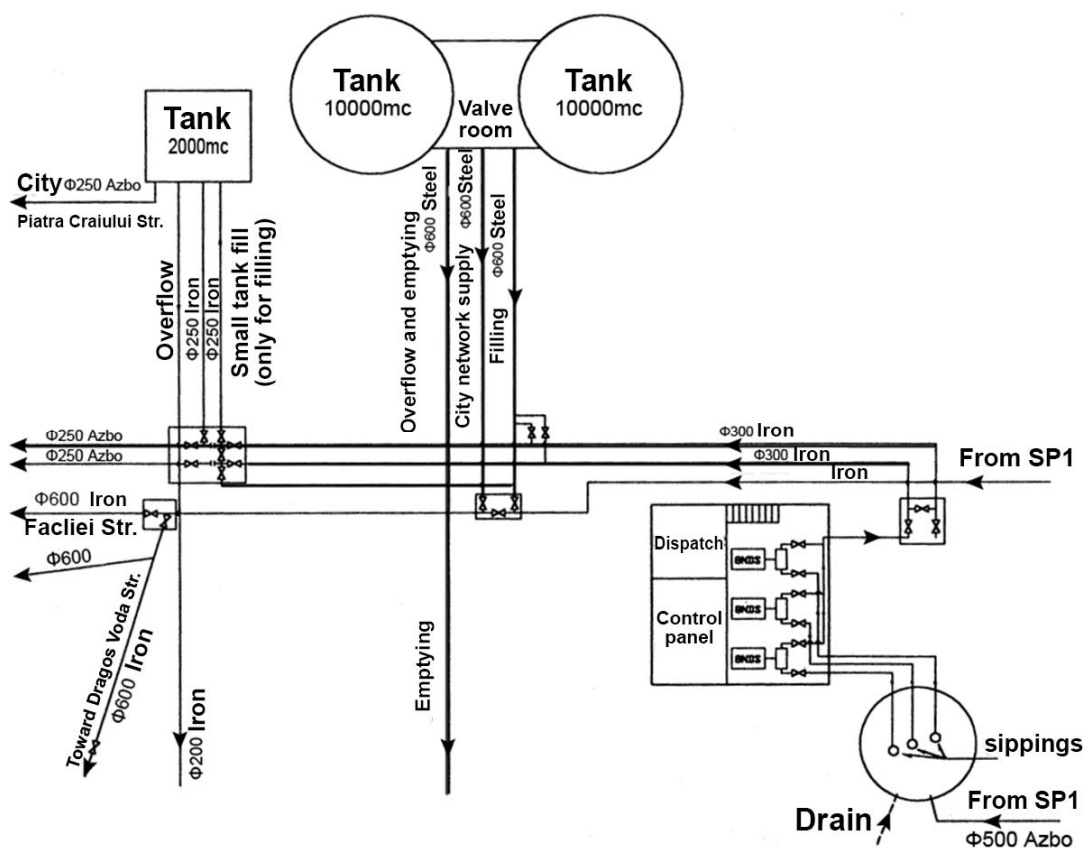


Fig. 3.2. – Functional diagram of Pumping Station no. 3 – ORADEA

To illustrate the load level of the SP, figures 4.11 and 4.12 show the monthly load curves.

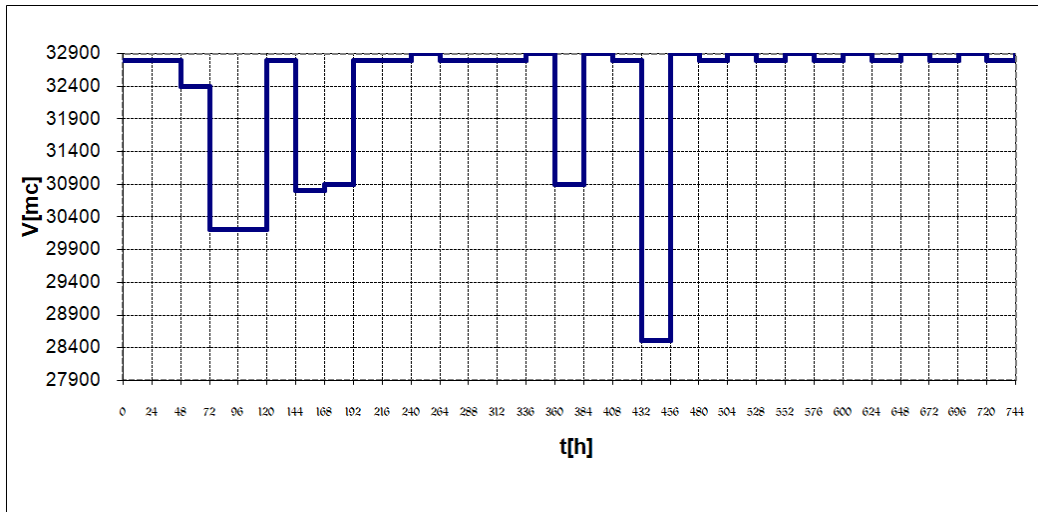


Fig. 3.3. - Monthly load curve of SP1 (January 2012)

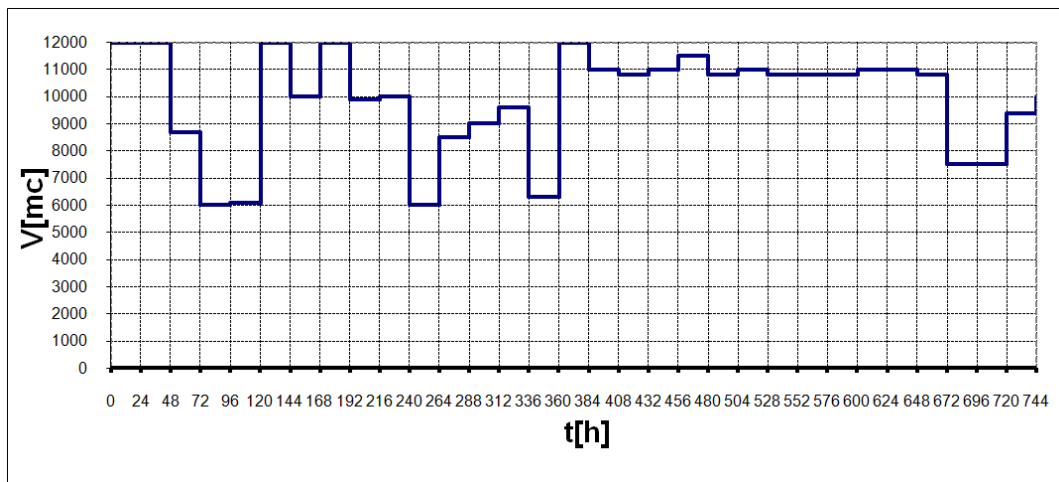


Fig. 3.4. - Monthly load curve of SP3 (January 2012)

4. Conclusions

The operational reliability (FO) study of SP1 and SP3 is extended over a period $T = 10.5$ years, comprising data collected in the interval $[01.01.2011 \div 30.06.2021]$. Some elements that characterize the level of demand of the equipment in the structure of S.P. 1 and S.P. 2 are:

SP1:

- average annual operating duration of a group: 5840 hours / year;
 - average load degree: 78% of the nominal value;
 - number of maneuvers: 40 maneuvers / year;
 - characterization of the working environment: average temperature 220C;
- quality of pumped water: potable; humid environment.

SP3:

- average annual operating duration of a group: 5840 hours / year;
- average load degree: 60% of the nominal value;
- number of maneuvers: 20 maneuvers / year;
- characterization of the working environment: average temperature 220C, quality of pumped water: potable; humid environment.

Since the equipment in the structure of the two SPs has different characteristics, the FO study was carried out separately for each station. The tracking of the equipment in the SPO structure was carried out based on the operation and intervention registers, which can be equated with a FO study typical for “truncated tests with replacement” [12].

The random variables (VA) of interest for the FO study of the S.P. are: “good operating time” (TBF) and “corrective maintenance time” (TMC). The statistical data taken from the registers allowed us to establish – with reference to the groups – the series of values for the two VAs and highlight the failure modes and the share of component failures in the failure of the groups. Detailed statistical data are presented in [152], where the variational series of the values of the two VAs is also presented. The volume of the selection ($r = 437 \rightarrow$ S.P. 1 and $r = 216 \rightarrow$ S.P. 3) is large enough to admit that the results obtained from the study have sufficient credibility. Based on the models, algorithm and FRVA program, commonly applied to the processing of statistical data [7], [9], these data were processed, testing three theoretical distributions (exponential, Weibull and normal) to establish the best estimate of the empirical distribution.

The results are presented in table 4.1.

Table 4.1

Pumping station structure					
Station	Distribution function	TBF (F)		TMC (M)	
		Parameter values	D_{\max}	Parameter values	D_{\max}
S.P. 1 $r = 437$	Exponential	$\lambda = 3,33 \cdot 10^{-5} \text{ h}^{-1}$	0,083	$\mu = 0,738$	0,522
	Weibull	$\eta = 3,29 \cdot 10^4 \text{ h}$ $\beta = 0,83$	0,08	$\eta_M = 1,74 \text{ h}$ $\beta_M = 1,42$	0,508
	Normal	$m = 3,17 \cdot 10^4 \text{ h}$ $\sigma = 2,76 \cdot 10^4 \text{ h}$	0,142	$m_M = 1,34 \text{ h}$ $\sigma = 1,87 \text{ h}$	0,443
S.P. 3 $r = 216$	Exponential	$\lambda = 3,48 \cdot 10^{-5} \text{ h}^{-1}$	0,095	$\mu = 0,69$	0,326
	Weibull	$\eta = 3,08 \cdot 10^4 \text{ h}$ $\beta = 0,83$	0,097	$\eta_M = 1,48 \text{ h}$ $\beta_M = 1,54$	0,407
	Normal	$m = 3,01 \cdot 10^4 \text{ h}$ $\sigma = 2,79 \cdot 10^4 \text{ h}$	0,127	$m_M = 1,34 \text{ h}$ $\sigma = 1,85 \text{ h}$	0,4

The FD expressions and the meaning of the parameters are as indicated in [12].

Therefore, the recommended distribution function expressions for the groups of the two pumping stations, with reference to the two random variables, are:

- Pumping station 1 (SP 1)

- TBF random variable:

$$R(t) = e^{-3,33 \cdot 10^{-5} t} \quad (1)$$

- TMC random variable:

$$M(t) = 1 - e^{-\left(\frac{t}{1,74}\right)^{1,42}} \quad (2)$$

- Pumping station 2 (SP 2)

- Random variable TBF:

$$R(t) = e^{-3,48 \cdot 10^{-5} t} \quad (3)$$

- TMC random variable:

$$M(t) = 1 - e^{-0,69 t} \quad (4)$$

Statistical data on events occurring at pumping stations 1 and 3 are presented in Annex 1. Based on these tables, failure rates for groups, respectively pumps, were calculated and represented. The absolute and percentage values of the variable $v(T)$, for groups and their components are given in table 4.2., and table 4.3. presents the contribution of the components in the structure of the electric motors driving the pumps, to their failure.

Table 4.2

**Absolute and percentage values of the variable $v(T)$,
with reference to the analyzed SP**

SP1	Trimmings		Motor		Valve		Flap			
	No. of defetcts	%	No. of defetcts	%	No. of defetcts	%	No. of defetcts	%		
GR I	64	72,72	20	22,72	2	2,27	2	2,27		
GR II	54	69,23	21	26,92	1	1,28	2	2,56		
GR III	50	68,49	20	27,39	1	1,36	2	2,73		
GR IV	43	69,35	16	25,80	2	3,22	1	1,61		
GR V	58	76,31	16	21,05	1	1,31	1	1,31		
GR VI	54	72	17	22,66	3	4	1	1,33		
S.P. 1	323	71,46	110	24,33	10	2,21	9	1,99		
SP3	Trimmings		Motor		Valve		Flap		Pump grease	
	No. of defetcts	%	No. of defetcts	%	No. of defetcts	%	No. of defetcts	%	No. of defetcts	%
GR I	35	54,68	10	18,75	2	1,56	1	1,56	15	23,43
GR II	47	59,49	10	15,19	2	1,26	1	1,26	18	22,78
GR III	40	55,55	7	15,27	4	1,38	1	1,38	19	26,38
S.P. 3	122	56,74	35	16,27	3	1,39	3	1,39	52	24,18

Table 4.3

**Absolute and weighted values of the variable $v(T)$,
with reference to the engines in the SP structure analyzed**

<i>Motor S.P. 1</i>														
	Bushings		Bearings		Shaft		Rotor		Stator		Coil Breakdown		Oil change	
	No. def.	%	No. def.	%	No. def.	%	No. def.	%	No. def.	%	No. def.	%	No. def.	%
GR I	1	5	2	10	1	5	2	10	2	10	1	5	11	55
GR II	3	14,28	2	9,52	2	9,52	1	4,76	1	4,76	1	4,76	11	52,38
GR III	1	5	2	10	1	5	2	10	2	10	1	5	11	55
GR IV	-	-	2	13	1	6,25	1	6,25	1	6,25	1	6,25	10	62,5
GR V	-	-	2	13	1	6,25	1	6,25	1	6,25	1	6,25	10	62,5
GR VI	-	-	2	11,76	1	5,88	1	5,88	1	5,88	1	5,88	11	64,7
S.P. 1	5	4,54	12	10,90	7	6,36	8	7,27	8	7,27	6	5,45	64	58,18
<i>Motor S.P. 3</i>														
	Bushings		Bearings		Shaft		Rotor		Stator		Coil Breakdown		Coupling replacement	
	No. def.	%	No. def.	%	No. def.	%	No. def.	%	No. def.	%	No. def.	%	No. def.	%
GR I	1	8,33	2	16,66	4	33,33	2	16,66	2	16,6	1	8,33	-	-
GR II	2	16,66	2	16,66	2	16,66	2	16,66	1	8,33	2	16,66	1	8,33
GR III	1	9,09	4	36,36	2	18,18	1	9,09	1	9,09	2	18,18	-	-
S.P. 3	4	11,42	8	22,85	8	22,85	5	14,28	4	11,42	5	14,28	1	2,85

References

1. BÎRSAN, E., IGNAT, C. – O modalitate de realizare a controlului rețelelor de distribuție a apei. Conferința de Instalații pentru Construcții, Iași, 2008.
2. IONESCU, G. L. – The optimization of energy consumption in water supply systems – Conferința Națională (cu participare internațională) „TEHNOLOGII MODERNE PENTRU MILENIUL III” – Analele Universității din Oradea – Fascicula Construcții și instalații hidroedilitare, 2009.
3. IONESCU, GH. C. – Contribuții la studiul și optimizarea fiabilității instalațiilor hidraulice din cadrul sistemelor de alimentare cu apă a centrelor urbane – Teză de doctorat, Universitatea din Oradea, martie, 2003.
4. IONESCU, GH. C. – Creșterea siguranței funcționării sistemelor de alimentare cu apă – Conferința Națională (cu participare internațională) „TEHNOLOGII MODERNE PENTRU MILENIUL III” – Analele Universității din Oradea – Fascicula Construcții și instalații hidroedilitare, 2007.
4. IONESCU, GH. C., IONESCU, G. L. – Sisteme de Alimentare cu apă. Editura Matrix Rom, București, 2010.
5. IONESCU, GH. C. – Optimizarea fiabilității instalațiilor hidraulice din cadrul sistemelor de alimentare cu apă – Editura Matrix Rom, București, 2004.
6. IONESCU, GH. C.; GLIGOR, E. – Probleme de fiabilitate generală a sistemelor de alimentare cu apă – Conferința Națională (cu participare internațională) „TEHNOLOGII MODERNE PENTRU MILENIUL III” – Analele Universității din Oradea – Fascicula Construcții și instalații hidroedilitare, 2008.
7. IONESCU, GH. C.; IONESCU, DANIELA-SMARANDA – Increasing the efficiency of water supply systems by optimizing the electrical energy consumption - The 19th DAAAM

- INTERNATIONAL SYMPOSIUM “Intelligent Manufacturing & Automation” 22-25th, October 2008 – Trnava, SLOVAKIA-ISI.
8. IONESCU, GH. C.; IONESCU, DANIELA-SMARANDA – Phisycal and Chemical Techniques for Removing Nitrogen and Phosphorus from Residual Waters – International Symposia Risk Factors for Environment and Food Safety & Natural Resources and Sustainable Development, Faculty of Environmental Protection, Nov. 6-7, Oradea, 2009.
 9. IONESCU, GH. C.; IONESCU, DANIELA-SMARANDA – Advanced Water Treatment Technologies – International Symposia Risk Factors for Environment and Food Safety & Natural Resources and Sustainable Development, Faculty of Environmental Protection, Nov. 6-7, Oradea, 2009.
 10. SOARE DAVID (Bursașiu Arghir) – Making good use frequency converters for increasing the efficiency of water supply systems – Lucrare prezentată la Conferința Națională (cu participare internațională) „TEHNOLOGII MODERNE PENTRU MILENIUL III” – Oradea, 2011.
 11. KOVACS TIBERIU, GH. CONSTANTIN IONESCU – Optimization of electrical energy consumption in water supply systems - 19th edition of The National Tehnical-Scientific Conference „Modern Technologies for the 3rd Millenium, April 5-6, 2020, Oradea, România <http://www.arhiconoradea.ro/Conferinta/HOME.htm>
ISBN 978-88-7587-724-8 Published: 2020 ISI PROCEEDINGS
 12. SZABO STEFAN, KOVACS TIBERIU, IONESCU GEORGE – LUCIAN, CZISZTER K. ISTVAN – ANDRAS, IONESCU DANIELA – SMARANDA, SĂRĂCUȚ-ARDELEAN ANDREI-FLORIN - Comparative studies and research on optimizing electric consumption of water supply systems - JOURNAL OF APPLIED ENGINEERING SCIENCES, VOL. 12(25)1-2022 B+ by the same C.N.C.S.I.S. Our journal is accepted in five International Databases (IDB), (WOS) Web of Science
(see: <http://mjl.clarivate.com/cgi-bin/jrnlst/jlresults.cgi?PC=MASTER&Full=Journal%20of%20Applied%20Engineering%20Sciences>)
 13. CZISZTER K. ISTVAN – ANDRAS, IONESCU GHEORGHE – CONSTANTIN, SĂRĂCUȚ-ARDELEAN ANDREI-FLORIN, SZABO STEFAN, KOVACS TIBERIU, IONESCU GEORGE – LUCIAN - Comparative studies and research on energy optimization of non-residential buildings - JOURNAL OF APPLIED ENGINEERING SCIENCES, VOL. 1-2022 B+ by the same C.N.C.S.I.S. Our journal is accepted in five International Databases (IDB), (WOS) Web of Science (see: <http://mjl.clarivate.com/cgi-bin/jrnlst/jlresults.cgi?PC=MASTER&Full=Journal%20of%20Applied%20Engineering%20Sciences>)
 14. EUROPEAN PARLIAMENT - Energy Efficiency in Buildings.
http://ec.europa.eu/energy/efficiency/buildings/buildings_en.htm, vizualizat 2021/07/03, 10:00
 15. X X X – Revista "Instalații pentru construcții" – colecție.
 16. X X X – Revista "Instalatorul" – colecție.
 17. X X X – Revista "Detectivii apei pierdute" – colecție 2012-2021.
 18. X X X – SR 1343-1 iunie 2006.
 19. X X X – Legea 311- 28 iunie 2004.
 20. X X X – Standarde și normative în vigoare.

A general review on night ventilation systems used to reduce energy consumption in buildings

Recenzie generală a sistemelor de ventilare pe timp de noapte utilizate pentru reducerea consumului de energie în clădiri

Marius Adam¹, Adriana Tokar¹, Alexandru Dorca¹, Dănuț Tokar¹
Alexandru Filipovici¹

¹ Universitatea Politehnica Timișoara.
Piața Victoriei 2, Timișoara 300006

E-mail: marius.adam@upt.ro, adriana.tokar@upt.ro, alexandru.dorca@upt.ro, danut.tokar@upt.ro,
alexandru.filipovici@upt.ro

DOI: 10.37789/rjce.2025.16.3.6

Abstract. The night ventilation process is carried out in order to reduce the energy consumption required to cool the space during the day. This process proposes a sustainable approach to generate a comfortable indoor environment, with relatively low energy consumption. Following an extensive study documenting existing research in the field, the paper aims to describe the elements that influence night ventilation and the impact of these elements on energy efficiency and thermal comfort.

Key words: night ventilation, energy efficiency, thermal mass, air changes per hour, climate zones, thermal comfort

1. Introducere

Sistemele de ventilare de noapte au primit o atenție sporită în ultimii ani datorită potențialului lor de economisire a energiei și a protecției mediului atunci când sunt utilizate în răcire pasivă sau semi-pasivă, în loc de răcire activă [1]. Supraîncălzirea este o problemă în continuă creștere în clădiri, introduce sarcini mari de răcire în clădiri, ceea ce reprezintă o provocare serioasă în faza de proiectare și în timpul funcționării acestora [2].

Răcirea cu sisteme de ventilare pe timp de noapte a fost studiată pe larg, pentru diferite tipuri de clădiri și de condiții climatice [3], unul dintre primii cercetători în acest domeniu este Givovi, care a subliniat că răcirea masei structurale a unei clădiri pe timp de noapte se realizează prin convecție din interior. În ultimele decenii, un număr semnificativ de studii au demonstrat aplicarea ventilației nocturne în clădiri rezidențiale [4], supermarketuri [5], clădiri de biblioteci [6] și clădiri de birouri [7, 8].

La mijlocul anilor 1990, Kolokotroni are mai multe studii privind ventilarea nocturnă, în care face referire la regimul de neocupare a clădirilor pe timpul nopții [9],

prin urmare, nivelul de zgomot și curenții de aer nu influențează dimensionarea sistemelor de ventilare. Inerția termică a materialelor de construcție și masei termică au o influență ridicată asupra eficienței de răcire a ventilației nocturne.

Ultimele cercetări arată o preocupare tot mai mare pentru sistemele de ventilare de noapte în contextul creșterii temperaturilor medii de vară sub influența schimbărilor climatice [10; 11]. O creștere cu până la 275% a cererii de energie de răcire a clădirilor comerciale este prevăzută în 2050, comparativ cu utilizarea actuală [12].

Chiar dacă ventilarea mecanică pe timp de noapte ar putea duce la o economisire a energiei electrice de la sursa de răcire de până la 0,9 kWh/(m²•an) la clima actuală extremă, ar putea reduce nesemnificativ consumul total de energie electrică pentru răcirea spațiului (până la 2 %) pentru toate climatele viitoare anticipate [13].

2. Elementele care influențează ventilarea de noapte

2.1 Coeficientul de convecție interior la transfer termic (CCITT)

Determinarea valorii lui CCITT este foarte importantă pentru evaluarea cu precizie a performanței sistemului de ventilare de noapte. În tabelul 1 sunt prezentate valorile CCITT, folosite la determinarea rezistenței termice a elementelor de construcție.

Tabel 1

Valorile coeficienților de convecție

Direcția și sensul fluxului termic	Elemente de construcții în contact cu:		Elemente de construcții în contact cu spații ventilate neîncălzite:	
	• exteriorul • pasaje deschise (ganguri) • rosturi deschise		• subsoluri și pivnițe • poduri • balcoane și logii închise • rosturi închise • alte încăperi	
	α_i/R_{si}	α_e/R_{se}	α_i/R_{si}	α_e/R_{se}
$T_i \rightarrow T_e(T_u)$	8/0,125	24/0,042*	8/0,125	12/0,084
$\alpha_e \rightarrow T_e(T_u) \rightarrow T_i$	8/0,125	24/0,042*	8/0,125	12/0,084
$\alpha_i \rightarrow T_i \rightarrow T_e(T_u)$	6/0,167	24/0,042*	6/0,167	12/0,084

Zhang și colaboratorii [14] au studiat o combinație de două sisteme diferite - un tavan difuz montat împreună cu un sistem radiant. Coeficienții de transfer termic măsurați în placă au fost de 2,5 și 7,7 W/m²K, în varianta cu și respectiv fără panourile de tavan instalate, ceea ce demonstrează că panourile care formează tavanul suspendat realizează o barieră de transfer termic, așa cum susțin alți autori [15].

Pentru determinarea CCITT în diferite regimuri de curgere a aerului [16] s-au realizat studii experimentale și corelații care au fost implementate în instrumente de software, cum ar fi Energy Plus [17].

Studiile experimentale anterioare au propus corelații CCITT adaptate pentru răcirea nocturnă cu ventilare difuză pe tavan (VNRD) și ventilare mixtă (VM). A fost propusă o metoda de simulare și optimizare a energiei clădirii pentru validarea corelațiilor determinate experimental. Rezultatele validării au demonstrat că, corelațiile propuse au prezis cu exactitate temperaturile de suprafață cu o eroare medie de $1,9^{\circ}\text{C}$. Pentru un birou dotat cu instalație de climatizare, răcirea nocturnă, cu VNRD, a economisit cu aproximativ $0,2 \text{ kWh/m}^2$ energie totală de răcire și a furnizat un procent mediu estimat de persoanelor nemulțumite în timpul orelor de lucru (un PPD) cu până la 3,1% mai scăzut față de cel cu sistem VM [18].

Fiind unul dintre cele mai fierbinți și mai umede orașe din China, Chongqing se confruntă cu o temperatură ușor diferită a aerului exterior și a aerului interior pe timp de noapte în timpul verii. Efectuând analize termice bazate pe relația de echilibru termic dintre transferul de căldură conductiv, transferul de căldură convectiv și transferul de căldură radiativ, valoarea medie globală a coeficientului de transfer de căldură convectiv la suprafața peretelui intern, în timpul ventilației nocturne, este de $10,79 \text{ W/m}^2\text{K}$ [19].

2.2 Numărul de schimburi orare sau debitul de aer ventilat

Studiile anterioare au arătat că un număr mai mare de schimburi de aer pe oră (n), de până la $10 [\text{h}^{-1}]$ sau mai mult, dacă este cazul, poate fi astfel utilizat pentru a mări eficiența ventilării nocturne, în special pentru clădirile neocupate noaptea [20]. Valoarea debitului depinde și de sistemul de ventilare ales. Pentru obținerea unui consum de energie redus cu $11,96 \text{ kWh}/(\text{m}^2 \cdot \text{an})$, în cazul ventilării naturale nocturne s-au determinat $10 [\text{h}^{-1}]$ schimburi orare iar în cazul ventilării mecanice s-a determinat un număr mediu de $8 [\text{h}^{-1}]$ schimburi orare [21].

Pentru o clădire de tip bibliotecă, situată în Irlanda și care este supusă unui climat de tip maritim, creșterea numărului de schimburi orare pentru ventilarea de noapte până la $10 [\text{h}^{-1}]$, a avut un efect semnificativ asupra reducerii temperaturii uscate, dar creșterile suplimentare ale schimbărilor de aer au avut un efect neglijabil [3].

Alte studii au examinat o clădire situată în Franța, zona maritimă și au indicat că, pentru o sarcină de răcire de aproximativ 20 W/m^2 , era posibilă o reducere de energie cu ventilare nocturnă de ordinul a 25%. Aceste economii au fost realizate la un debit de aer calculat la un număr de schimburi orare de 8-10 $[\text{h}^{-1}]$ [22]. În acest caz s-a observat că ventilarea nocturnă a reușit să reducă temperaturile diurne ale aerului între $1,5^{\circ}\text{C}$ și 2°C , cu o îmbunătățire a condițiilor de confort.

Pentru o clădire de tip rezidențial, situată în Algeria, care se află într-un climat mediteranean temperat, s-au realizat simulări dinamice, folosind software-ul TRNSYS pentru a studia impactul strategiilor de răcire pasivă cu ajutorul ventilării naturale de noapte și s-a determinat că pentru un număr de schimburi orare de $8 [\text{h}^{-1}]$, se reduce consumul de energie de răcire cu aproximativ $10 \text{ kWh}/(\text{m}^2 \cdot \text{an})$ [4].

Pentru clădiri de birouri din normativul I5/2022, în anexa 7, sunt prezentate valorile recomandate pentru numărului de schimburi orare de aer, între 4 $[\text{h}^{-1}]$ și 8 $[\text{h}^{-1}]$.

^{1]}, pentru evaluarea valorilor propuse pentru debitul total de climatizare. O mărire a debitului de aer pentru ventilarea de noapte de la 5 [h⁻¹] la 15 [h⁻¹] schimburi orare, în cazul clădirilor de birouri aduce o scădere a sarcinii termice de răcire cu 5% [23].

2.3 Capacitatea termică a clădirii

Capacitatea termică este capacitatea unui material de a absorbi, stoca și elibera căldură. Întârzierea termică este viteza cu care un material eliberează căldura stocată. Pentru cele mai comune materiale de construcție, cu cât masa termică este mai mare, cu atât decalajul termic este mai mare.

Comparativ cu o bază de referință a clădirii existente, s-a constatat că, creșterea masei clădirii realizează o reducere a temperaturilor interne între 2°C și 3°C, atunci când masa a crescut de la 800 kg/m² la 1600 kg/m² [3]. Studii ulterioare au arătat că ventilarea pe timp de noapte a generat o putere de răcire între 12 kWh/(m²*an) și 16 kWh/(m²*an), în timp ce pentru o clădirea mai ușoară a rezultat o valoare mult mai mica, între 2-4 kWh/(m²*an).

S-a determinat că pentru clădiri cu o capacitate termică medie, folosind ventilarea naturală de noapte, se poate reduce necesarul anual de răcire cu până la 3,0 kWh/(m²*an) [24].

Tot în această direcție, ca o alternativă sau completare la materialele de construcție clasice, au apărut materiale cu schimbare de fază care asigură o eficiență ridicată pentru sistemele de ventilare de noapte. S-a constatat, în cazul unei clădiri rezidențiale, la care s-au folosit materiale cu schimbare de fază și ventilare naturală de noapte, temperatura aerului interior s-a redus cu 1,1°C și numărul orelor de disconfort termic au scăzut cu 34% [25].

Utilizarea sistemelor de ventilare de noapte este de multe ori asociată cu utilizarea materialelor cu schimbare de fază [26, 27], noțiunea de acoperiș verde [28] și alte strategii de energie regenerabilă.

2.4 Condițiile climatice

Pentru a cuantifica posibilitatea de răcire a clădirilor prin ventilare de noapte în diferite condiții climatice a fost determinat un indice al potențialului de răcire climatică, care se bazează pe diferența de temperatură dintre structura clădirii și aerul exterior în grade-ore [29,30]. Rezultatele arată un potențial de răcire nocturnă foarte ridicat pentru întreaga Europă de Nord și China de Nord și un potențial relativ semnificativ în Europa Centrală.

Luând în considerare cerințele anuale de răcire pentru o clădire de birouri din Regatul Unit, Kolokotroni [31] afirmă că energia de răcire realizată de ventilarea nocturnă este capabilă să furnizeze până la 20 kWh/m² de răcire pe an, în timp ce energia necesară pentru climatizarea unei clădiri de birouri standard din Regatul Unit este de aproximativ 30 kWh/m² pe an [32].

Într-un studiu realizat în Belgia [33], pentru climă moderată, pentru clădirile comerciale sarcină de răcire variază de la 30 W/m² la 100 W/m². În funcție de

proiectarea clădirii, ventilarea pe timp de noapte este capabilă să asigure o sarcină de răcire $10\text{--}40 \text{ W/m}^2$. Această concluzie este întărită de condițiile climatice belgiene, unde se înregistrează o temperatură medie anuală de $9,7^\circ\text{C}$, respectiv valoarea medie a valorile maxime înregistrate vara de $21,8^\circ\text{C}$ [34].

Pentru condițiile climatice din Franța, cercetările asupra sistemelor de ventilare de noapte atât prin metode experimentale, cât și prin metode numerice, au concluzionat o reducere a temperaturii diurne a aerului interior de $1,5^\circ\text{C}$ - 2°C , ceea ce determină un consum energetic redus [7].

Condițiile climatice din zona de nord a Chinei favorizează utilizarea ventilării de noapte care contribuie la reducerea consumului anual de energie electrică pentru răcirea spațiului cu $1,15 \text{ kWh}/(\text{m}^2 \cdot \text{an})$ într-o clădire de birouri. Cu un număr de schimburi orare de $10 [\text{h}^{-1}]$, temperatura medie radiantă a suprafeței interioare a scăzut cu până la $3,9^\circ\text{C}$ [23].

Pentru orașul Beijing, sistemele de ventilare naturală de noapte funcționează mai bine pentru o temperatură minimă sub 22°C , în timpul nopții, dar cu un risc ridicat de apariție a condensului. Pentru Shanghai, răcirea pasivă cu ajutorul sistemelor de ventilare de noapte nu poate fi considerată de succes [35].

3. Concluzii și direcții viitoare de cercetare

Lucrarea își propune efectuarea unei analize și sinteze documentare privind evoluția utilizării sistemelor de ventilare de noapte, descrierea elementelor principale care influențează eficiența ventilării și impactul acestora asupra consumului de energie electrică pentru răcirea clădirilor.

Valoarea maximă a coeficientul de convecție interior la transfer termic este de $10,79 \text{ W/m}^2\text{K}$ și influențează într-o mică măsură consumul de energie pentru răcire, respectiv o economie de aproximativ $0,2 \text{ kWh/m}^2$.

Numărul de schimburi orare are o implicație majoră asupra reducerii consumului de energie pentru răcire, astfel se pot obține valori mai reduce cu până la $11,96 \text{ kWh}/(\text{m}^2 \cdot \text{an})$, în cazul ventilării naturale nocturne, cu un număr de schimburi orare de $10 [\text{h}^{-1}]$. Rezultate mai bune se înregistrează atunci când tariful orar al energiei electrice variază zi/noapte și se aplică ventilarea mecanică nocturnă, aceasta asigurând un număr mai mare de schimburi orare, până la $15 [\text{h}^{-1}]$.

Capacitatea termică a clădirii poate influența consumul de energie electrică pentru răcire cu până la $3 \text{ kWh}/(\text{m}^2 \cdot \text{an})$. Această influență se poate mări prin utilizarea materialelor cu schimbare de fază.

Cea mai importantă influență asupra sistemelor de ventilare de noapte o are zona climatică care poate realiza o energie pentru răcire de până la 20 kWh/m^2 pe an, în zona de nord a Europei.

În consecință, analizând toate elementele care influențează ventilarea de noapte și toate aspectele pozitive care rezultă din utilizarea acestor sisteme, ne propunem pe viitor, să cercetăm teoretic, experimental și pe baza simulărilor dinamice, un astfel de sistem pentru o clădire de învățământ superior din Timișoara.

Referințe

- [1] *Miguel Lança a, Pedro J. Coelho a, João Viegas*, Numerical simulation of a night cooling strategy in an office room, *Energy & Buildings* 252 (2021) 111359
- [2] *M. Kolokotroni, P. Heiselberg*, Ventilative Cooling: State-Of-The-Art Review, Aalborg Univ. Aalborg, Denmark, 2015. <https://www.buildup.eu/en/node/52462>.
- [3] *Donal P. Finn a, Darragh Connolly b, Paul Kenny*, Sensitivity analysis of a maritime located night ventilated library building, *Solar Energy* 81 (2007) 697–710
- [4] *K. Imessad, L. Derradji, N.A. Messaoudene, F. Mokhtari, A. Chenak, R. Kharchi*, Impact of passive cooling techniques on energy demand for residential buildings in a Mediterranean climate, *Renew. Energy* 71 (2014) 589e597, <https://doi.org/10.1016/j.renene.2014.06.005>.
- [5] *W. Li-xia, Z. Jia-ning, W. Zhao-jun*, Night ventilation and active cooling coupled operation for large supermarkets in cold climates, *Energy Build.* 38 (2006) 1409e1416, <https://doi.org/10.1016/j.enbuild.2006.02.011>.
- [6] *K. Goethals, H. Breesch, A. Janssens*, Sensitivity analysis of predicted night cooling performance to internal convective heat transfer modelling, *Energy Build.* 43 (2011) 2429e2441, <https://doi.org/10.1016/j.enbuild.2011.05.033>.
- [7] *P. Blondeau, M. Sp_erandio, F. Allard*, Night ventilation for building cooling in summer, *Sol. Energy* 61 (1997) 327e335, [https://doi.org/10.1016/S0038-092X\(97\)00076-5](https://doi.org/10.1016/S0038-092X(97)00076-5).
- [8] *G. Young, K. Steemers*, Night-time naturally ventilated offices: statistical simulations of window-use patterns from field monitoring, *Sol. Energy* 84 (2010) 1216e1231, <https://doi.org/10.1016/j.solener.2010.03.029>.
- [9] *M. Kolokotroni*, Annex 28: Low Energy Cooling - Night Ventilation in Commercial Buildings, 1995.
- [10] *Sun, H., Kaiser, J., Jimenez-bescos, C.*, 2022. Examining the regulating impact of thermal mass on overheating, and the role of night ventilation, within different climates and future scenarios across China. *Clean. Eng. Technol.* 9 (January), 100534. <https://doi.org/10.1016/j.clet.2022.100534>.
- [11] *Machard, A., Inard, C., Alessandrini, J.M., Pel'e, C., Rib'eron, J.*, 2020. A methodology for assembling futureweather files including heatwaves for building thermal simulations from the European coordinated regional downscaling experiment (EURO-CORDEX) climate data. *Energies* 13 (13), 1–36. <https://doi.org/10.3390/en13133424>.
- [12] *Santamouris, M.*, 2016. Cooling the buildings – past, present and future. *Energy Build.* 128, 617–638. <https://doi.org/10.1016/j.enbuild.2016.07.034>.
- [13] *Hossein Bakhtiari, Sana Sayadi, Jan Akander, Abolfazl Hayati, Mathias Cehlin*, A framework for assessing the current and future capability of mechanical night ventilation in the context of climate change, *Energy Reports* 12 (2024) 4909–4925,
- [14] *C. Zhang, P.K. Heiselberg, Q. Chen, M. Pomianowski*, Numerical analysis of diffuse ceiling ventilation and its integration with a radiant ceiling system, *Build. Simul.* 10 (2) (2017) 203–218.
- [15] *L.M. Domínguez, O.B. Kazanci, N. Rage, B.W. Olesen*, Experimental and numerical study of the effects of acoustic sound absorbers on the cooling performance of thermally active building systems, *Build. Environ.* 116 (2017) 108–120.
- [16] *L. Peeters, I. Beausoleil-Morrison, A. Novoselac*, Internal convective heat transfer modeling: critical review and discussion of experimentally derived correlations, *Energy Build.* 43 (2011) 2227e2239, <https://doi.org/10.1016/j.enbuild.2011.05.002>.
- [17] U.S. Department of Energy, EnergyPlus 9.3 engineering reference. <https://bigladdersoftware.com/epx/docs/9-3/engineering-reference/>, 2020.

- [18] Rui Guo *, Yue Hu, Per Heiselberg, Hicham Johra, Chen Zhang, Pei Peng, Simulation and optimization of night cooling with diffuse ceiling ventilation and mixing ventilation in a cold climate, *Renewable Energy* 179 (2021,) 488 – 501.
- [19] W. Ji, Q. Luo, Z. Zhang, H. Wang, T. Du, P.K. Heiselberg, Investigation on thermal performance of the wall-mounted attached ventilation for night cooling under hot summer conditions, *Build. Environ.* 146 (2018) 268e279, <https://doi.org/10.1016/j.buildenv.2018.10.002>.
- [20] A. O'Donovan, A. Belleri, F. Flourentzou, G.-Q. Zhang, G.C. da Graca, H. Breesch, M. Justo-Alonso, M. Kolokotroni, M.Z. Pomianowski, P. O'Sullivan, Others, Ventilative Cooling Design Guide, Aalborg University, Department of Civil Engineering, 2018. <https://venticool.eu/wp-content/uploads/2016/11/VC-Design-Guide-EBC-Annex-62-March-2018.pdf>.
- [21] Li, X.X., Huang, K.L., Feng, G.H., Li, W.Y., Wei, J.X., 2022. Night ventilation scheme optimization for an Ultra-low energy consumption building in Shenyang, China. *Energy Rep.* 8, 8426–8436. <https://doi.org/10.1016/j.egyr.2022.06.059>.
- [22] Blondeau, P., Sperandio, M., Allard, F., 1997. Night ventilation for building cooling in summer. *Solar Energy* 61 (5), 327–335.
- [23] Wang, Z., Yi, L., Gao, F., 2009. Night ventilation control strategies in office buildings. *Sol. Energy* 83 (10), 1902–1913. <https://doi.org/10.1016/j.solener.2009.07.003>.
- [24] Brambilla, A., Bonvin, J., Flourentzou, F., Jusselme, T., 2018. Life cycle efficiency ratio: a new performance indicator for a life cycle driven approach to evaluate the potential of ventilative cooling and thermal inertia. *Energy Build.* 163, 22–33. <https://doi.org/10.1016/j.enbuild.2017.12.010>.
- [25] Jamil, H., Alam, M., Sanjayan, J., Wilson, J., 2016. Investigation of PCM as retrofitting option to enhance occupant thermal comfort in a modern residential building. *Energy Build.* 133, 217–229. <https://doi.org/10.1016/j.enbuild.2016.09.064>.
- [26] C. Stetiu, H.E. Feustel, Phase-Change Wallboard and Mechanical Night Ventilation in Commercial Buildings, Lawrence Berkeley Natl. Lab., 1998, pp. 1e14.
- [27] X. Chen, Q. Zhang, Z. John, X. Ma, Potential of ventilation systems with thermal energy storage using PCMs applied to air-conditioned buildings, *Renew. Energy* 138 (2019) 39e53, <https://doi.org/10.1016/j.renene.2019.01.026>.
- [28] J. Ran, M. Tang, Passive cooling of the green roofs combined with night-time ventilation and walls insulation in hot and humid regions, *Sustain. Cities Soc.* 38 (2018) 466e475, <https://doi.org/10.1016/j.scs.2018.01.027>.
- [29] Y. Liu, Climatic Analysis and Architectural Design Strategies for Bio-Climatic Design (In Chinese), Xi'an University of Architecture and Technology, 2003.
- [30] N. Artmann, Climatic potential for passive cooling of buildings by night-time ventilation in Europe, *Appl. Energy* 84 (2007) 187e201, <https://doi.org/10.1016/j.apenergy.2006.05.004>.
- [31] Kolokotroni, M., Webb, B.C., Hayes, S.D., 1998. Summer cooling with night ventilation for office buildings in moderate climates. *Energy and Buildings* 27, 231–237.
- [32] CIBSE, 2000. Chartered Institute of Building Services Engineers, Guide H, CIBSE.
- [33] Gratia, E., Bruyere, I., DeHerde, A., 2004. How to use natural ventilation to cool narrow office buildings. *Building and Environment* 39, 1157–1170.
- [34] Breesch, H., Brossaer, A., Janssens, A., 2005. Passive cooling in a lowenergy office building. *Solar Energy* 79, 682–696.
- [35] G. Carrilho da Graça, Q. Chen, L.R. Glicksman, L.K. Norford, Simulation of winddriven ventilative cooling systems for an apartment building in Beijing and Shanghai, *Energy Build.* 34 (1) (2002) 1–11.

The role of ventilation systems on indoor air quality. Analysis and Solutions for a Healthy Environment

Rolul sistemelor de ventilare asupra calitatii aerului interior. Analiză și soluții pentru un mediu sănătos

Cristian Pacurar¹, Adriana Tokar¹, Marius Adam¹

University Politehnica Timisoara

Traian Lalescu 2, Timisoara 300223, Romania

E-mail: cristian.pacurar@upt.ro, adriana.tokar@upt.ro, marius.adam@upt.ro

DOI: 10.37789/rjce.2025.16.3.7

Abstract. This paper presents the relation between indoor air quality (IAQ) and the efficiency of ventilation systems in indoor spaces, given their impact on the health and comfort of occupants. In the context of urbanization and modern construction trends, in which the tightness of buildings has increased significantly, inadequate ventilation can lead to the accumulation of internal pollutants, such as carbon dioxide (CO₂), volatile organic compounds (VOCs), fine particles, and biological agents (molds, bacteria). The paper presents the different types of ventilation systems used in homes (natural, mechanical and hybrid ventilation), analyzing their effectiveness in maintaining a healthy indoor environment. The study highlights that proper ventilation not only prevents the build-up of pollutants, but also helps to improve occupant performance, reducing risks to respiratory and mental health. In conclusion, this paper highlights the need for a balance between energy efficiency and occupant health protection by implementing sustainable and smart ventilation solutions in modern homes.

Key words: indoor air pollution, IAQ, heat recovery technologies (HRV), indoor pollutants, ambient comfort, ventilation systems, healthy environment, mechanical ventilation, natural ventilation, hybrid ventilation, CO₂ concentrations,

1. Introduction

Indoor air quality (IAQ) is a determinant of health and comfort in the residential environment, especially in the context in which individuals spend, on average, more than 90% of their time indoors [1]. The air inside homes can contain a variety of contaminants, both from internal sources (building materials, domestic activities) and external sources (traffic, industry, pollen). In this paper, the main categories of pollutants encountered in the residential environment are analyzed, along with their sources, accumulation mechanisms and effects on human health. Proper ventilation of

spaces is essential for maintaining good indoor air quality and preventing the build-up of pollutants [2].

2. Content of the paper

Indoor air quality (IAQ) has become a topic of major interest only in recent decades but concerns about home ventilation can be traced back to ancient times. In ancient Rome, architects designed dwellings with open atriums to allow air circulation and the dispersion of smoke from cooking or heating [3]. Until the nineteenth century, most homes benefited from natural ventilation through cracks in buildings, frequently opened windows and the use of chimney stoves. Although uncontrolled and energy-inefficient, this natural ventilation reduced the build-up of pollutants. Since the Industrial Revolution (19th century), urbanization and the intensive use of fossil fuels have led to an increase in pollution, and concerns about home hygiene have increased, but from the perspective of infectious diseases rather than indoor air. A turning point was the energy crisis of the 1970s, when the focus was on sealing homes to reduce heat loss. This measure, although energy-efficient, has led to the emergence of problems with the accumulation of pollutants in the indoor air, especially in residential spaces. In the 1980s and 1990s, the first systematic studies on Sick Building Syndrome (SBS) and the effects of indoor pollution on health began to appear [4]. The World Health Organization (WHO) and ASHRAE have begun to develop standards and recommendations on acceptable levels of indoor pollutants (such as CO₂, VOCs, PM_{2.5}, formaldehyde). Since the 2000s, with technological advancement and the digitalization of homes, mechanical ventilation systems with heat recovery (HRV), air quality sensors and smart home solutions have been developed, which allow precise monitoring and control of ventilation [5].

Today, in the context of increasing time spent indoors (over 90% of the day, according to recent studies) and long-term health concerns, indoor air quality in homes is recognized as an essential factor for physical and mental well-being, being increasingly integrated into sustainable design norms and public health policies. [1]. Changes in construction, energy cost, materials and health concerns are shifting ventilation philosophy once again. Buildings are now a source of contamination. Health, economics and aesthetics are becoming more important than comfort in determining the specification for ventilation. Table 1 is described as an extension of the concept presented by Fanger in 1996 and shows the paradigm for ventilation design. [6]. There is expected to be in a transition period over the next 5 to 10 years, because the design industry struggles to incorporate qualitative attributes into prescriptive standards. Performance criteria based on developing indices for quantifying the health hazard of air composed of a mixture of contaminants or subjective rating schemes are likely to emerge. In 1869 Lewis Leeds told to Franklin Institute that “We are thus to conclude that our own breath is our greatest enemy”. [6]

Table 1

Paradigms in the philosophy of ventilation since 1800 [Extension of Fanger -1996]

<i>Years</i>	<i>Pollution Sources</i>	<i>Paradigm</i>
1800	People	Poison
1900		Contagion
1935		Comfort
1975	People Buildings	Comfort + Health
2000	People Buildings Outside Environment	Comfort + Health + Productivity
2050		Personal aesthetics

Studies show that proper ventilation systems play a crucial role in maintaining indoor air quality. In the absence of adequate ventilation, internal pollutants (such as CO₂, VOCs, fine particles) can reach dangerous concentrations, affecting the health of occupants. Also, the accumulation of moisture, combined with insufficient air exchange, can favor the development of mold and other biological contaminants.

As main pollutants we mention chemical and biological pollutants, particulate matter and radon. Chemical pollutants include gaseous or volatile substances that can affect the respiratory, cardiovascular or nervous systems. Among the most relevant are: carbon dioxide, volatile organic compounds, carbon monoxide and nitrogen oxides. Carbon dioxide (CO₂) is an indirect marker of insufficient ventilation, accumulating especially in bedrooms and poorly ventilated spaces. Although it is not toxic at normal concentrations, values above 1000 ppm can indicate discomfort, decreased cognitive capacity and the feeling of "closed" air [7].

Volatile organic compounds (VOCs) are a large group of substances emitted by common products: adhesives, varnishes, paints, furniture materials, detergents and room fragrances. Among the most common are benzene, toluene and formaldehyde – a chemical agent recognized as a potential carcinogen by the International Agency for Research on Cancer (IARC). Carbon monoxide (CO) and nitrogen oxides (NO_x) occur predominantly in homes where combustion sources are used: gas stoves, stoves, fireplaces without adequate draught. Carbon monoxide, being colorless and odorless, poses an increased risk of poisoning, especially in poorly ventilated spaces. Fine particles, classified according to aerodynamic diameter (PM₁₀, PM_{2.5}, PM_{0.1}), are transported into the indoor air from both internal (cooking, smoking, cleaning, candles) and external (road traffic, industry) sources. PM_{2.5} particles can penetrate deep into the respiratory tract, favoring the appearance of cardiovascular and respiratory diseases [8]. In conditions of high humidity and poor ventilation, homes can become a favorable environment for the development of biological contaminants, such as: mold spores, allergens, bacteria and airborne viruses. Mold spores (*aspergillus*, *cladosporium*) colonize the walls or ceiling in the presence of condensation. Allergens such as dust mites, animal hair, pollen, are associated with allergic reactions, rhinitis or asthma. Airborne bacteria and viruses are found

especially in crowded spaces or without efficient air circulation. Radon is a natural radioactive gas, resulting from the decay of uranium in the soil, which can enter homes through cracks in the foundation or through building materials. Depending on the geographical area, concentration can vary significantly. According to the World Health Organization (WHO), prolonged exposure to radon is considered the second leading cause of lung cancer, after smoking [9].

Indoor CO₂ concentrations are used as an indicator of indoor air quality. The rate at which carbon dioxide is generated and oxygen is consumed depends on physical activity. These relationships between these two and breathing rates are shown in Figure 1 to maintain the steady-state CO₂ concentration below a given limit [6], [10].

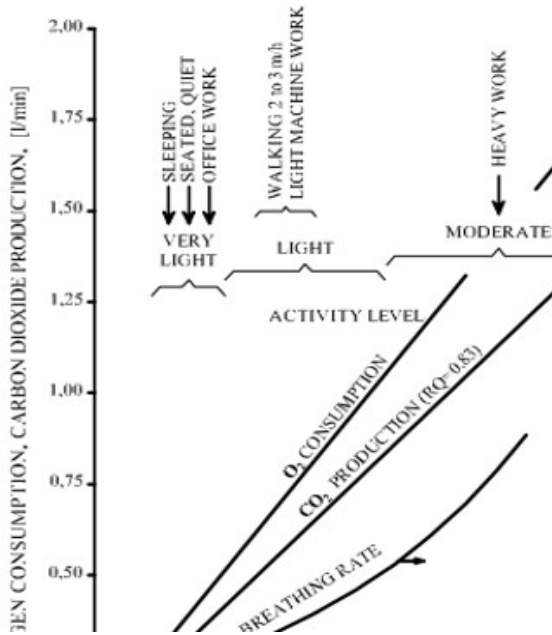


Fig.1 . Metabolic data

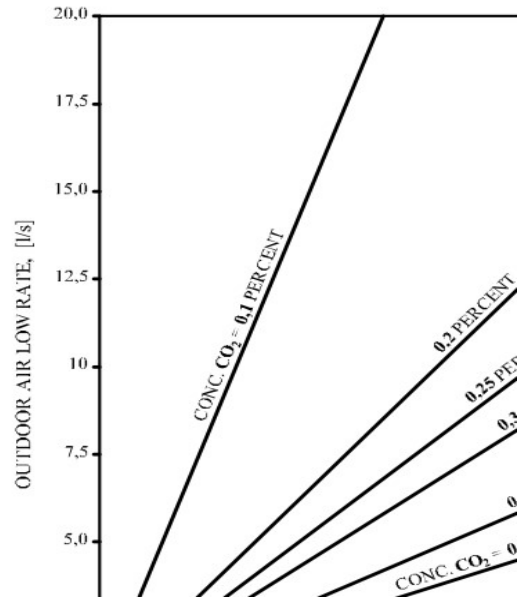


Fig.2. Ventilation requirements

The mass balance equation gives the outdoor air flow rate needed to maintain the steady-state CO₂ concentration below a given limit and Equation 1 presents the outdoor air flow rate per person:

$$V_o = \frac{N}{(C_s - C_o)} \quad (1)$$

Where: V_o= outdoor air flow rate per person; N= CO₂ generation rate per person.

C_s=CO₂ concentration in a specific space; C_o = CO₂ concentration in outdoor air [10],[11]. In Figure 2 the ventilation requirements are presented as a report between the outdoor air flow rate required and physical activity. The required ventilation must be increased if the physical activity level is greater than 1.2 met, in order to have the

same carbon dioxide level. In equation 1 the decrease in oxygen content of the room air could be substituted for carbon dioxide concentration [10].

$$C_s - C_o = \frac{N}{V_o} \quad (2)$$

Considering equation 1, CO₂ generation rate per person has a negative value because oxygen is consumed rather than generated.

$$C_s = C_o - \frac{N}{V_o} \quad (3)$$

When the activity level is reached at 1.2 met, the oxygen consumption rate is 0.36 l/min.

Ventilation is essential for maintaining good indoor air quality, but the method of achieving this can vary. Two primary approaches are natural ventilation and mechanical ventilation. Each has its advantages and disadvantages, and the choice between them often depends on the specific needs of a building and its occupants. Natural ventilation is the process by which fresh air enters the home through hardware openings, window hardware or cracks in construction, and is eliminated through air vents (either through exhaust hardware or chimneys) [5]. It was the main way of ventilating homes before the industrial revolution, but also in regions where the climate allowed the frequent opening of hardware stores. The main advantage it has is that it allows a natural air exchange, based on temperature and pressure differences. Another advantage is that it is an inexpensive and simple to implement ventilation system, which does not require additional equipment. As a disadvantage, natural ventilation can lead to significant losses of thermal energy, especially in the cold period of the year. The efficiency of natural ventilation depends on external weather conditions (wind, temperature), which makes the system inefficient in extreme weather conditions or in thermally insulated buildings. Mechanical ventilation uses electrical equipment, such as fans, to control the flow of air inside the home. It is divided into two main types: mechanical ventilation with extraction and mechanical ventilation with air intake. Mechanical extraction ventilation involves extracting stale air from rooms, and fresh air enters through passive openings or non-airtight hardware. It is often used in bathrooms, kitchens and other spaces with high humidity or pollutant emissions. Mechanical air intake ventilation (VMA) involves supplying fresh air from the outside, constantly, while stale air is exhausted. VMA systems can include heat exchangers (HRVs – Heat Recovery Ventilators) to recover heat from the exhaust air and transfer it to fresh air, thus reducing heat energy losses. Mechanical ventilation systems, especially those with heat recovery, have demonstrated superior efficiency in reducing pollutant concentrations and improving thermal comfort. These systems not only improve air quality, but also contribute to reducing energy consumption, which is essential in the context of energy efficiency requirements in modern construction. They have higher efficiency in removing pollutants, especially in modern buildings

with high tightness. As a disadvantage is the possibility of accumulation of pollutants in ventilation systems if they are not properly maintained. Hybrid ventilation combines the advantages of natural and mechanical ventilation, using both passive airflow and mechanical equipment to ensure optimal air exchange. In favorable weather conditions, natural ventilation can be used, and when conditions do not allow this, the system switches to mechanical ventilation [5], [6], [12].

3. Conclusions

Ventilation is more than just a building requirement; it's a critical component that affects the health and comfort of building occupants. Poor ventilation can have a range of negative consequences, from minor discomforts to severe health risk. In the absence of an efficient air exchange, the pollutants emitted inside accumulate. Ventilation has the role of diluting internal pollutants, achieved through the intake of clean air, but also that of evacuating contaminated air, especially through mechanical systems or natural ventilation. The more efficient the ventilation is, the lower the concentration of pollutants substances.

References

- [1] I. Sarbu, C. Pacurar, „Experimental and numerical research to assess indoor environment quality and schoolwork performance in university classrooms”, Building and Environmental, 2015.
- [2] Y. AlHorr, M. Arif, A. Kaushik, A. Mazroei, M. Katafygiotou, E. Elsarrag, „Occupant productivity and office indoor environment quality: A review of the literature”, Building and Environment, Volume 105, 15 August 2016, pp. 369-389.
- [3] V. Van Tran, D. Park, Y.C. Lee, „Indoor Air Pollution, Related Human Diseases, and Recent Trends in the Control and Improvement of Indoor Air Quality”, International Journal of Environmental Research and Public Health, vol. 17, no. 8, April 23, 2020, ID Article: 2927.
- [4] Enviroliteracy Team, „How Did The Industrial Revolution Affect the Environment?”, 2024.
- [5] S. Dimitroulopoulou, et al., „Indoor air quality guidelines from across the world: An appraisal considering energy saving, health, productivity, and comfort”, Environment International vol. 178, August 2023, ID Article:108127.
- [6] ASHRAE Handbook—2005 Fundamentals, Chapter 8. 2005. American Society of Heating, Refrigerating and Air-Conditioning Engineers, Inc., Atlanta, GA.
- [7] A Seppänen, W J Fisk, M J Mendell, „Association of ventilation rates and CO₂ concentrations with health and other responses in commercial and institutional buildings”, Indoor Air 1999.
- [8] The World Health Report 2010, Health Systems Financing: Path to Universal Coverage, 2012
- [9] N.E. Klepeis,; W.C. Nelson, W.R. Ott, J. Robinson, A.M. Tsang, P. Switzer, J.V. Behar, S. Hern, W. Engelmann, The National Human Activity Pattern Survey (NHAPS): „A Resource for Assessing Exposure to Environmental Pollutants”, in Journal of Exposure Science & Environmental Epidemiology, 2021.
- [10] ANSI/ASHRAE Standard 62.1-2016 Ventilation for Acceptable Indoor Air Quality.
- [11] L.A. McHattie, “Graphic visualization of the relations of metabolic fuels: Heat: O₂, CO₂, H₂O: Urine N”,. in Journal of Applied Physiology Vol. 15, No. 4, 1960, pp. 677–83.
- [12] S. Sadrizadeh et al, “A systematic review of operating room ventilation”, in Journal of Building Engineering, vol. 40, August 2021, ID Article: 102693.

Experimental Analysis of Thermo-Mechanical Effects on Geothermal Piles

Analiză experimentală a efectelor termo-mecanice asupra piloților geotermici

Bahadır Kivanç¹, Florescu Virgil²

¹ Societatea Romana Geoexchange
2F Fabricilor Str., Oradea, Romania
e-mail: bahadir.kivanc@phd.utcb.ro

² Technical University of Civil Engineering Bucharest
124 Lacul Tei Blvd., Bucharest, Romania
e-mail: virgil.florescu@utcb.ro

DOI: 10.37789/rjce.2025.16.3.8

Abstract. The growing global population necessitates sustainable energy solutions to meet escalating energy demands. Geothermal energy, abundant and continuous, ranks as a leading alternative after solar energy. Integrating geothermal energy into building systems requires specialized structures. For shallow geothermal applications, thermo-active piles offer a cost-effective and efficient solution regarding both investment and operational expenses. Distinct from traditional piles, these energy piles enable thermal exchange between the pile and surrounding soil, supporting building heating, cooling, and hot water needs. Their design mandates a coupled thermo-hydro-mechanical analysis. This study presents a numerical model of a field-scale energy pile experiment conducted in Houston, Texas, validated through stress and temperature data collected during the experiment.

Key-words: geothermal piles, experiment, solar energy

1 Case study on the numerical modelling of energy piles

Energy piles combine structural foundations with geothermal heating and cooling systems, using the ground as a renewable energy source. This dual-function system has gained attention in sustainable building design due to its environmental and economic benefits. Numerical modelling helps predict their thermal and mechanical performance under various operating and environmental conditions.

The global population is experiencing a rapid increase, with current estimates nearing 8 billion and projections indicating a rise to approximately 9.8 billion by 2050

[1]. This demographic trend has led to a significant escalation in global energy demand. Presently, nearly 60% of this demand is met through the consumption of fossil fuels [2].

The reliance on fossil fuels presents two critical challenges: the intensification of environmental degradation due to greenhouse gas emissions, and the inherent non-renewability of these resources. In response to these issues, geothermal energy has emerged as a viable alternative. Defined as the thermal energy stored within the Earth's crust, geothermal energy ranks as the second most abundant renewable resource globally, following solar energy.

One of the key advantages of geothermal energy lies in its uninterrupted availability, independent of atmospheric conditions, thereby ensuring a consistent and reliable energy supply [3]. Due to its sustainability and minimal environmental impact, geothermal energy has garnered increasing interest as a clean energy solution.

Among the various technologies employed to harness shallow geothermal resources, thermo-active piles (commonly referred to as energy piles) have gained prominence [4]. These structural elements differ from conventional piles by integrating pipe systems that enable heat exchange between the subsurface and the built environment. The temperature of the fluid circulating within these pipes is modulated via a heat pump, allowing for the delivery of thermal energy throughout the structure to satisfy heating, cooling, and domestic hot water requirements.

Extensive research has been conducted to investigate the thermal performance of energy piles under load. Their response to thermal loading has been documented through field experiments [5], [6], [7], and subsequently validated using numerical simulations [8], [9].

In the present study, a comprehensive numerical model was developed to simulate the behavior of an energy pile tested at field scale in Houston, Texas. The model was validated using stress and temperature measurements obtained from the experiment, thereby providing a reliable framework for further investigations into the thermo-mechanical performance of energy piles.

2 Field experiment

2.1 Energy Pile Characteristics

An in-situ energy pile test was carried out in Houston, Texas [7]. The pile, constructed using the Augered Cast-In Place (ACIP) method, has a diameter of 45.7 cm and a total length of 15.24 m. To monitor the pile's mechanical behavior, vibrating wire strain gauges were installed at five different depths along the reinforcement cage (Figure 1).

The pile incorporates high-density polyethylene (HDPE) pipes to facilitate heat exchange between the ground and the structure. These pipes have a diameter of 25.4 mm and a wall thickness of 3.2 mm. A single U-shaped pipe configuration is positioned centrally within the pile. The heat transfer fluid circulating within the pipe is composed of 80% water and 20% antifreeze. During testing, the fluid circulated at a constant flow rate of 0.88 m/s. The thermal conductivity of the pipe material is 0.42 W/m/°C.

The energy pile has a modulus of elasticity of 36 GPa and a linear thermal expansion coefficient of $1.29 \times 10^{-5} \mu\epsilon/^{\circ}\text{C}$. The instrumentation was placed at depths of -2.7 m, -5.7 m, -8.7 m, -11.6 m, and -14.5 m, respectively.

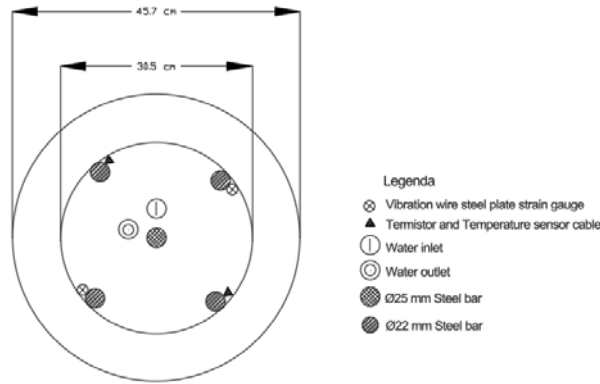


Figure 2-1 Energy Pile instrumentation

2.2 Soil properties

Based on the findings from the geotechnical investigations conducted at the site, the subsurface profile consists of a clay layer extending to a depth of 9.8 meters, beneath which a sand stratum is located. The groundwater table was identified at a depth of 3.7 meters below the surface. The geotechnical parameters utilized in the numerical analysis are presented in Table 1.

Table 1

Soil parameter

Ground layer	Terzaghi (Mpa)	Poisson	Kohezyon (kPa)	Internal friction angle (°)
Clay	45	0.495	114	0
Sand	75	0.3	5	43

2.3 Purpose of the Experiment

As part of this study, the energy pile was subjected to a static load test in the field, and its vertical load capacity was determined to be 2558 kN. After the static load was removed, cyclic thermal loading was applied. This thermal loading consisted of five thermal cycles and lasted for a total of six weeks. The temperature of the fluid circulated through the pipes inside the pile is shown in Figure 2.

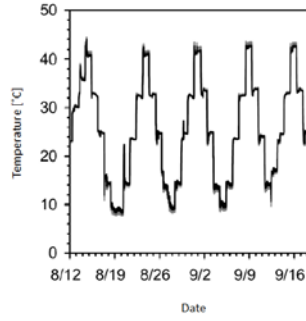


Figure 2-2 Thermal loading cycles

3 Physico-Mathematical Models for the Simulation of Transfer Processes in Geothermal Piles

Analytical solutions are widely used due to their simplicity and computational efficiency. Most analytical approaches for analyzing geothermal heat pump systems assume conduction-dominated systems (neglecting the natural flow of groundwater) and are based on the infinite line source theory or the cylindrical source theory

$$\frac{T_r - T_e}{T_i - T_e} = \sum_{n=1}^{\infty} \frac{2J_1(\varepsilon_n)}{\varepsilon_n [J_0^2(\varepsilon_n) + J_1^2(\varepsilon_n)]} J_0\left(\frac{r}{R} \varepsilon_n\right) \exp(-\varepsilon_n^2 Fo) \quad 3-1$$

These models are particularly applied for in-situ evaluation of geothermal systems using the Thermal Response Test (TRT), which typically lasts between 12 and 60 hours. However, they are less suitable for long-term analysis, as the effects usually become significant after approximately 1.6 years of operation, depending on the hydrogeological and operational conditions of the geothermal system. The temperature response in an infinite line source model (without groundwater flow) cannot reach steady-state conditions, and the thermal anomaly will increase indefinitely with operating time. Therefore, by using software such as COMSOL, long-term simulations can be performed, allowing for the analysis of axial effects and groundwater flow influence on the temperature distribution along the walls of geothermal foundation structures.

3.1 Model “Infinite Line Source” (ILS) *Reg* [10].

The Infinite Line Source (ILS) model is a direct application of Lord Kelvin’s heat source approach [11] to ground heat exchangers. This model is based on the idea that any line can be considered as a series of closely spaced point sources. It begins by calculating the temperature change at a specific location within an infinite homogeneous medium using the point heat source formula, and then, through integration, it accounts for the effects of the other point sources at the target location (Figure 3-1).

The following general assumptions were made for the derivation of this model:

1. The soil is considered a homogeneous medium, and its thermophysical properties are assumed to remain constant with temperature
2. The medium has a uniform initial temperature
3. The heating rate per unit length is constant from the start until the end of the thermal loading

The infinite line heat source model is the analytical solution of the conductive heat transfer equation in a homogeneous and isotropic medium, expressed in radial coordinates according to [12] [13]

$$\frac{\delta^2 T}{\delta r^2} + \frac{1}{r} \times \frac{\delta T}{\delta r} = \frac{\rho c_p}{k} \times \frac{\delta T}{\delta t} \quad (3.1)$$

unde,

T : temperatura mediului,

r : distanta radiala de la sursa de caldura,

ρ : densitatea mediului,

c_p : caldura specifica a mediului

k : conductivitatea termica a mediului,

t : timp.

To solve the equation, it is assumed that the system is initially at a constant temperature ($T(r, t=0) = T_0$), and that the boundaries located at an infinite distance from the heat source ($r=\infty$) always remain at a constant temperature ($T(r=\infty, t) = T_0$). The surrounding medium is considered homogeneous and isotropic

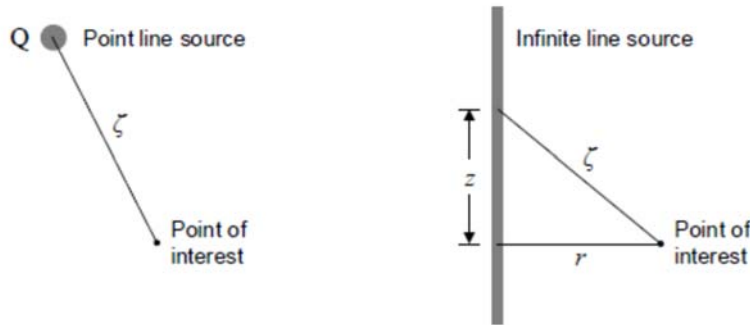


Figure 3-1 "Point Line Source" and "Infinite Line Source" models according to [10]

Ingersoll and Plass (1948) [14] demonstrated that the temperature change at time t and at a distance ζ from a point heat source emitting a constant heat rate q can be calculated as follows:

$$\Delta T(t) = \left(\frac{q\alpha}{k}\right) \left(\frac{1}{2\sqrt{\pi\alpha t}}\right)^3 \exp\left(-\frac{\zeta^2}{4\alpha t}\right) \quad (3.2)$$

The following integral is then used to estimate the temperature change caused by an infinite linear heat source. Again, the linear source is represented by adjacent points, for each of which the distance to the location of interest is $2\zeta=r+z$, as illustrated in (Figure 3-1)

$$\Delta T = \int_{-\infty}^{+\infty} \left(\frac{q\alpha}{k} \right) \left(\frac{1}{2\sqrt{\alpha\pi t}} \right)^3 e^{-(r^2+z^2)/4\alpha r} dz = \frac{q}{4\pi k t} e^{\frac{-r^2}{4\alpha t}} \quad (3.3)$$

Since the heat source continuously emits from time 0 to t, the temperature change at the point of interest can be estimated as:

$$\Delta T = \frac{q}{4\pi k} \int_0^t \frac{e^{\frac{-r^2}{4\alpha t}}}{t} dt \quad (3.4)$$

Assuming an infinite linear heat source located at $r=0$ and represented by a constant heat flux per unit length, and given the prescribed initial and boundary conditions, the solution to equation (3.5) can be expressed as the following temperature increment $\Delta T(r,t)=T(r,t)-T_0$, which depends on the distance r from the source and time t

$$\Delta t(r, t) = -\frac{q}{4\pi k} Ei \left(-\frac{r^2}{4\alpha t} \right) \quad (3.5)$$

where,

$Ei(u)$: exponential integral,

q : heat flux injected per unit length of the borehole

The exponential integral in equation (3.6) can be derived as the following Taylor series expansion [15].

$$Ei(u) = \gamma + \ln(u) + \sum_{i=1}^{\infty} \frac{u^i}{i \cdot i!} \quad (3.6)$$

γ is the Euler–Mascheroni constant ($\gamma = 0.57721\dots$).

For large values of t/r^2 , $Ei(u)$ can be approximated as:

$$\Delta T(r_b, t) = \frac{q}{4\pi k} \left[\ln \left(\frac{4\alpha t}{r_b^2} \right) - \gamma \right] \quad (3.7)$$

The relationship between the measured average fluid temperature (T_f) during a thermal response test and the temperature at the borehole wall is:

$$T_f(t) = T_0 + qR_b + \frac{q}{4\pi k} \left[\ln \left(\frac{4\alpha t}{r_b^2} \right) - \gamma \right] \quad (3.8)$$

where,

T_0 : initial (undisturbed) ground temperature,

R_b : borehole thermal resistance.

The slope of the curve gives:

Equation (3.9) can be expressed in the form

$$T_f(t) = m \cdot \ln(t) + n,$$

In order to determine the thermal conductivity of the ground. In this way, by using the slope of the evolution of the average fluid temperature with respect to the natural logarithm of time, the thermal conductivity can be evaluated. The slope of the curve gives:

$$m = \frac{q}{4\pi k} \quad (3.9)$$

The thermal conductivity of the ground can be evaluated using this slope, according to the following relation:

$$k = \frac{q}{4\pi m} \quad (3.10)$$

The ILS model does not account for the finite length of typical heat exchangers. The finite length causes an edge effect, which results in a reduction of the temperature change at the ends of the line. This axial effect becomes significant at approximately $t \approx H^2/180\alpha t$ for a single line source, where H is the length of the heat exchanger. This limiting time is even shorter if there is interaction between multiple line sources [16].

Representing the heat exchanger as a linear heat source does not provide accurate results for short time periods and in the case of vertical heat exchangers with large diameters, such as thermal piles (which also function as heat exchangers).

3.2 Standard Finite Line Source Model (FLS) [17]

Traditionally, heat transfer in the porous soil medium without groundwater flow is described by the heat conduction equation as follows [17] :

$$\rho c \frac{\delta T}{\delta t} - \nabla * (\lambda \nabla T) = 0 \quad (3.11)$$

where:

- ρ is the density of the soil [kg/m^3],
- c is the specific heat capacity of the soil [$\text{J}/\text{kg} \cdot \text{K}$],
- T is the temperature [$^{\circ}\text{C}$ or K],
- t is time [s],
- k is the thermal conductivity of the soil [$\text{W}/\text{m} \cdot \text{K}$],
- Q is the internal heat source term [W/m^3].

$$\rho c = n\rho_w c_w + (1 - n)\rho_s c_s \quad (3.12)$$

λ – Thermal conductivity [$\text{W}/\text{m} \cdot \text{K}$]

ρc – Volumetric heat capacity of the porous medium

$\rho_s c_s$ – Weighted average of the solids in the aquifer medium

$\rho_w c_w$ – Weighted average of the water in the aquifer medium

The solution of the partial differential equation for heat transfer from a source in a porous medium with an initial uniform temperature T_0 is given by the relation:

$$\Delta T(x, y, z, t) = \frac{Q}{4\pi\lambda r} \operatorname{erfc} \left[\frac{r}{\sqrt{4at}} \right] \quad (3.13)$$

The temperature difference in the borehole, $\Delta T = T_0 - T$, where T_0 is the initial uniform temperature and T is the local temperature, is related to the heat Q extracted or injected from the borehole. The thermal diffusivity is defined as $(a = \frac{\lambda}{\rho c})$, where λ is the thermal conductivity and ρc is the volumetric heat capacity of the porous medium. The distance $r = \sqrt{x^2 + y^2 + (z - z')^2}$ to the heat source, located along the z -axis at coordinates $(0, 0, z')$

The Finite Line Source (FLS) model can be expressed as follows (H.Y. Zeng, N.R. Diao, Z.H. Fang, 2002): [18], [19].

$$\Delta T_{FLS}(x, y, z, t) = \frac{q_L}{4\pi\lambda} \left[\int_0^H \frac{1}{r} \operatorname{erfc} \frac{1}{\sqrt{4at}} dz' - \int_{-H}^0 \frac{1}{r} \operatorname{erfc} \frac{r}{\sqrt{4at}} dz' \right] \quad (3.14)$$

4 Numerical Model

4.1 Standard Finite element numerical model

A three-dimensional numerical model of the energy pile was developed using COMSOL Multiphysics software (refer to Figure 3). The dimensions of the numerical model are 50 m x 50 m x 40 m. The boundary conditions of the model are such that the edges are constrained with sliding supports in the vertical direction, while the base of the model is anchored. Thermal boundary conditions were applied by thermally isolating the model boundaries, with the exception of the upper surface. The initial temperature of the pile and surrounding soil was set to 21.6°C, as determined from field measurements. For the clay and sand soils, the Mohr-Coulomb material model was employed, while a linear elastic material model was used for the thermal pile. The first of the five thermal cycles, as illustrated in Figure 2, was applied to the numerical model for thermal loading. The initial stress conditions are representative of the geostatic state.

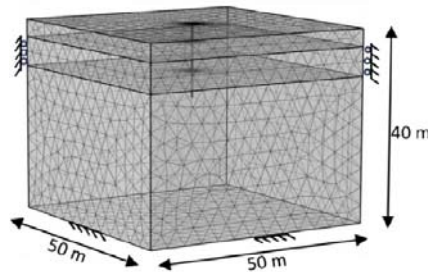


Figure 4-1 Numerical model and boundary conditions

5 Comparison of the field experiment and numerical model results

In the field experiment, the temperatures measured along the pile and the values calculated by the numerical model are presented for the first three days in Figure 4. Temperature and strain measurements along the pile were made using vibration wire strain gauge sensors, as shown in Figure 1. All values presented in the graphs are the averages of the readings obtained from these two sensors. There are positional differences in the pipe and sensor placements in the field due to manufacturing variations. The distance of the sensors from the center varies between 11.7 cm and 12.9 cm. Therefore, the numerical model results are provided for this range. The D1 and D2 values shown in Figure 4 represent the analysis results at distances of 11.7 cm and 12.9 cm from the center of the pile, respectively. As seen in Figure 4, the temperature values

measured in the field and those calculated by the finite element numerical model are in good agreement.

The stresses generated by thermal loading are presented in Figure 5. The stress value obtained from the sensor located at a depth of approximately 8.7 m is higher than the value obtained from the numerical model. Apart from this exception, the stresses measured in the field are in good agreement with the values calculated by the numerical model.

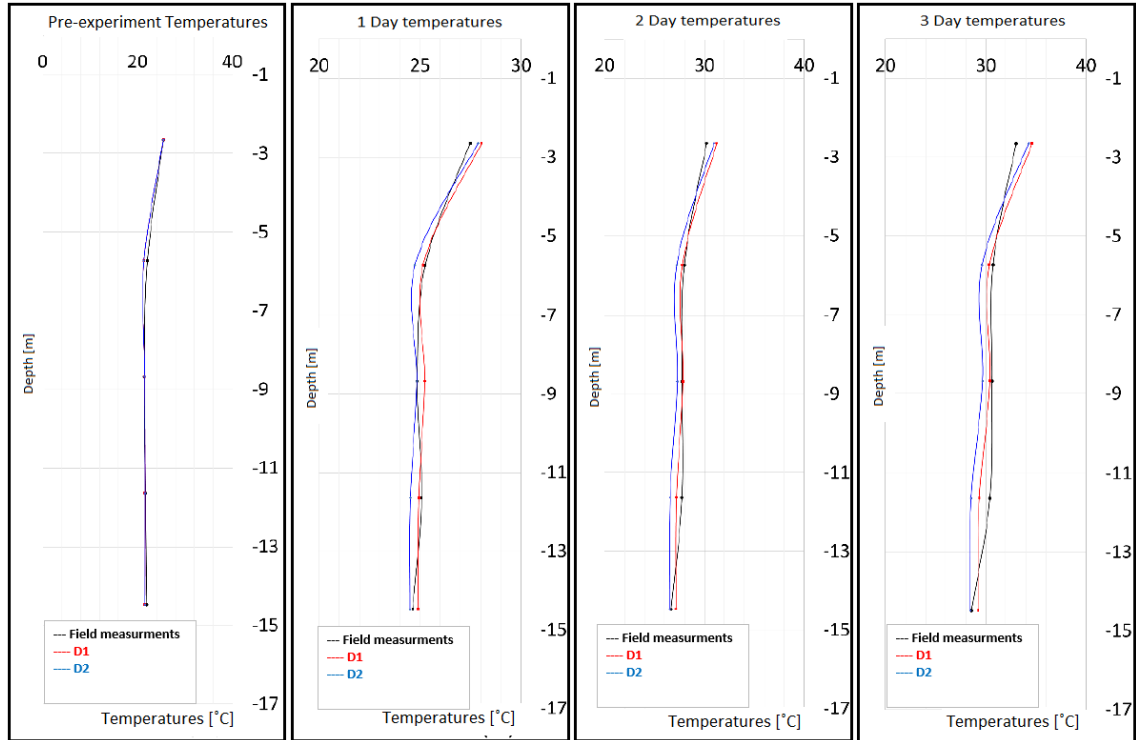


Figure 5-1 Measured and Calculated Temperatures Along the Pile Before and During Thermal Loading

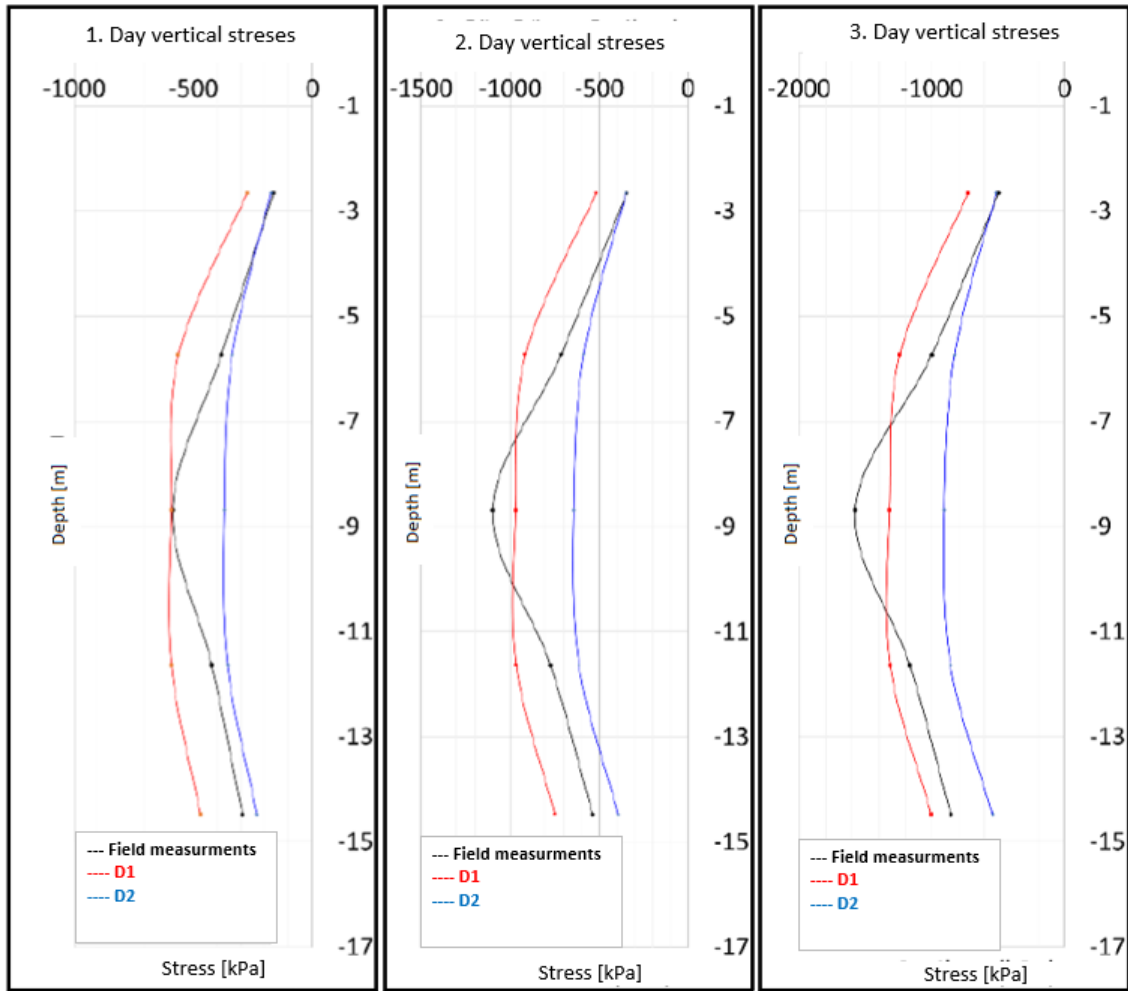


Figure 5-2 Measured and calculated temperatures along the pile during thermal loading

6 Conclusions

As a result of the numerical analyses conducted, the thermomechanical behavior of the pile under thermal effects was investigated. The temperatures and stresses measured along the pile in the field were compared with the results of the numerical model. The thermal fluid circulated through the pipes within the pile led to an increase in the pile's temperature. The temperature increases measured in the field were consistent with those calculated by the finite element numerical model. The temperature rise within the pile caused thermal expansion, which, depending on the boundary conditions of the pile, induced additional axial stresses along its length. Except for the sensor located at a depth of 8.7 m, the stress increases measured in the field due to thermal expansion were in agreement with those obtained from the numerical model. The discrepancy at this depth can be attributed to a change in sensor positioning during pile installation in the field.

Important Considerations in the Numerical Modeling of Energy Piles: There are several important factors that must be taken into account when numerically modeling energy piles. The first is the definition of thermal boundary conditions, which must ensure that the surface temperatures of both the pile and the surrounding soil are consistent with those obtained from field experiments. Secondly, the positioning and installation of sensors in the field-tested pile is critical. Sensors should be placed on the reinforcement in such a way that their positions are not affected by external influences or the construction process. A third important consideration, particularly in water-saturated soils, is the need to account for the thermal properties of water, as it significantly influences heat transfer behavior.

7 Bibliography

- [1] United Nations, „World Population Prospects,” Department of Economic and Social Affairs, New York, 2019.
- [2] International Energy Agency, I. E. A., „Key World Energy Statistics,” International Energy Agency, PARIS, 2016.
- [3] Sunggyu Lee, James G. Speight, Sudarshan K. Loyalka, „Handbook of Alternative Fuel Technologies,” CRC Press, London, 2007.
- [4] Brandl, H., „Energy foundations and other thermo-active ground structures,” *Géotechnique*, vol. 56, nr. E-ISSN 1751-7656 / ISSN 0016-8505, pp. 81-122, 2006.
- [5] Bourne-Webb, P.J., Amatya, B., Soga, K., Amis, T., Davidson, C., Payne, P., „Géotechnique,” in *Geotechnical and thermodynamic aspects of pile response to heat cycles*, London, Emerald Publishing, 2015, pp. 237-248.
- [6] Laloui, L., Nuth, M., Vulliet, L., „Experimental and numerical investigations of the behaviour of a heat exchanger pile,” in *Numerical and Analytical Methods in Geomechanics*, Wiley Online Librar, 2006, pp. 763-781.
- [7] Sutman, M., „Thermo-mechanical behavior of energy piles,” in *Full-scale field testing and numerical modeling*, Virginia Tech, 2016.
- [8] Moradshahi, A., Faizal, M., Bouazza, A., McCartney, J.S., „Cross-sectional thermo-mechanical responses of energy piles,” in *Computers and Geotechnics*, 2021, p. 138.
- [9] Gao, J., Zhang, X., Liu, J., Li, K., Yang, J., „Numerical and experimental assessment of thermal performance of vertical energy piles,” *Appl. Energy*, 2008, pp. 901-910.
- [10] T. Y. ÖZÜDOĞRU, „The use of geothermal heat exchanger piles for sustainable design,” Istanbul Technical University, Istanbul, Sept 2015.
- [11] W. (J. K. Thomson, *Mathematical and Physical Papers*, London: Cambridge University Press,, 1884, pp. 41-60.
- [12] C. H.S, *Mathematical Theory of the Conduction of Heat in Solids*, New York, USA: Dover Publications, 1945.
- [13] H.S. Carslow, „*Mathematical Theory of the Conduction of Heat in Solids*,” New York, Dove Publication, 1945.
- [14] Ingersoll, L. R. and Plass, H. J., *Theory of the ground pipe heat source for the heat pump*, vol. 47, ASHVE Transactions, 1948, p. 339–348..
- [15] Abramovitz, M. and Stegun, I. A., *Handbook of mathematical functions*, Washington ,USA: US Government Printing Office, 1964.
- [16] Lamarche, L. and Beauchamp, B., „A new contribution to the finite line-source model for geothermal boreholes,” *Energy Build*, vol. 39, nr. doi:10.1016/j.enbuild.2006.06.003, p. 188–198., 2006.
- [17] H.S. Carslaw, J.C. Jaeger, *Conduction of Heat in Solids*, second ed, New York: Oxford University Press, 1959.
- [18] D. Marcotte, P. Pasquier, F. Sheriff, M. Bernier, „The importance of axial effects for borehole design of geothermal heat-pump systems,” in *Renew. Energ.*, *Renew. Energ.*, 2010, pp. 763-770.
- [19] L. Lamarche, B. Beauchamp, „A new contribution to the finite line-source model for geothermal boreholes,” in *Energy Build*, 2007, pp. 188-198.

Numerical modeling of thermal transfer through a refrigeration room wall - thermal bridge phenomenon highlighting

Simulare numerică transfer termic prin perete camera frigorifică – evidențierea fenomenului de punte termică

Mirela Tomoșoiu¹, GrațIELa Maria Țârlea¹

¹Universitatea Tehnică de Construcții București
Bulevardul Lacul Tei 124, București 020396, Romania
E-mail: mirela.tomosoiu@phd.utcb.ro

DOI: 10.37789/rjce.2025.16.3.9

Abstract. *The CFD simulations play an important role in heat transfer processes field, enabling heat transfer mechanism the analysis through conduction, convection and/or radiation, identifying critical points in thermal insulation systems, predicting the evolution of certain parameters in systems where heat transfer processes occur, optimizing the heat transfer system design, and improving their energy efficiency. Among the systems based on thermal transfer phenomena, the refrigeration systems require some of the highest energy consumption. Therefore, one of the most effective methods for these systems cost reducing is ensuring an optimal thermal insulation for the walls. CFD simulations can become a very useful tool in cold room parameters evaluation, such as temperature and humidity, as well as for critical areas identifying, where thermal bridges may occur, with results in uncontrolled thermal flows.*

Key words: CFD, computational fluid dynamics, cold room, refrigeration, thermal bridge, Ansys, thermal transfer modeling, convection, conduction

Rezumat. *Realizarea simulărilor CFD are un rol important în domeniul proceselor de transfer termic, permițând analiza mecanismelor transferului de căldură prin conducție, convecție și/sau radiație, identificarea punctelor critice în sistemele de izolație termică, estimarea evoluției unor parametri ai sistemelor în care au loc procese de transfer termic, optimizarea proiectării sistemelor de transfer termic și eficientizarea energetică a acestor sisteme. Între sistemele bazate pe fenomene de transfer termic, sistemele de refrigerare necesită unele din cele mai ridicate consumuri de energie. De aceea, una dintre cele mai utile metode de reducere a costurilor acestor sisteme este asigurarea unei optime izolații termice a pereților. Simulările CFD pot fi un instrument foarte util în evaluarea parametrilor de funcționare ai unei camere frigorifice, respectiv temperatură, umiditate, dar și pentru identificarea zonelor critice în care pot apărea punți termice generând fluxuri termice necontrolate.*

Cuvinte cheie: CFD, camere frigorifice, refrigerare, punte termică, Ansys, transfer termic, flux termic, simulare transfer termic, convecție, conducție

1. Introducere

Refrigerarea este una dintre tehnologiile mari consumatoare de energie, fiind răspunzătoare de aproximativ 35% din energia electrică consumată în industria alimentară [1]. De altfel costul energiei electrice are o pondere importantă în valoarea totală a costurilor operaționale de stocare în industria alimentară [2,3]. De aceea, identificarea unor metode de reducere a consumului de energie aferent funcționării camerelor frigorifice reprezintă un punct de mare interes pentru mulți cercetători din domeniu [4].

Fenomenul de punte termică apare atunci când într-o zonă a anvelopei unei clădiri rezistența termică se modifică semnificativ din diferite cauze: a) o străpungere totală sau parțială a anvelopei de materiale cu conductivități termice diferite și/sau b) o modificare a grosimii materialului și/sau c) o diferență între zonele interioară și exterioară cum sunt joncțiunile dintre perete/pardoseală/tavan [5].

O punte termică este o zonă din anvelopa unei clădiri în care fluxul termic este diferit (de obicei mai ridicat) comparativ cu zonele adiacente. Efectele unei punți termice pot fi: creșterea temperaturii suprafeței interioare, care în cele din urmă poate duce la acumularea umidității în interiorul peretelui și apariția mușgaiului și b) creșterea fluxului termic și prin urmare pierdea căldurii în exterior [6].

Puntea termică este zona în care intră în contact materiale cu conductivități termice diferite și prin care are loc o pierdere de căldură. În cazul camerelor frigorifice prin zonele unde se formează punți termice are loc un aport nedorit de căldură din exterior ceea ce duce inevitabil la afectarea mediului din interiorul camerei frigorifice cu un impact atât în consumul de energie cât și în deteriorarea produselor depozitate.

Există multe elemente în camerele frigorifice care pot duce la formarea unor punți termice, având ca rezultat fluxuri termice necontrolate cu consecințe în creșterea consumului de energie [7].

Astfel că, identificarea, încă din faza de proiectare, a zonelor în care se pot forma punți termice, poate aduce beneficii importante. Acest lucru poate fi realizat cu ajutorul simulărilor CFD (Computational Fluid Dynamics).

CFD reprezintă o ramură a mecanicii fluidelor care utilizează metode numerice și algoritmi pentru a rezolva și analiza probleme referitoare la curgerea fluidelor și transferul de căldură, permițând cercetătorilor și inginerilor să realizeze “experimente numerice” în “laboratoare virtuale” [8].

Analiza fenomenelor fizice complexe precum dinamica fluidelor, transferul de căldură sau propagarea undelor, se poate face utilizând ecuații diferențiale cu derivate parțiale care uneori pot avea un număr considerabil de variabile. Rezolvarea acestor ecuații sau sisteme de ecuații se face prin intermediul analizei cu elemente finite [9].

Unul dintre cele mai mari beneficii ale softurilor CFD este capacitatea de a rezolva ecuațiile care descriu curgerea fluidelor și transferul de căldură. Acest lucru se realizează prin discretizarea domeniului de lucru, respectiv descompunerea în volume de mici dimensiuni care apoi sunt studiate și asupra cărora se aplică ecuațiile matematice ce descriu fenomenele fizice pentru a se determina proprietățile fizice cum ar fi presiune, viteză și/sau temperatură. Rezolvarea ecuațiilor și determinarea soluției

numerice presupune parcurgerea unui proces iterativ care necesită resurse de calcul importante. Din acest motiv, aplicarea simulărilor CFD a luat o amploare deosebită în paralel cu evoluția capacității de calcul a computerelor [10].

Exemple de programe utilizate pentru realizarea de simulări CFD sunt: Ansys, COMSOL Multiphysics, SimFlow.

2. Metodologie

Lucrarea de față își propune să evidențieze modul în care poate fi evaluat comportamentul unui perete multistrat al unei camere frigorifice în condițiile nominale de lucru, respectiv modul în care realizarea diferită, uneori defectuoasă a îmbinărilor la colțurile pereților poate duce la crearea de punți termice.

Pentru aceasta se utilizează o simulare cu ajutorul software-ului Ansys versiunea 2024 R2 Student, respectiv a modulului Steady-State Thermal.

Se consideră o porțiune dintr-o zonă de colț a unei camere frigorifice realizată din panouri tip sandwich cu grosime de 100mm din poliuretan având la exterior tablă de oțel. Caracteristicile constructive și proprietățile materialelor din care este alcătuit peretele termoizolant sunt prezentate în Tabelul nr.1.

Tabelul 1

Caracteristici perete tip sandwich

Denumire strat	Material	Grosime (mm)	Coefficient conductivitate termică λ (W/mK)
Perete exterior	tablă oțel	1	0,022
Strat izolator	poliuretan	98	50,2
Perete interior	tablă oțel	1	0,022

Pentru a pune în evidență felul în care simularea va arăta zona în care apare fenomenul de punte termică, se iau în considerare două variante de îmbinare a pereților în zona de colț a camerei frigorifice.

Astfel într-o primă variantă, în zona de colț pereții au fost îmbinați fără a îndepărta porțiunea de tablă care intră în contact cu panoul alăturat în zona poliuretanului, iar stratul de poliuretan rămâne expus la exterior, nefiind protejat, așa cum se vede în Fig.1a. Acest tip de îmbinare este deficitară întrucât porțiunea de tablă din interior care ajunge la exteriorul peretelui va permite un transfer de căldură dinspre exterior către interior care va afecta negativ funcționarea camerei frigorifice.

În varianta a doua, îmbinarea s-a făcut după decuparea porțiunii de tablă și lipirea straturilor de poliuretan, asigurând și acoperirea integrală a poliuretanului la exterior Fig.1b.

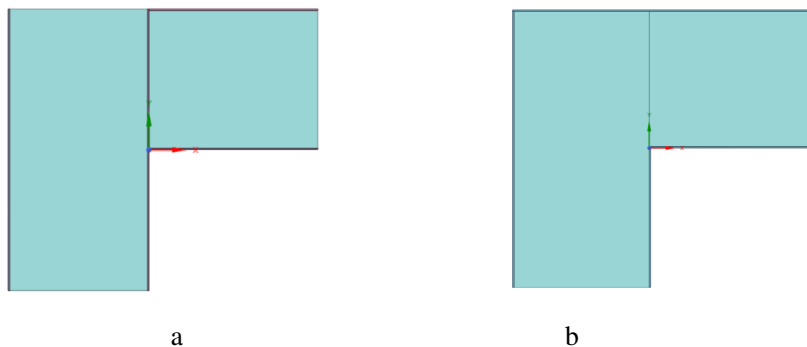


Fig. 1. Îmbinare de colț cameră frigorifică
a) Îmbinare de colț defectuoasă, b) Îmbinare de colț corectă

Pentru a realiza simularea modului în care se realizează transferul de căldură prin peretele camerei frigorifice într-o zonă în care este probabilă apariția fenomenului de punte termică, este necesară parcurgerea mai multor module ale aplicației de simulare.

În prima etapă se definește geometria elementului analizat.

În acest caz, este vorba de o porțiune de colț din peretele unei camere frigorifice așa cum se arată în Fig.2.

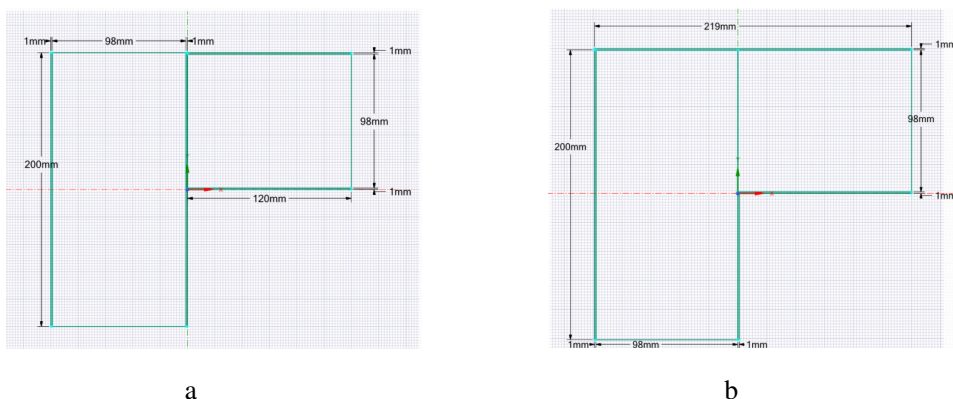


Fig. 2. Geometria elementului de construcție analizat
a) Îmbinare de colț defectuoasă, b) Îmbinare de colț corectă

În etapa următoare se definesc materialele componente peretelui multistrat și proprietățile acestora, urmând apoi să fie asociat fiecărei suprafețe materialul și implicit proprietățile aferente (Fig.3).

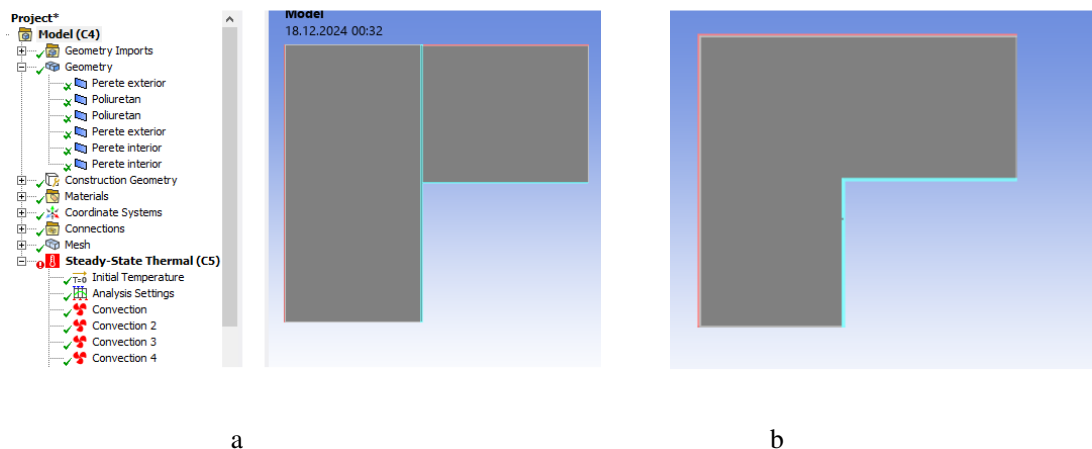


Fig. 3. Atribuirea materialelor și a caracteristicilor pentru fiecare suprafață în parte
a) Îmbinare de colț defectuoasă, b) Îmbinare de colț corectă

Următoarea etapă presupune stabilirea grilei de calcul, respectiv rețeaua de noduri necesară discretizării fiecărui domeniu în parte pentru aplicarea algoritmilor de calcul. (Fig.4)

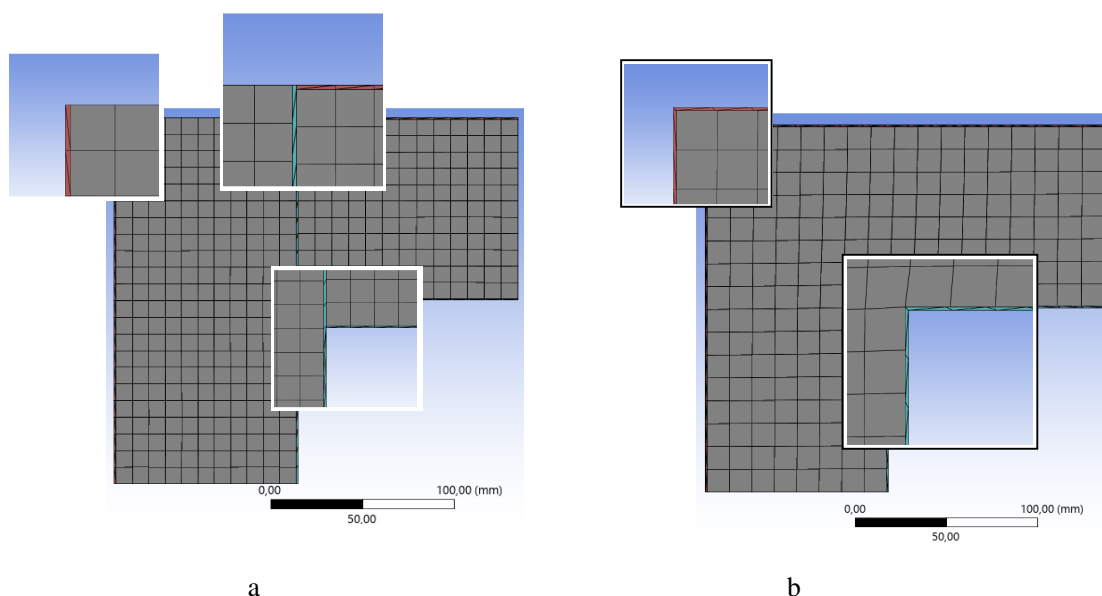


Fig. 4. Construirea rețelei cu nodurile de discretizare
a) Îmbinare de colț defectuoasă, b) Îmbinare de colț corectă

Este necesar să fie definite condițiile la limită, respectiv să fie definite fenomenele fizice ce se desfășoară la limitele elementului de construcție studiat.

Condițiile la limită (boundary conditions) sunt elemente extrem de importante în simularea numerică deoarece sunt principala modalitate prin care poate fi configurat cazul la care se lucrează prin simulare numerică.

Condițiile la limită descriu parametri/mărimile pe frontiera domeniului de interes, această informație de pe frontieră propagându-se în domeniul de calcul prin intermediul modelului matematic din cadrul programului de simulare numerică.

“Evident că, dacă condițiile la limită nu vor fi suficient de bine configurate/alese, și rezultatele obținute vor avea de suferit. În limba engleză expresia consacrată în domeniul CFD pentru acest lucru este “Garbage IN, Garbage OUT!”. Adică, dacă se vor introduce date de intrare/condiții la limită neconforme și rezultatele obținute vor fi greșite / neconforme / departe de realitate” [11].

Astfel, la interior are loc un fenomen de convecție între peretele interior și stratul de aer din imediata vecinătate a acestuia.

Datele necesare pentru configurarea condițiilor la limită pentru peretele rece (interior) sunt: valoarea coeficientului de convecție termică la interior care are valoarea de $8\text{W/m}^2\text{K}$ și temperatura la interior -18°C .

Pentru configurarea condițiilor la limită pentru peretele cald (exterior) sunt: valoarea coeficientului de convecție termică la exterior care are valoarea de $23\text{W/m}^2\text{K}$ și temperatura la exterior 22°C .

Pentru zonele în care elementul de perete este decupat pentru limitarea zonei studiate (evidențiate cu culoare albastră în fig.2) se consideră că valoarea fluxului termic este egală cu 0, transferul de căldură realizându-se numai pe direcția transversală a peretelui, de la temperatura mai mare (peretele exterior) la temperatura mai joasă (peretele interior).

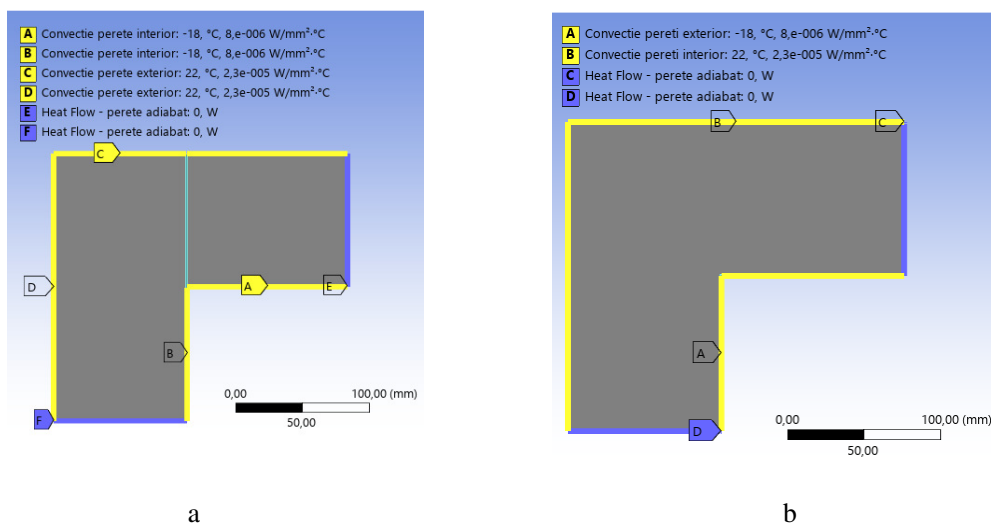


Fig. 5. Stabilirea condițiilor la limita domeniului studiat
a) Îmbinare de colț defectuoasă, b) Îmbinare de colț corectă

După definirea condițiilor la limită, se poate trece la aplicarea și rezolvarea modelului matematic și apoi la prelucrarea rezultatelor.

3. Rezultate

Programul permite obținerea mai multor tipuri de informații.

De interes pentru aplicația de față ar fi, în primul rând, distribuția valorilor temperaturii în interiorul peretelui (Fig.6). Pot fi puse în evidență punctele în care temperatura atinge valoarea maximă, respectiv minimă și de asemeni poate fi indicată temperatura într-un anumit punct de interes.

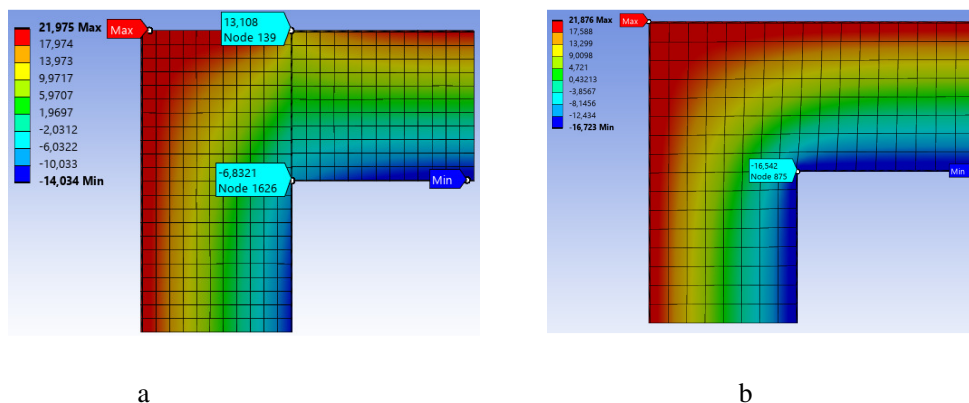


Fig. 6. Distribuția temperaturii în perete
a) Îmbinare de colț defectuoasă, b) Îmbinare de colț corectă

Pentru situația studiată se observă în primul rând o afectare evidentă a profilului temperaturilor în zona în care în interiorul peretelui a rămas stratul interior de tablă, față de situația în care acest strat a fost îndepărtat. De asemeni se evidențiază faptul că există o diferență importantă între valorile temperaturilor în colțul interior al peretelui în cele două cazuri: $-6,8^{\circ}\text{C}$ față de $-16,5^{\circ}\text{C}$.

Informații de interes pot fi obținute și prin evidențierea distribuțiilor fluxului termic prin perete. Cum era ușor de intuit, în zona stratului de tablă rămas în interiorul peretelui, fluxul termic are valori mult mai mari comparativ cu restul peretelui, putând fi determinate și valorile numerice ale acestuia. (Fig.7)

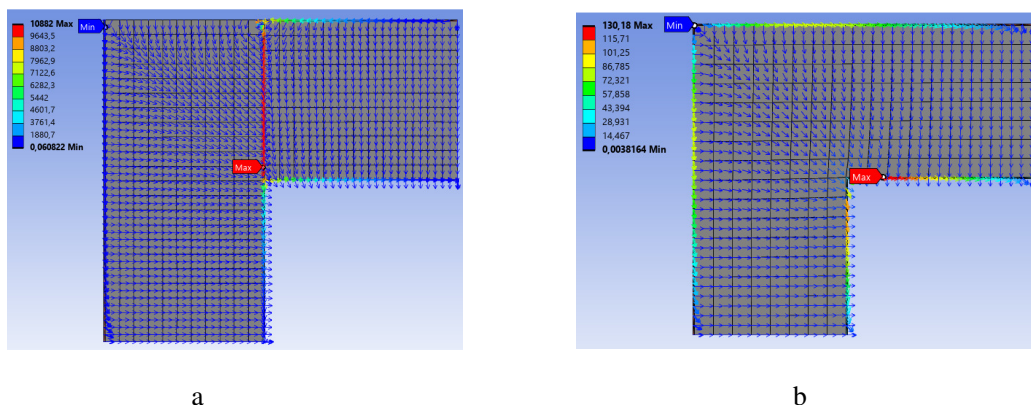
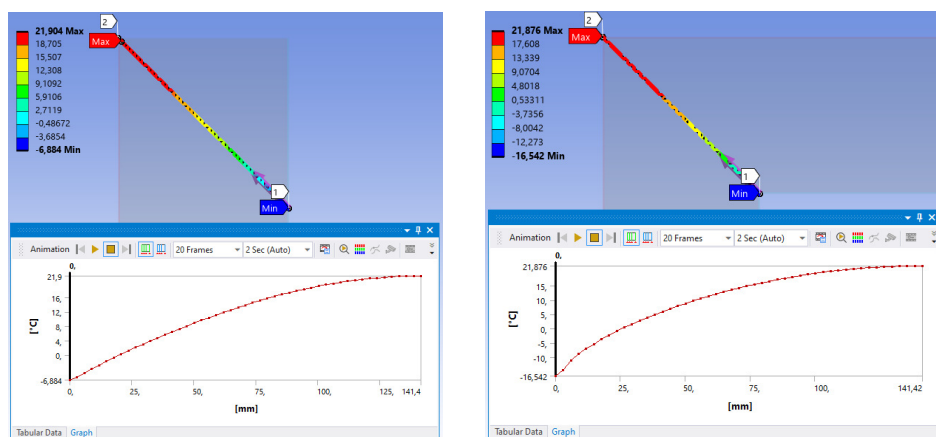


Fig. 7. Distribuția fluxului termic prin perete
a) Îmbinare de colț defectuoasă, b) Îmbinare de colț corectă

Simulare numerică transfer termic prin perete camera frigorifică – evidențierea fenomenului de punte termică

O altă variantă de extragere a unor informații utile permite stabilirea unei anumite secțiuni a peretelui în care să poată fi studiat în detaliu profilul unui anumit parametru, în cazul de față profilul de temperaturi. (Fig.8)



a b
Fig. 8. Distribuția temperaturii în zona de colț a peretelui
a) Îmbinare de colț defectuoasă, b) Îmbinare de colț corectă

Aceste informații pot fi obținute atât grafic, cât și tabelar, ceea ce permite exportarea datelor într-un fișier Excel și utilizarea lor la întocmirea unor grafice comparative. (Fig.9)

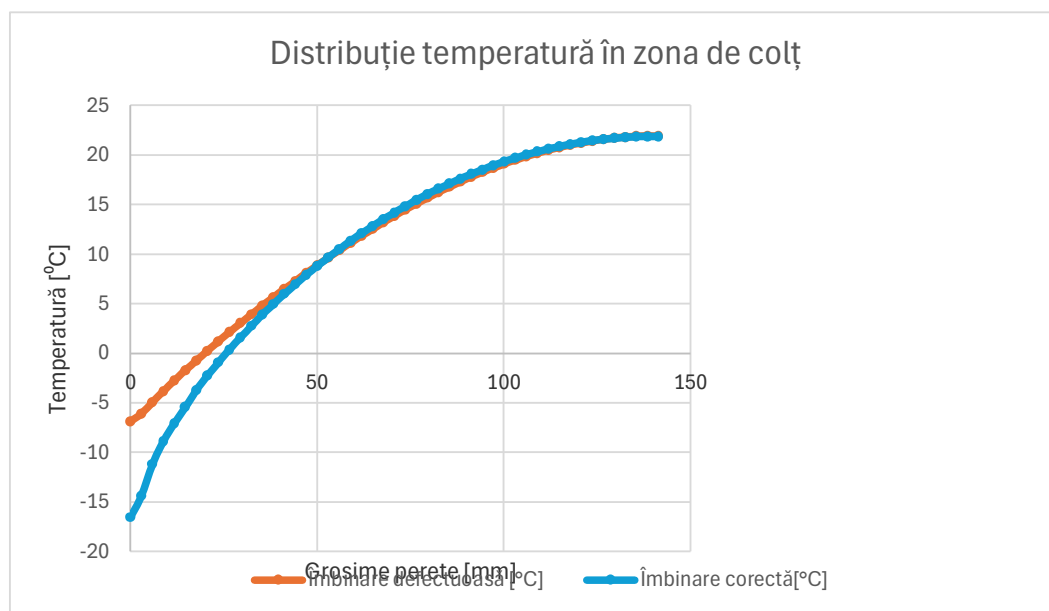


Fig.9. Reprezentarea comparativă a distribuției temperaturii în zona de colț a peretelui

4. Concluzii

Datorită progreselor înregistrate în ultimele decenii în domeniul tehnicii de calcul, simulările CFD au devenit un instrument deosebit de puternic în domeniul cercetării și al ingineriei.

Realizarea simulărilor CFD are un rol important în domeniul proceselor de transfer termic, permițând analiza mecanismelor transferului de căldură prin conducție, convecție și/sau radiație, identificarea punctelor critice în sistemele de izolație termică, estimarea evoluției unor parametri ai sistemelor în care au loc procese de transfer termic, optimizarea proiectării sistemelor de transfer termic și eficientizarea energetică a acestor sisteme.

În concluzie, Computational Fluid Dynamics (CFD) ar putea deveni un instrument indispensabil pentru simularea proceselor de transfer de căldură și dinamicii fluidelor în diverse aplicații. Capacitatea de analiză și optimizare a performanței termice, identificarea punctelor sensibile încă din faza de proiectare a sistemelor duce la îmbunătățirea eficienței energetice, a siguranței în utilizare și a fiabilității acestora. Posibilitatea de predicție a comportamentului unui sistem în diferite condiții de funcționare, fără a fi necesare costuri asociate realizării unor prototipuri sau standuri de încercări, fac din CFD un real sprijin pentru cercetătorii din multe domenii ingineresti, inclusiv HVAC-R, iar pe măsură ce cererea pentru sisteme eficiente din punct de vedere energetic și de înaltă performanță continuă să crească, importanța CFD în simularea termică va crește, devenind o componentă critică în dezvoltarea soluțiilor tehnice.

Referințe

- [1] X.Q. Li, P.E. Campana, H.L. Li, J.Y. Yan, K. Zhu, Energy storage systems for refrigerated warehouses, *Energy Procedia* 143 (2017) 94–99.
- [2] J.A. Evans, E.C. Hammond, A.J. Gigiel, A.M. Foster, L. Reinholdt, K. Fikiin, C. Zilio, Assessment of methods to reduce the energy consumption of food cold stores, *Appl. Therm. Eng.* 62 (2014) 697–705.
- [3] A.M. Foster, L.O. Reinholdt, T. Brown, Reducing energy consumption in cold stores using a freely available mathematical model, *Sustain. Cities Soc.* 21 (2016) 26–34.
- [4] X..Jiang, A. Lin, H.Ma,X. Li, Y. Li, Minimizing the thermal bridge through the columns in a refrigeration room, *Applied Thermal Engineering* 165 (2020) 114565.
- [5] EN ISO 10211-1, Thermal bridges in building construction: heat flows and surface temperatures. Part 1. General Calculation Methods, 1995.
- [6] "Definition and effects of thermal bridges []". *passipedia.org*. Retrieved 2017-11-05.
- [7] I. Garrido, S. Lagüela, P. Arias, Thermal-based analysis for the automatic detection and characterization of thermal bridges in buildings, *Energy Build.* 158 (2018) 1358–1367.
- [8] <http://server.ce.tuiasi.ro/~ddiaconu/download/FOC/Imprastierea%20fumului%20si%20gazelor%20fierbinti%20-%20analiza%20CFD.pdf> - drd. ing. Zeno Grigoras
- [9] <http://ro.insta3dm.com/info/what-is-finite-element-analysis-and-how-does-i-63479542.html>
- [10] <https://sim-flow.com/download/cfd-simulation-software/>
- [11] Bode F. Simularea numerică a proceselor de transfer termic – Aplicații, UTPRESS Cluj-Napoca, 2021, ISBN 978-606-737-505-3

- [12] A. Kecebas, M. Kayveci, Effect on optimum insulation thickness, cost and saving of storage design temperature in cold storage in Turkey, *Energy Education Science and Technology Part A: Energy Science and Research* 2010 Volume (Issue) 25(2): 117-127
- [13] J.A. Evans, A.M. Foster, J.-M. Huet, L. Reinholdt, K. Fikiin, C. Zilio, et al., Specific energy consumption values for various refrigerated food cold stores, *Energy Build.* 74 (2014) 141–151.
- [14] X.Q. Li, P.E. Campana, H.L. Li, J.Y. Yan, K. Zhu, Energy storage systems for refrigerated warehouses, *Energy Procedia* 143 (2017) 94–99.
- [15] J.A. Evans, E.C. Hammond, A.J. Giegel, A.M. Foster, L. Reinholdt, K. Fikiin, C. Zilio, Assessment of methods to reduce the energy consumption of food cold stores, *Appl. Therm. Eng.* 62 (2014) 697–705.
- [16] A.M. Foster, L.O. Reinholdt, T. Brown, Reducing energy consumption in cold stores using a freely available mathematical model, *Sustain. Cities Soc.* 21 (2016) 26–34.
- [17] I. Garrido, S. Lagüela, P. Arias, Thermal-based analysis for the automatic detection and characterization of thermal bridges in buildings, *Energy Build.* 158 (2018) 1358–1367.
- [18] A. Reilly, O. Kinnane, The impact of thermal mass on building energy consumption, *Appl. Energy* 198 (2017) 108–121.

Retrofit of refrigeration installations with low GWP refrigerants

Modernizarea instalațiilor frigorifice cu agenți frigorifici cu GWP scăzut

Mihai Adrian, Tokar Adriana

¹Universitatea Politehnica Timișoara
Timisoara, Piața Victoriei, nr. 2, Romania
E-mail: mihaiadrian@yahoo.com, adriana.tokar@upt.ro

DOI: 10.37789/rjce.2025.16.3.10

Abstract. Technological developments in the refrigerant industry based on the limitations imposed by REGULATION (EU) 2024/573 OF THE EUROPEAN PARLIAMENT AND OF THE COUNCIL of 7 February 2024 on fluorinated greenhouse gases, amending Directive (EU) 2019/1937 and repealing Regulation (EU) No. 517/2014 have aligned with this regulation and, together with refrigeration equipment manufacturers, have begun to introduce refrigerants with a GWP (Global Warming Potential) of less than 150 units into the European market. This paper presents a method for the modernization of small and medium-sized commercial refrigeration installations using refrigerants such as R448A or R449A, as well as the technical implications that must be taken into account in the modernization process.

Key words: Retrofit, commercial refrigeration, R449A, R448A, R455A, GWP

Rezumat. Evoluția tehnologică în industria agenților refrigeranți bazată pe limitările impuse de REGULAMENTUL (UE) 2024/573 AL PARLAMENTULUI EUROPEAN ȘI AL CONSILIULUI din 7 februarie 2024 privind gazele fluorurate cu efect de seră, de modificare a Directivei (UE) 2019/1937 și de abrogare a Regulamentului (UE) nr. 517/2014 s-a aliniat acestui regulament și împreună cu producătorii de echipamente frigorifice au început introducerea în piața europeană a refrigeranților cu GWP (Potential de Încălzire Globală) mai mic de 150 unități.

Prezenta lucrare prezintă o metodă de modernizare a instalațiilor frigorifice comerciale de puteri mici și medii ce utilizează refrigeranți precum R448A sau R449A, cât și implicațiile tehnice care trebuie luate în considerare în procesul modernizării.

Cuvinte cheie: Retrofit, refrigerare comercială, R449A, R448A, R455A, GWP

1. Introducere

Având în vedere Regulamentul (UE) 2024/573 al Parlamentului European și al Consiliului din 7 februarie 2024 privind gazele fluorurate cu efect de seră, de

modificare a Directivei (UE) 2019/1937 și de abrogare a Regulamentului (UE) nr. 517/2014, instalațiile frigorifice trebuie modernizate, atât cele existente cât și cele noi proiectate. Noile condiții de funcționare impuse de noii refrigeranți care îndeplinesc condițiile regulamentului ce a început să fie aplicat încă din 11 martie 2024, impun măsuri noi de limitare a pierderilor.

Având în vedere faptul că noua generație de refrigeranți cu GWP redus sunt ușor inflamabili trebuie să ne asigurăm că echipamentele și condițiile de exploatare sunt adecvate.

Modernizarea unui sistem frigorific trebuie realizată în colaborare cu un inginer în instalații frigorifice și trebuie realizată de asemenea cu maximă responsabilitate față de mediu, personal și bugetul alocat unei astfel de investiții, luând în considerare și impactul total generat asupra mediului TEWI (Total Equivalent Warming Impact), care se determină prin calcul.

Înainte de toate și poate cel mai important aspect de urmărit în procesul modernizării este acela ca toate tipurile de agenți frigorifici inflamabili trebuie utilizați doar în echipamente frigorifice ce au fost proiectate să funcționeze cu astfel de refrigeranți respectând standardele și normele în construcții.

Clasificarea categoriilor de inflamabilitate ne ajută să înțelegem și ce acțiuni trebuie realizate, astfel că avem următoarele categorii de clasificare conform standardului ISO 817:

Litera indică nivelul de toxicitate

A = Agenți frigorifici cu toxicitate redusă ;

B = Agenți frigorifici cu toxicitate ridicată;

Numărul indică nivelul de inflamabilitate

1 = neinflamabil;

2L = ușor inflamabil;

2 = inflamabil;

3 = foarte inflamabil.

Cei mai mulți agenți frigorifici folosiți în prezent în instalațiile din România sunt clasificați ca A1 (toxicitate redusă și neinflamabili).

Astfel de refrigeranți cum sunt R134a, R407C, R404A, R448A, R449A, R452A sunt utilizați cu precădere în aplicații de climatizare auto, climatizare industrială, pompe de căldură, refrigerare comercială și industrială.

Totodată refrigeranții din categoria A2L deja prezenți în instalațiile frigorifice de climatizare în special fie rezidențiale, fie auto sau industriale precum R32, R-1234yf și R1234ze, R454C, R455A, au o toxicitate redusă și sunt ușor inflamabili.

În privința refrigeranților prezenți în special în aplicații domestice cât și în aplicații comerciale de puteri foarte mici și mici precum R290, R600a și R1270, ei fiind clasificați A3, adică au o toxicitate redusă și sunt foarte inflamabili.

În aplicațiile industriale de puteri mari de ordinul sutelor de kilowați devine eficientă folosirea refrigerantului R717 (NH₃- amoniac) însă el este clasificat ca B2L adică are o toxicitate ridicată și ușor inflamabil.

Alte caracteristici importante de luat în considerare când se caracterizează nivelul de inflamabilitate precum 1, 2L, 2 sau 3 al unui refrigerant este viteza de ardere, limita maxima (UFL) și minimă (LFL) de inflamabilitate, energia minimă de aprindere (MIE) și căldura degajată prin ardere (HOC). Aceste caracteristici limitează aria de aplicativitate, pentru că trebuie să respecte standardele de siguranță și standardele generale de siguranță ale instalațiilor și aparatelor frigorifice.

Standardele de siguranță dau liniile directe și referințe importante care pot fi folosite uneori și ca îndrumări practice sub forma unor reguli de respectat ca bună practică și dacă sunt respectate întocmai pot fi folosite ca metoda de a demonstra conformitatea cu legislația.

Frigotehniștii cât și utilizatorii echipamentelor frigorifice și de climatizare trebuie întotdeauna să urmeze instrucțiunile de instalare și de utilizare ale producătorilor de echipamente. Producătorii la rândul lor trebuie să asigure respectarea legislației locale (EX.: normele în construcții). Dacă nu există astfel de instrucțiuni, de exemplu atunci când un tehnician sau un utilizator modifică echipamentele sau assemblează echipamentul propriu, tehnicianul sau utilizatorul devine „producător“ și prin urmare, va fi responsabil pentru siguranța echipamentului respectiv.

Standardul general de siguranță în instalații frigorifice EN378:2016 și standardele de siguranță ale aparatelor, cum ar fi EN60335-2-40, EN60335-2-89, oferă informații relevante, de exemplu pentru a se asigura că instalațiile nu depășesc încărcătura maximă de agent frigorific într-o anumită zonă.

Referitor la EN378:2016 este un standard general al instalațiilor frigorifice, în timp ce EN60335-2-40, EN60335-2-89 și EN60335-2-24 sunt exemple de standarde ale aparatelor. Uneori, standardele generice ale instalațiilor și cele ale aparatelor se referă la cerințe similare, de exemplu încărcătura maximă admisibilă pentru anumite încăperi. În astfel de cazuri, cerințele standardelor aparatelor prevalează asupra celor menționate în standardul general al instalațiilor. De exemplu, pentru aparatele de climatizare sau pompele de căldură, prevalează încărcătura maximă admisibilă pentru agenți inflamabili din standardul EN60335-2-40. Pe de altă parte, în privința toxicității, prevalează cerințele EN378:2016, deoarece acest aspect nu este inclus în standardul aparatelor.

2. Conținutul lucrării

Studiul de caz se referă la modernizarea unei instalații frigorifice aferentă unei camere frigorifice cu spațiu vitrat de expunere și desfacere cum sunt cele din benzinării. În proiectarea inițială a instalației s-a ținut cont de reglementările în vigoare și cele viitoare , selectându-se echipamente compatibile cu noii refrigeranți A2L cu GWP sub 150 unități, în speță R455A. Dar din motive de disponibilitate precară și la un cost ridicat a refrigerantului în momentul punerii în opera a investiției s-a optat pentru un refrigerant cu GWP sub 2500 unități (R449A-GWP1397), fiind admis la

vremea aceea. Odată cu modificarea legislației se dorește modernizarea ei, astfel încât să corespundă noilor reglementări. Sistemul cu expansiune directă inițial analizat este compus din agregat carcasat insonorizat Emerson model ZXMY-020E-TFD, vaporizator Kelvion KSC-301-6BE-FX28, valvă electronică pulsatorie Danfoss AKV10P4, electroventil Danfoss EVO 101 și tablou electric de comanda și control Pego ECP 200 Expert Pulse funcționare cu agent frigorific R449A, GWP = 1397; grupa A1.

Sistemul modernizat implică înlocuirea agentului frigorific cu R455A, GWP = 148; grupa A2L și analiza noilor parametri ai instalației astfel încât să fie menținuți parametrii aplicației.

Tema de analiza realizată comparativ, s-a efectuat pentru o cameră frigorifică cu perete vitrat și uși pentru autoservire (Fig.1.) având ca scop minimizarea impactului modificărilor aduse prin înlocuirea refrigerantului urmărind:

- compararea parametrilor tehnico-economici;
- compararea consumului de energie;
- impactul asupra mediului.



Fig.1. Cameră frigorifică cu autoservire

2.1 Descrierea incintei analizate

Analiza de fezabilitate a soluției s-a pretat pentru o cameră frigorifică având plafonul și pereții din panou tristrat 80mm (Fig.2), finisat la interior cu tablă de oțel, vopsea plastifiată albă, nontoxică, certificată pentru uz alimentar. Pardoseala este pavată cu gresie antiderapantă A1FL, 33,3x33,3 0,95 cm, montată cu rosturi de 2mm. Izolația panourilor este spumă de înaltă densitate 40-42kg/m³ care nu întreține arderea, conform ISO3582, fără CFC. Coeficient de conductibilitate termică: $\lambda=0,33 \text{ W/m}^2\text{K}$.

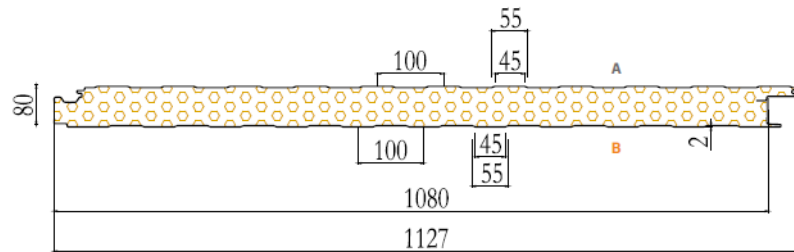


Fig.2. Panou tristrat 80mm; PIR 80

Suprafața camerei analizate este $S = 9 \text{ m}^2$ și o înălțime $H = 2,5 \text{ m}$ (Fig.3)
 Pardoseala de beton de 20 cm grosime este pentru o capacitate portanta de 50 kN/mp.

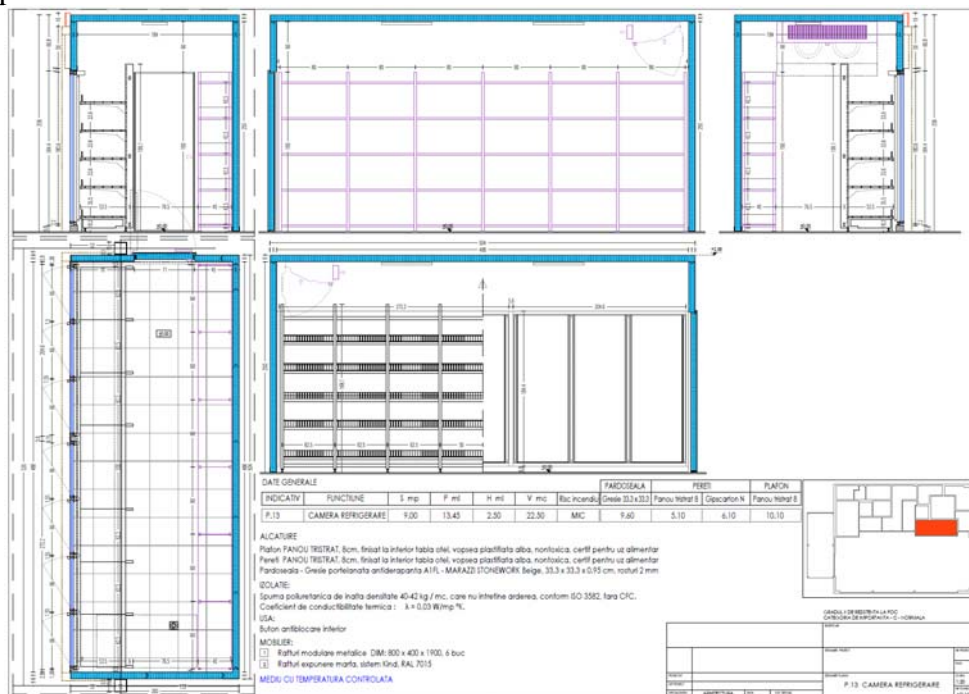


Fig. 3. Camera frigorifica analizata

Mai jos sunt datele de intrare extrase din programul de calcul al necesarului termic (Fig.4):

Cold Store Cooling Load Calculator.

Client:
Project:

Enquiry N°.
Date. 4/24/2025

Cold Store Dimensions (Internal)

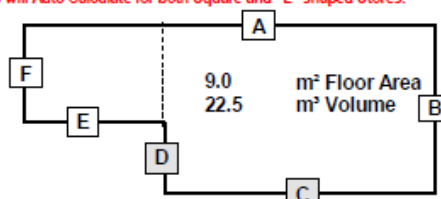
Inputs

Cold Store Configuration.

For a Square or Rectangular Store input Dimensions A & B only. C & D will Auto Calculate for both Square and "L" shaped Stores.

Dimension for Wall A
Dimension for Wall B
Dimension for Wall C
Dimension for Wall D
Dimension for Wall E
Dimension for Wall F
Cold Store Height.

5	m
1.8	m
5	m
6	m
0	m
0	m
2.5	m



Information

Cold Store Temperature .

Ambient Temperature Wall A.
Ambient Temperature Wall B.
Ambient Temperature Wall C.
Ambient Temperature Wall D.
Ambient Temperature Wall E.
Ambient Temperature Wall F.
Ambient Temperature Ceiling.
Ambient Temperature Floor.

Inputs

2	°C
23	°C
23	°C
23	°C
23	°C
	°C
	°C
30	°C
16	°C

Values used in Calculation.

21	Wall TD °C
21	Wall TD °C
21	Wall TD °C
21	Wall TD °C
	Wall TD °C
	Wall TD °C
	Wall TD °C
28	Ceiling TD °C
14	Floor TD °C

Wall Insulation.

Wall Insulation Thickness.

Ceiling Insulation.

Ceiling Insulation Thickness.

Floor Insulation.

Floor Insulation Thickness.

Polyurethane (PUR)

80 mm

80 mm

80 mm

Concrete (No Insulation)

200 mm

0.025 K Value. W/m.K

0.313 U Value. W/m².°C

0.025 K Value. W/m.K

0.313 U Value. W/m².°C

0.550 K Value. W/m.K

2.750 U Value. W/m².°C

Product.

Approx. Product Mass per m³
Product Input Load per Day.
Total Weight of Product in the Store.
Temperature of Product Entering Store.
Final Product Temperature.

Water

230 Kg/m³

700 Kg

2000 Kg

20 °C

4 °C

4.19 SH above Freezing. kJ/Kg°C

2.10 SH below Freezing. kJ/Kg°C

334 Latent Heat. kJ/Kg.

Respiration. kJ/kg/24h.

Freezing Temperature °C

Air Changes per Day

Store Usage Factor.

Heavy Traffic

21.1 Air Changes/24hr.

2 Factor

Number of Personnel

Personnel Hours per Day

2

1 Hrs.

330 Watts / Person.

Number of Trucks

Rating of Truck. (Typically 3000 Watts)
Trucks Hours per Day

1

1 Watts
Hrs.

Watts

Lighting in Watts

or

Lighting in Watts per m²

Lighting Hours per Day.

100

Watts

100

Watts

Watts / m²

Hrs.

Watts

Additional Loads.

100

Watts/hr

100

Watts

Wall A	13.3	m ²	87.4 Watts.	
Wall B	5.1	m ²	33.2 Watts.	
Wall C	13.3	m ²	87.4 Watts.	
Wall D	5.1	m ²	33.2 Watts.	
Wall E		m ²	Watts.	
Wall F		m ²	Watts.	
Ceiling	9.0	m ²	78.8 Watts.	
Floor	9.0	m ²	346.5 Watts.	
Insulation Total			666.4 Watts.	25.8%
Product Load				
SH above Freezing	4.19	kJ/Kg°C	543.1 Watts.	
SH below Freezing.		kJ/Kg°C	Watts.	
Latent		kJ/Kg	Watts.	
Respiration		kJ/Kg/24h	Watts.	
Product Total			543.1 Watts.	21.0%
Air Change Load	71	kJ/m ³	781.1 Watts.	30.3%
Personnel Load			27.5 Watts.	1.1%
Truck Load			Watts.	
Lighting Load based on Wattage			Watts.	
Lighting Load based on Watt/m²			Watts.	
Additional Load			100.0 Watts.	3.9%
Total Load (Net)			2118.1 Watts.	
Hours Run per Day	20	Hrs.	2541.7 Watts.	
Cooler Fan Motor Input Power.	145	Watts.	196.1 Watts.	6.3%
Guide Value (Click Box if accepted)	145	Watts		
Applicable for KÜBA Coolers Only.				
Defrost Heat Load.	1195	Watts.	78.8 Watts.	2.5%
Guide Value (Click Box if accepted)	1195	Watts.		
Defrosts per Day.	4			
Defrost System.	Electric Defrost (Time Control)			
Contingency Allowance %	10	%	281.7 Watts.	9.1%
Total Cooling Load.			3.1 kW	

Fig. 4. Necesar termic camera frig

2.2 Variantele generate de refrigerantul utilizat

Soluțiile tehnice analizate constau în compararea funcționării unei instalații de refrigerare cu detentă directă ce funcționează cu refrigerant R449A respectiv, după modernizare, cu refrigerant R455A raportându-ne la consumul de energie, protecția mediului și măsurile de siguranță în exploatare.

Prima instalație ce funcționează cu refrigerant A1L, R449A este compusă din agregat frigorific ZMY-020E-TFD (Fig.5) carcasat și complet automatizat frigorific și electronic pregătit și pentru refrigeranți A2L, cu un compresor marca Copeland model YB12K1E-TFD (Fig.6) și un vaporizator marca Kelvion model KSC-301-6BE-FX28(Fig.7) complet echipate cu valvă termostatică pulsatorie Danfoss AKV10PS4

068F4034 (Fig.8), robineti de separatie, electroventil Castel (Fig.9) si tablou automatizare Pego ECP200 Expert Pulse (Fig.10) .



Fig. 5. ZMY-020E-TFD



Fig. 6. YB12K1E-TFD



Fig. 7. KSC-301-6BE-FX28



Fig. 8. AKV10PS4



Fig. 9. Electroventil Castel A2L



Fig. 10. ECP200 Expert Pulse

Parametrii tehnici ai agregatului Copeland ZMY-020E-TFD – R449A sunt prezentați mai jos în Fig.11. și performanțele energetice în Fig. 12.

Refrigerant	R449A Arith. Mean Temp.
High Side Properties:	
Condensing Temperature, °C	45.40
Abs. Condensing Pressure, bar	20.06
Dew Point, °C	47.50
Bubble Point, °C	43.30
Saturated vapour enthalpy, kJ/kg	415.00
Specific volume of saturated vapour, dm³/kg	10.50
Low Side Properties:	
Evaporating Temperature, °C	-10.00
Evaporating Abs. Pressure, bar	3.84
Dew Point, °C	-8.30
Bubble Point, °C	-13.80
With vapour at, °C	1.70
Specific volume, dm³/kg	62.30
Enthalpy, kJ/kg	404.00
Operating Conditions:	
Evaporating Temperature, °C	-10.00
Suction Superheat, K	10.00
Ambient, °C	38.00
Condensing Unit Selected	ZXMY-020E-TFD

Fig. 11. Parametrii ZMY-020E-TFD – R449A

PERFORMANCE AT SPECIFIED OPERATING POINT
ZXMY-020E-TFD Data at 50 Hz

Evaporating Abs. Pressure, bar	3.84
Abs. Condensing Pressure, bar	20.06
Cooling Capacity, kW	3.28
Total Power Input, kW	1.72
COP	1.90
Current at 400 V, A	3.01
Mass Flow, g/s	23.90
Heating Capacity, kW	4.80
Condensing Temperature, °C	45.40
Subcooling at the Unit's outlet, K	0.00

Fig. 12. Performante energetice ZMY-020E-TFD – R449A

Parametrii tehnici ai vaporizatorului Kelvion KSC-301-6BE-FX28 R449A sunt prezentați în Fig. 13, iar parametrii fizici sunt prezentați în Fig 14.

Capacity [kW]	3,49	Sensible heat ratio (SHR) [-]	0,72	Refrigerant	R449A (Dupont XP40)
Air inlet temp. [°C]	0,0	Air outlet temp. [°C]	-4,6	Operation mode	EC
Rel. humidity [%]	85,0	Evaporation temp. [°C] (Mid point)	-10,0		

AIR DATA	HEAT EXCHANGER	MATERIALS
Air volume flow 1.500 m³/h	Surface 11,4 m²	Tubes Copper
Ext. static pressure 0 Pa	Fin spacing 7 mm	Fins Alu
Air throw 10 m	Internal volume 3,7 dm³	End plates Alu
Altitude 0 m	Liquid temp. 22,0 °C	Casing Alu
Air outlet rel. humidity 97,8 %	Superheating temp. -2,8 °C	Finish powder coated, white (RAL 9010)
	Max. operating pressure 32 bar	

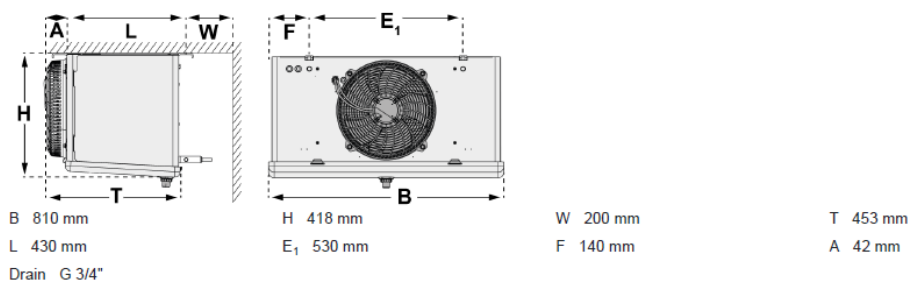
FAN(S)

1 PIECE(S): 230V/1PH/50-60HZ; IP54	SELECTED SPEED DATA (PER FAN) ⁽³⁾	FAN SET SERIAL PLATE DATA (PER FAN)
Fan diameter 300 mm	Operation mode EC - S1	Operation mode EC
Range of temp. -40,0 to 60,0 °C	Speed 1650 rpm	Speed 1640 rpm
Sound power LwA 67 dB(A)	Power input 94 W	Power nominal 110 W
Sound pressure LpA (3m) ⁽²⁾ 46 dB(A)	Operating current 0,6 A	Current draw 1,0 A
Optional controller, on site ⁽⁵⁾ EC controller	Control voltage EC 10 V	Protector Built in protector, connected internal
ErP 2015	Energy efficiency class C	

CONNECTIONS ⁽⁷⁾	WEIGHT ⁽⁴⁾	DEFROST
Inlet Cu 12 mm	Dry weight 22 kg	Electric defrost
Outlet Cu 22 mm	Weight incl. packing 27 kg	Coil 1,61 kW
Refrigerant distribution Venturi		Drip tray 0,54 kW
		Total 2,15 kW

Fig. 13. Parametrii KSC-301-6BE-FX28 – R449A

DIMENSIONS ⁽⁴⁾



Packing dimensions (height x length x width): 530 x 910 x 600 mm

Fig. 14. Parametrii gabaritici KSC-301-6BE-FX28 – R449A

Cea de-a doua variantă modernizată, are aceleași componente ca și cea de mai sus însă funcționează cu refrigerant A2L – R455A. Acest nou refrigerant din cauza că are alte proprietăți fizico-chimice necesită verificarea parametrilor agregatului în noile condiții, iar faptul este ușor inflamabil schimbă un pic datele soluției tehnice inițiale pentru ca necesită măsuri suplimentare de siguranță în exploatare precum detector de refrigerant în camera frigorifică DGS-SC HFC grup 1* 080Z2803 (Fig.15).



Fig.15 DGS-SC HFC grup1

* HFC grup 1: R1234ze, R454C, R1234yf, R454A, R455A, R452A, R454B, R513A.

Parametrii tehnici ai agregatului Copeland ZMY-020E-TFD – R455A sunt prezentați mai jos în Fig.16 și performantele energetice în Fig. 17.

Refrigerant	R455A Arith. Mean Temp.
High Side Properties:	
Condensing Temperature, °C	46.40
Abs. Condensing Pressure, bar	20.47
Dew Point, °C	51.00
Bubble Point, °C	41.80
Saturated vapour enthalpy, kJ/kg	414.00
Specific volume of saturated vapour, dm ³ /kg	10.40
Low Side Properties:	
Evaporating Temperature, °C	-10.00
Evaporating Abs. Pressure, bar	3.91
Dew Point, °C	-6.20
Bubble Point, °C	-18.50
With vapour at, °C	3.80
Specific volume, dm ³ /kg	61.50
Enthalpy, kJ/kg	399.00
Operating Conditions:	
Evaporating Temperature, °C	-10.00
Suction Superheat, K	10.00
Ambient, °C	38.00
Condensing Unit Selected	ZXMY-020E-TFD

Fig. 16. Parametrii ZMY-020E-TFD – R455A

PERFORMANCE AT SPECIFIED OPERATING POINT
ZXMY-020E-TFD Data at 50 Hz

Evaporating Abs. Pressure, bar	3.91
Abs. Condensing Pressure, bar	20.47
Cooling Capacity, kW	3.13
Total Power Input, kW	1.76
COP	1.77
Current at 400 V, A	3.06
Mass Flow, g/s	23.30
Heating Capacity, kW	4.69
Condensing Temperature, °C	46.40
Subcooling at the Unit's outlet, K	0.00

Fig. 17. Performante energetice ZMY-020E-TFD – R455A

Parametrii tehnici ai vaporizatorului Kelvion KSC-301-6BE-FX28 – R455A sunt prezentați în Fig. 18, iar parametrii fizici sunt prezentați în Fig. 19.

Modernizarea instalațiilor frigorifice cu agenți frigorifici cu GWP scăzut

Capacity [kW]	3,37	Sensible heat ratio (SHR) [-]	0,8	Refrigerant	R455A (Solstice® L40X)
Air inlet temp. [°C]	0,0	Air outlet temp. [°C]	-4,5	Operation mode	EC
Rel. humidity [%]	85,0	Evaporation temp. [°C]	(Mid point) -10,0		

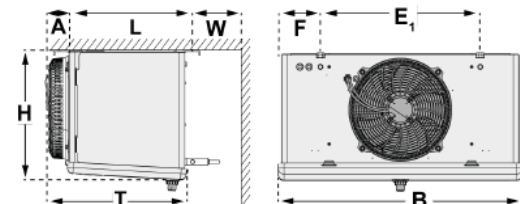
AIR DATA	HEAT EXCHANGER	MATERIALS
Air volume flow	Surface	Tubes
Ext. static pressure	Fin spacing	Fins
Air throw	Internal volume	End plates
Altitude	Liquid temp.	Casing
Air outlet rel. humidity	Superheating temp.	Finish
	Max. operating pressure	

FAN(S)

1 PIECE(S): 230V/1PH/50-60HZ; IP54	SELECTED SPEED DATA (PER FAN) ⁽³⁾	FAN SET SERIAL PLATE DATA (PER FAN)
Fan diameter	Operation mode	Operation mode
Range of temp.	Speed	Speed
Sound power L _{WA}	Power input	Power nominal
Sound pressure L _{pA} (3m) ⁽²⁾	Operating current	Current draw
Optional controller, on site ⁽⁵⁾	Energy efficiency class	Protector
ErP		

CONNECTIONS ⁽⁷⁾	WEIGHT ⁽⁴⁾	DEFROST
Inlet	Dry weight	Electric defrost
Outlet	Weight incl. packing	Coil
Refrigerant distribution		Drip tray
Venturi		Total

Fig. 18. Parametrii KSC-301-6BE-FX28 – R455A

DIMENSIONS ⁽⁴⁾

B 810 mm L 430 mm Drain G 3/4"
H 418 mm E ₁ 530 mm
W 200 mm F 140 mm
T 453 mm A 42 mm

Packing dimensions (height x length x width): 530 x 910 x 600 mm

Fig. 19. Parametrii gabaritici KSC-301-6BE-FX28 – R455A

3. Rezultate

Pentru a putea înțelege comparativ diferențele tehnico-economice, consumul de energie și impactul asupra mediului au fost calculate costurile de instalare și de funcționare, costul cu modernizarea și impactul asupra mediului la nivel de GWP.

Tabelul 1

Costurile sistemelor de refrigerare considerate în studiu de caz

Sistem de refrigerare	Costuri instalare [Euro]	Costuri mentenanță anuală [Euro]	Cost consum energie electrică anual [Euro]	Cost modernizare [Euro]	Costuri anuale totale [Euro]
R449A	6810	500	911	2763	10984
R455A	7215	600	946	-	8761

Costul anual al energiei necesare alimentării echipamentelor de refrigerare s-a considerat aproximativ un preț de 0,08 EUR/kWh.

Durata de viață a instalației având asigurat service anual este între 10 și 20 de ani.

4. Discuții

Din punct de vedere al costurilor de instalare, punere în funcție, funcționare, exploatare, întreținere și modernizare cele două soluții propuse diferă cu 21% (2223 Euro). Aceste costuri trebuie însă analizate întotdeauna de la începutul investiției, iar pe termen lung mai trebuie considerate și o eventuală modernizare a instalației prin realizarea înlocuirii agentului refrigerant pentru ca legislația a devenit clară.

Impactul asupra mediului din punct de vedere legislativ, începe să primeze înaintea costurilor de exploatare, chiar dacă consumurile de energie sunt sensibil egale.

5. Concluzii

Rezultatele studiului arată că folosirea refrigerantului A2L R455A încă de la implementarea proiectului are avantaje nete pe termen mediu și lung, atunci când vorbim de instalații de capacități comerciale mici și medii.

Eficiență energetică a instalației ce funcționează cu refrigerant A2L R455A, este similară cu cea a instalației ce funcționa cu refrigerant A1L, neinflamabil, R449A.

Impactul asupra mediului este foarte mult diminuat, de la 1397 unități GWP la 148 unități / kg refrigerant folosit. Sau mai exact de la un total de 4191 m³ la 0,44 m³ echivalent tone CO₂.

Din punct de vedere al investiției inițiale balanța cost investiție- siguranță exploatare rămâne înclinată în favoarea refrigeranților A1L dacă nu se consideră necesitatea modernizării și alinierii tehnologice și legislativ a instalației.

Investiția într-un refrigerant mai puțin poluant (cu GWP cât mai mic) are efect benefic atât pentru mediul în care trăim.

Referințe

- [1] Regulament EU F-Gas- 2024 https://climate.ec.europa.eu/eu-action/fluorinated-greenhouse-gases/f-gas-legislation_en.
- [2] © R.STAPLEY 2000 :Cold Store Cooling Load Calculation Software.
- [3] Danfoss <https://store.danfoss.com/en/Climate-Solutions/Climate-Solutions-for-cooling/>.
- [4] Kelvion Select Software - <https://selectrt.kelvion.com/selector/parameter/>.
- [5] Castel – Producator de elemente de automatizare instalații frigorifice, <https://castel.it/catalog/product-lines>.
- [6] Copeland – Producator de agregate frigorifice, <https://www.copeland.com/en-fr/shop/3274820>.

Fine porosity-cellular glass obtained by microwave-assisted heat treatment using the expansion ability of glycerol together with water glass

Sticlă celulară cu porozitate fină obținută prin tratament termic asistat de microunde folosind capacitatea de expansiune a glicerolului împreună cu apă de sticlă

Sorin Mircea Axinte^{1,2}, Lucian Paunescu³

¹National University of Science and Technology „Politehnica”, Faculty of Applied Chemistry and Materials Science

1-7 Gh. Polizu street, sector 1, Bucharest 011016, Romania

E-mail: sorinaxinte@yahoo.com

²Daily Sourcing & Research SRL

95-97 Calea Grivitei, sector 1, Bucharest 010705, Romania

E-mail: sorinaxinte@yahoo.com

³Daily Sourcing & Research SRL

95-97 Calea Grivitei, sector 1, Bucharest 010705, Romania

E-mail: lucianpaunescu16@gmail.com

DOI: 10.37789/rjce.2025.16.3.11

Abstract. Results of microwave-assisted manufacturing fine porosity-cellular glass using a liquid carbonic foaming agent (glycerol) together with water glass are presented in this paper. Under the conditions of developing the process in oxidizing atmosphere of the oven, the water glass role was to avoid the premature burning of carbon resulted after glycerol decomposing. The use of authors' own version of microwave heating applied in the last experiments reconfirmed the solution viability and its remarkable energy efficiency. Also, as an original technique measure, water glass proportion in the mix was increased to 8-12 % leading to growing the fineness of specimen porosity

Key words: high porosity, cellular glass, microwave, glycerol, water glass.

Rezumat. Rezultatele fabricării cu asistența microundelor a sticlei celulare cu porozitate fină utilizând un agent de spumare carbonic lichid (glicerol) împreună cu apă de sticlă sunt prezentate în această lucrare. În condițiile desfășurării procesului în atmosfera oxidantă a cuptorului, rolul apei de sticlă a fost evitarea arderii premature a carbonului rezultat după descompunerea glicerolului. Utilizarea versiunii proprii a autorilor privind încălzirea cu microunde aplicată în ultimele experimente a reconfirmat viabilitatea soluției și remarcabila sa eficiență energetică. De asemenea, ca o măsură tehnică originală, proporția apei de sticlă în amestec a fost crescută la 8-12 % conducând la creșterea fineței porozității probelor.

Cuvinte cheie: porozitate înaltă, sticlă celulară, microunde, glicerol, apă de sticlă.

1. Introduction

A wide variety of cellular products using recycled residual glass was designed and made in the last few decades. Properties of these products could be modeled depending on several factors: foaming agent type and mineral addition materials, heating rate and holding time at the foaming temperature, final process temperature. Their appropriate choice allowed to obtain cellular materials with physical, thermal, mechanical, and microstructural characteristics quite different depending on the requirements of the application domain [1]. On industrial-scale, several cellular glass types are manufacturing mainly in the form of thermal insulation boards and blocks, the most known products in the world being „Technopor” under license of the Swiss company Misapor Switzerland and several branches in Europe and „Foamgla” under license of the North-American company Pittsburgh Corning with branches in the United States, Europe, and China. According to information in the literature, fine and ultra-fine porosity cellular glass are not industrially manufactured, but only on an experimental small-scale and on the type of these products the current work is focused.

Recycling glass waste of which generation has been continuously increasing over the last 30-40 years, became a major problem, because storing this waste in landfills is now unacceptable for environmental reasons.

Recycling the glass waste and its reintroduction into the manufacturing process of new glass is practiced in the glass industry, but to a rather small extent due to the high costs of the quantitative sorting operations (by colour) of the waste. It has been experimentally found that glass recycling for the purpose of manufacturing new material types, especially in construction, would be an appropriate procedure due to the attractive properties of this material after a relatively unexpensive processing (sintering, foaming). The so-called cellular glass simultaneously meets several properties such as: low weight, rigidity, non-degradability, non-toxicity, chemical resistance, compression resistance, resistance to humidity, steam, bacteria, insects, rodents, etc. [1].

Sodium silicate aqueous solution is considered a cheap and environmentally friendly category of alkali silicates. According to [2], the investigation of structural peculiarities of the sodium silicate aqueous solution subjected to heating showed that important structural changes occur through its reorganization due to the water elimination. The water amount remaining in the system complies with Arrhenius' theory [3], quantified by an energy activation of $30 \text{ kJ} \cdot \text{mol}^{-1}$. The measurement results carried out by the authors showed that the new structure becomes almost similar to the characteristic structure of hydrated silicate glasses.

In another work [4], the research of possibility to expand drinking bottle waste with water glass into air atmospheric-oven was performed. Experimental results indicated that by growing the water glass amount, heat conductivity and crystallinity of products decrease. The remaining crystal content affects however the forming

process of closed-porous froth. It has found that by the addition of only water glass, without another traditional expanding agent, the production mechanisms of cellular glass into air and respectively, into argon atmosphere are different. Under the conditions of carrying out the experiment without protection atmosphere, the lowest density of the expanded material was $0.123 \text{ g}\cdot\text{cm}^{-3}$ and the minimum value of heat conductivity was $0.053 \text{ W}\cdot\text{m}^{-1}\cdot\text{K}^{-1}$, the closed porosity being 50 %. The starting mixture was composed of glass waste mentioned above, water glass (12 wt. %) as an expanding agent as well as boron trioxide (2 wt. %), aluminum phosphate (2 wt. %), and tripotassium phosphate (2 wt. %) as additives.

In the glass expansion process, the direct contribution of water glass is well-known. However, this process mechanism has not yet been validated on an experimental basis. To prove this situation, Hriba et al. [5] made an experiment, in which the evolution of the mix containing cathode ray tube waste and water glass was investigated during the foaming process. Structurally, water glass is perceived as a colloidal suspension of the Na_2SiO_3 aqueous solution, having as main components colloids and anions (or molecules) of silicate. Between these components there is the water as OH groups or water molecules. Drying the water glass solution leads to generation a xerogel with a glass-like structure, that by further heating softens and begins to expand due to the evaporation of the remaining water. As a result of these structural changes, connectivity of the pore network increases. The powder glass-water glass mix favours the sintering process and decreases the expanding temperature. Also, the presence of water glass allows to apply carbon-based foaming processes in atmospheric air without the danger of premature carbon burning. The current literature explains the expansion through releasing water structurally bound to water glass. However, the detection of water vapour at high temperatures during the water glass heating leads to the idea that water could be one of the main gases involved in expansion. Water glass as a soluble silicate reacts with CO_2 forming the alkaline carbonate (Na_2CO_3) that constitutes a traditional expanding agent for the powder glass. So, the effect of the oxidizing atmosphere of the oven on the mixture containing water glass is a favourable one.

In another work [6], experimental results of using only water glass as an expanding agent were exposed. The conclusion was that this method is viable, cellular glasses with fine porosity and closed pores with diameters between 4 nm and 800 μm being obtained. The mechanical resistance of expanded products was 1.7 MPa. In conformity with the same paper, conventional cellular glasses (made by foaming with traditional agents) commercially available have significantly higher pore size reaching 3 mm, while their strength is lower.

Aspects related to the preparation of cellular glass of mixed colours and water glass (15 wt. %) as a foaming agent, the mixture being uniaxially pressed at 10 MPa were presented in [7]. The sintering process occurs at 800 and respectively, 850 $^{\circ}\text{C}$. Results showed that by increasing the grain size of raw material and growing the temperature, the froth porosity increased, while the density decreased. The specimen microstructure indicated that the increase of pore homogeneity was favoured by the

fineness of glass grains and the higher sintering temperature led to larger pores, yet still remaining closed. Compression and flexural strength decreased with decreasing the grain size of raw material and increasing the sintering temperature. The heat conductivity did not exceed $0.25 \text{ W}\cdot\text{m}^{-1}\cdot\text{K}^{-1}$, this value being considered adequate for insulating material applications.

According to [8], making a cellular glass material with a high porous structure and density under $0.5 \text{ g}\cdot\text{cm}^{-3}$ requires the controlled use of glycerol, a liquid carbonic agent ($\text{C}_3\text{H}_8\text{O}_3$) together with water glass, which have the capability to provide optimal properties.

The use of an industrial-scale making recipe of cellular glass gravel, a porous material with heat insulation and load-bearing properties, mainly including glass waste, glycerol, and water glass is that applied by the German company Glapor Werk Mitterteich [9]. According to technical data provided by the manufacturer, apparent density has values between $0.13\text{-}0.21 \text{ g}\cdot\text{cm}^{-3}$, heat conductivity around $0.078 \text{ W}\cdot\text{m}^{-1}\cdot\text{K}^{-1}$, compression strength in the range of $4.9\text{-}6.0 \text{ MPa}$, and the pore size under $300 \mu\text{m}$ [10].

The experimental analysis of influence of glycerol/water glass ratio used for making glass foam by the sintering/foaming process of glass waste on the morphological characteristics of specimens was made in the work [11]. Glycerol as an expanding agent (between 1-1.5 %) associated with water glass as an enveloping material for the carbon particles (between 2-5 %) were used in this experiment. The process temperature had values in the range of $800\text{-}850 \text{ }^\circ\text{C}$, the heating rate having extremely high values between $26\text{-}166 \text{ }^\circ\text{C}\cdot\text{min}^{-1}$. As a result, fine porosity materials with pore size within the limits of $0.25\text{-}2 \text{ mm}$ were produced. The pore dimension varied depending on the heating rate value and the final temperature of the thermal process. The suitable proportions of glycerol and water glass were experimentally established being 1.5 % for glycerol and 5 % for water glass. The optimal temperature was $850 \text{ }^\circ\text{C}$ and the optimal heating rate was in the range of $50\text{-}80 \text{ }^\circ\text{C}\cdot\text{min}^{-1}$. Heat conductivity had comparable values with that of similar industrial products ($0.06\text{-}0.08 \text{ W}\cdot\text{m}^{-1}\cdot\text{K}^{-1}$).

Experimentally tested solution for manufacturing a lightweight glass froth is presented in [12]. The material mixture included container glass waste (92 %), water glass (3.5 %), and yellow glycerol (3.5 %) as a by-product of making biodiesel used as an expanding agent. Also, sodium carbonate (1 %) as a solid foaming agent was added. The final sintering/foaming temperature was $850 \text{ }^\circ\text{C}$, the average heating rate being $10 \text{ }^\circ\text{C}\cdot\text{min}^{-1}$. The sintered product was maintained at $850 \text{ }^\circ\text{C}$ for 30 min. The highest value of compression strength reached 16 MPa corresponding to the bulk density of $0.67 \text{ g}\cdot\text{cm}^{-3}$.

Some components of the authors' team of the current paper were previously interested in producing fine porosity-cellular glass obtained by the use of the liquid carbonic expanding agent (glycerol) in association with water glass in order to avoid the premature burning of fine carbon particles resulted by decomposing the glycerol [13]. Colourless flat glass waste (83-83.7 wt. %) from building demolition constituted the basic raw material, while glycerol (1.0-1.8 wt. %), water glass (5.3-7.5 wt. %), and

water addition (7.7-10 wt. %) completed the starting mixture. Unlike all manufacturing processes mentioned above, in this paper the effect of high energy efficiency of electromagnetic waves was used as an unconventional heating procedure of solid materials. The process temperature varied within the limits of 810-824 °C, average heating rate being in the range of 19.1-20.3 °C·min⁻¹, leading to obtaining very low specific energy consumptions between 0.81-0.88 kWh·kg⁻¹. Results showed excellent heat insulation properties (apparent density between 0.20-0.26 g·cm⁻³, porosity in the range of 85.5-88.2 %, and heat conductivity within the limits of 0.056-0.070 W·m⁻¹·K⁻¹, and in the same time high compression strength between 4.6-5.8 MPa.

In another work of Romanian authors [14], a different making method of a fine porosity-cellular glass using glass waste as raw material, borax as a fluxing agent (8-11 wt. %), and aqueous NaOH solution as a foaming agent (3-7 wt. %) was chosen. As in the paper [13], unconventional electromagnetic waves heating method in the own version was adopted. The process temperature had relatively low values (between 710-780 °C). Characteristics of the optimal making version were: apparent density of 0.26 g·cm⁻³, porosity of 87.6 %, heat conductivity of 0.069 W·m⁻¹·K⁻¹, and compression strength of 1.60 MPa. The specific energy consumption value was low (0.89 kWh·kg⁻¹).

Starting from own results obtained in the manufacture of fine porosity-cellular glass by microwave-assisted in 2020 [13], the main objective of the current work was to improve the performance regarding the fineness of the cellular material porosity by modifying its making recipes. Specifically, the water glass content of the starting mixture was significantly increased from 5.3-7.5 wt. % to 8.0-12.0 wt. % with growing the addition water content (between 10-13 wt. %).

2. Methods and materials

In general, the carbonic expanding agents can generate glass froth either by reaction with oxygen existing in the interstitials of the softened glass particles in the oxidizing atmosphere of the furnace or by carbon reduction of some glass components [1, 15]. For example, Na₂SO₄ from the glass can be reduced to Na₂S and dissolved into the glass molten. Thus, the reaction of SO₄²⁻ (from the glass) with the carbon forms S²⁻ (in glass) as well as CO and CO₂, that are pore-forming gases.

Carbon-containing liquid expanding agents (such as glycerol) develop the possibilities of penetration between the fine particles of powder glass. Glycerol from the glass mixture decomposes in the oxidizing conditions of the oven, generating a large range of chemical components from CO₂ and CO to pure carbon and hydroxyl compounds [15].

As stated above in this paper, in the case of using the carbon-expanding agent (e.g. glycerol), the role of water glass is essential in the foaming process to avoid premature burning the carbon resulting from the decomposition of this organic agent in the oxidizing environment of the furnace. Thus, water glass creates a protective layer

to envelop fine carbon particles, delaying the burning process and therefore the formation of CO and CO₂ as pore-forming gases.

The experiment presented in this work was conducted at the experimental base of the Romanian company Daily Sourcing & Research on an 800 W microwave-powered testing equipment. The equipment shown in Fig. 1 consists of a microwave oven commonly used in households for food preparation, adapted through constructive and operational modifications to allow much higher temperatures (up to 1200 °C) (a). The oven is equipped with a cylindrical tube made of SiC and Si₃N₄ (b) highly sensitive to microwaves, with the diameter of 1250 mm, height of 100 mm, and wall thickness of 2.5 mm, placed in the central area of the inner space of the oven on a 3 mm-metal plate. The location of the tube (made in China) has the role of tempering the intensely destructive effect of electromagnetic waves on the glass-based raw material upon their direct contact. The optimal size of the tube wall thickness was previously experimentally determined by the research team of Daily Sourcing & Research [16]. In this way, a lower, but predominant proportion (70-80 %) of emitted waves through the single waveguide placed in one of the oven walls completely penetrates the oven wall and comes into direct contact with the material subjected to heating. The remaining proportion of waves are absorbed in the wall mass, which is quickly and intensely heated, so that its hot inner surface at over 1000 °C transmits heat through thermal radiation to the same material. Direct microwave heating has some peculiarities that give it a higher energy efficiency than conventional heating systems. Thus, the heating process is started inside the material in its central area. There, the microwave power is converted into energy and the core of the material becomes the point with the highest temperature. Thus, the heat propagates volumetrically from the inside to the outside. The propagation mode is completely opposite to that which characterizes the heat transfer in conventional heating [17, 18]. Conventional methods require first heating the entire set of massive materials that make up the traditional oven (vault, walls, hearth, etc.) and only then the material effectively takes up the heat emitted by the conventional heating source. On the contrary, unconventional microwave heating has the ability of selectivity [18], i.e. the heating is focused only on the material susceptible to microwaves, the other materials not having the capacity to absorb the waves are insignificantly heated. Refractory materials that are traditional components of the oven masonry are practically not susceptible to microwaves, having in their composition high contents of silica and alumina.

Although electromagnetic waves have been known since the mid-20th century and their properties have been identified since the early years, their application has only materialized in the field of communications and radars and very few in the area of industrial heating processes, and those only at low temperatures in the range of 100-500 °C [19].

The list of materials chosen for this experiment includes: green and amber post-consumer drinking bottle as raw material, glycerol as a liquid carbonic expanding agent, aqueous solution of water glass, mainly used to avoid the premature burning of carbon resulted from the glycerol decomposition as well as distilled water addition for supplementary dilution of aqueous solution.

Fine porosity-cellular glass obtained by microwave-assisted heat treatment using the expansion ability of glycerol together with water glass

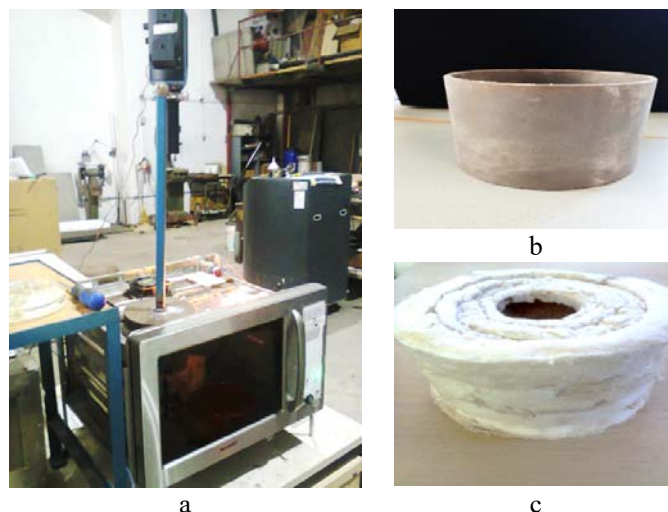


Fig. 1. Images of the experimental equipment
a – microwave oven including the radiation pyrometer for measuring the glass surface temperature,
b – SiC and Si₃N₄ ceramic tube; c – thermal protection of the tube.

The post-consumer drinking bottle was selected from green and amber drinking bottles in relatively equal weight proportions. After washing, the waste was broken, ground in a ball mill, and sieved for elimination glass particles over 80 μm . The oxide composition of the two glass waste previously measured with the AXIOS type fluorescence spectrometer from the Romanian Metallurgical Research Institute showed the following composition values [20] (Table 1).

Table 1

Glass type	Oxide composition of glass types							
	Oxide composition (wt. %)							
	SiO ₂	Al ₂ O ₃	Fe ₂ O ₃	CaO	MgO	Na ₂ O	K ₂ O	Cr ₂ O ₃
Green	71.8	1.9	=	11.8	1.2	13.1	0.1	0.1
Amber	71.1	2.0	0.2	12.1	1.1	13.3	0.1	-

In terms of chemistry, glycerol or glycerine (C₃H₈O₃) represents the simplest trihydroxy alcohol, being a slightly viscous liquid (1.28 g·cm⁻³), water and alcohol-soluble. Glycerol is found in all natural oils and fats in the form of long chain fatty acid esters (known also as glycerides). Also, it is naturally found in combined form in all vegetable and animal fats and oils, commonly as a triglyceride with fatty acids. Different industrial processes are used for obtaining glycerol, the most known being the propylene synthesis through the oil hydrolysis. If the glycerol proportion in vegetable oils is within the limits of 8-14 %, the yield of glycerol through industrial processes is about 10 % [21]. Glycerol grades for non-food applications can reach the maximum purity of 95 wt. %. The glycerol used in this experiment commercially purchased (originated from the Netherlands) had 89 wt. % of purity.

Water glass (sodium silicate-Na₂SiO₃), whose role has already specified above in this work, was procured from the market in form of an aqueous solution with 38 % concentration.

The investigation techniques of physical, heat, mechanical, and microstructural characteristics of cellular glass products were in general those usually applied for this cellular material type. Apparent density was measured using Archimedes' principle in accordance with the ASTM C373 standard and ISO 18754:2020 was applied for measuring the porosity. The compression strength of fine porosity-cellular glass samples was determined with a hydraulically operated compression testing machine with the pressing capacity of 107 MPa, according to the ASTM C133-97 (2015) standard. The water-absorption of specimens was identified in accordance with ASTM C373-18 standard by their immersion under water. Microstructural appearance of specimens was examined with Biological Microscope MT5000 model (1000 x magnification).

3. Results and discussion

Composition of the mixture versions adopted for experimentally making the fine porosity-cellular glass is presented in Table 2.

Table 2

Composition of the mixture versions for producing cellular glass

Composition	Version 1 (wt. %)	Version 2 (wt. %)	Version 3 (wt. %)	Version 4 (wt. %)
Green and amber post-consumer drinking bottle	81.00	78.75	76.50	73.25
Glycerol	1.00	1.25	1.50	1.75
Water glass	8.0	9.0	10.0	12.0
Water addition	10.0	11.0	12.0	13.0
Water glass/glycerol ratio	8.00	7.20	6.67	6.86

According to the data in Table 2, the water glass/glycerol weight ratio had values between 8 and 6.67, slightly decreasing from the first to the latest versions. Glycerol and water glass as well as water addition had growing values within the limits of 1-1.75 %, 8-12 %, respectively 10-13 %.

Operational parameters of the expanding process of fine porosity-cellular glass are shown in Table 3.

Table 3

Operational parameters of the expanding process of cellular glass

Version	Raw material/ cell glass amount (g)	Process temperature (°C)	Heating time (min)	Average rate (°C·min ⁻¹)		Specific energy consumption (kWh·kg ⁻¹)
				Heating	Cooling	
1	550/525	815	35	22.71	5.2	0.69
2	550/527	817	36	22.14	5.3	0.71
3	550/526	820	38	21.05	5.2	0.75
4	550/527	825	41	19.63	5.3	0.81

Fine porosity-cellular glass obtained by microwave-assisted heat treatment using the expansion ability of glycerol together with water glass

Cellular glass specimens corresponding to the four material mixtures mentioned above (Fig. 2) were obtained in the temperature range of 815-825 °C. According to the operational parameters shown in Table 3, by using the technique of microwave heating predominantly direct and partially indirect, reaching very high heating rates in all the four experimental versions (between 19.63-22.71 °C·min⁻¹) has been possible and also relatively short heating times until the appearance and development of foaming into the material mass (between 35-41 min).

The energy efficiency of the microwave-assisted procedure was excellent also in this case, the specific energy consumption being in the range of 0.69-0.81 kWh·kg⁻¹, lower or at most equal to the consumption industrially registered using conventional heating methods.

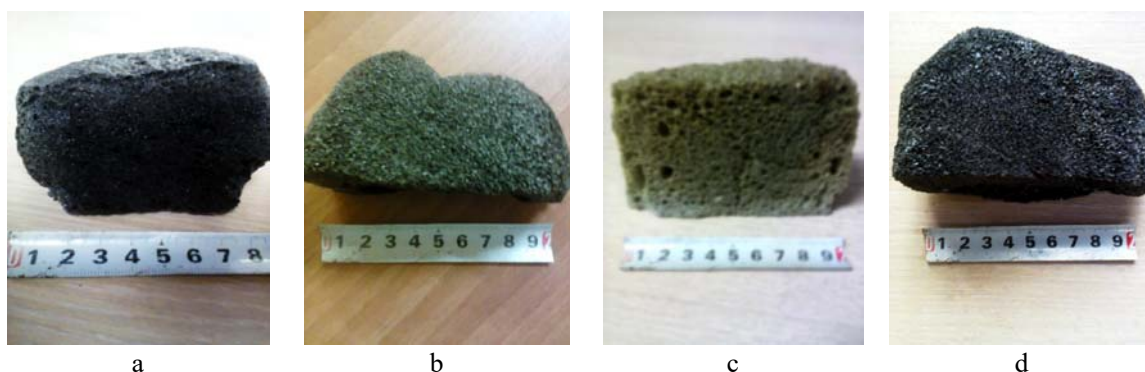


Fig. 2. Section images of the fine porosity-cellular glass
a – version 1; b – version 2; c – version 3; d – version 4.

The physical, heat, mechanical, and microstructural features of the cellular glass specimens are presented in Table 4.

Table 4

Physical, heat, mechanical, and microstructural features						
Version	Aparent density (g·cm ⁻³)	Porosity (%)	Heat conductivity (W·m ⁻¹ ·K ⁻¹)	Compression strength (MPa)	Water absorption (vol. %)	Pore size (μm)
1	0.20	88.3	0.055	2.1	2.3	40-120
2	0.21	87.5	0.058	2.5	2.3	60-230
3	0.23	86.7	0.061	2.7	2.5	70-240
4	0.15	90.8	0.049	1.8	2.1	20-90

In accordance with the results in Table 4, the work objective was reached. Fine porosity of cellular glass specimens was obtained in all tested experimental versions, the pore size being under 240 μm. The lowest values of cell diameter, fully closed, were reached in the case of version 4 characterized by the combined use of water glass and glycerol in the weight ratio of 12.0/1.75, i.e. 6.86, the temperature at the

moment of stopping the heating proces being the highest of the four version (825 °C). The identified range of pore size was 20-90 μm .

Apparent density corresponding to the specimen made by version 4 was extremely low ($0.15 \text{ g}\cdot\text{cm}^{-3}$), it also influencing the very small value of heat conductivity ($0.049 \text{ W}\cdot\text{m}^{-1}\cdot\text{K}^{-1}$) and the high value of porosity (90.8 %). Despite extremely low physico-thermal features of this specimen, compression strength of the mentioned product was more than satisfactory (1.8 MPa).

Although, the other tried versions allowed increasing the apparent density to $0.20\text{-}0.23 \text{ g}\cdot\text{cm}^{-3}$ as well as the heat conductivity to $0.055\text{-}0.061 \text{ W}\cdot\text{m}^{-1}\cdot\text{K}^{-1}$, the mechanical strength did not significantly increase, reaching a maximum of 2.7 MPa in the case of version 3.

The evolution of microstructural appearance of the fine porosity-cellular glass specimens under the influence of different proportions of glycerol and water glass introduced in the starting mixture of the four experimental versions is shown in Fig. 3.

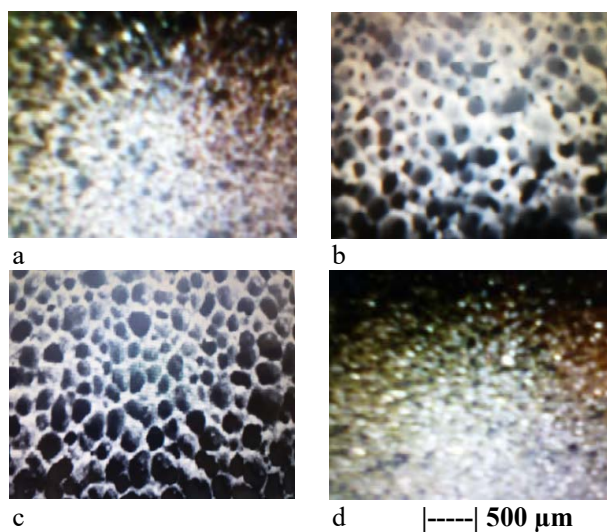


Fig. 3. Microstructural appearance of the fine porosity cellular glass specimens

a – version 1; b – version 2; c – version 3; d – version 4.

The simultaneous growing of glycerol and water glass in the proportions mentioned in Table 2 showed that firstly, the cellular glass registers increasing the pore size and then, the tendency to form a fine porosity structure is exhibited. The explanation could be that by the use of glycerol in a lower amount the foaming process is normally favoured and in addition, the water glass contribution, whose role is to protect the carbon particle surfaces created through the glycerol decomposition, is beneficial for delaying this process. By simultaneous growing the glycerol and water glass content, increasing the specimens porosity is evident, their size reaching over $200 \mu\text{m}$. Under the water glass/glycerol ratio value of about 7, the contribution of water glass to form fine porosity becomes more important than the contribution of

further increase of the glycerol content on the foaming and thus pore dimension enters in the reduction trend, reaching below 90 μm .

6. Conclusions

Having in view the work objective regarding making a fine porosity-cellular glass under conditions of higher energy efficiency compared to production of other similar products, the experimental results can be considered as a success in technological terms. In the experimental version (4) based on the combined use of water glass and glycerol in the ratio of 6.86 (water glass representing 12.0 wt. % and glycerol 1.75 wt. %), the apparent density reached extremely low value of $0.15 \text{ g}\cdot\text{cm}^{-3}$ as well as heat conductivity registered $0.049 \text{ W}\cdot\text{m}^{-1}\cdot\text{K}^{-1}$. Despite these low values of physical and thermal properties, the cellular material maintained a more than satisfactory level of compressive strength of 1.8 MPa. Obtaining these performances was made through the original growing the proportion of water glass up to 12 wt. % and choosing suitable ratio between water glass and glycerol. Also, adopting the unconventional microwave heating technique, unused in the world in heating processes of solids at temperatures above 500 $^{\circ}\text{C}$, constituted an important originality character of the paper.

References

- [1] G. Scarinci, G. Brusatin, E. Bernardo, „Glass Foams”, in Cellular Ceramics: Structure, Manufacturing, Properties and Applications, Scheffler M., Colombo P. (eds.), Wiley-VCH Verlag GmbH & Co. KGaA, Weinheim, Germany, 2005, pp. 158-176, ISBN: 3-527-31320-6.
- [2] H. Mohsin, S. Maron, I. Maurin, E. Burov, G. Tricot, L. Devys, E. Gouillart, T. Gacoin, „Thermal Behavior of Water Glass: Foaming and Xerogel-to-Glass Evolution”, in Journal of Non-Crystalline Solids, Elsevier, vol. 566, 2021. <https://doi.org/10.1016/j.jnoncrysol.2021.120872>
- [3] *** „Arrhenius Theory”, in Encyclopedia Britannica, 2024. <https://www.britannica.com/science/Arrhenius-theory>
- [4] Sonia Smiljanić, U. Hribar, M. Spreitzer, J. König, V. Gioncu, M. Ivan, „Water-Glass-Assisted Foaming in Foamed Glass Production”, in Ceramics, MDPI, G. Shekhgildyan, M.I. Ojevan (acad.ed.s.), vol. 6, no. 3, 2023, pp. 1646-1654. <https://doi.org/10.3390/ceramics6030101>
- [5] U. Hribar, M.B. Østergaard, N. Iversen, M. Spreitzer, J. König, „The Mechanism of Glass Foaming with Water Glass”, in Journal of Non-Crystalline Solids, Elsevier, vol. 600, 2023. <https://doi.org/10.1016/j.jnoncrysol.2022.122025>
- [6] Daniela Hesky, C.G. Aneziris, U. Gross, A. Horn, „Water and Waterglass Mixtures for Foam Glass Production”, in Ceramics International, vol. 41, no. 10, 2015. <https://doi.org/10.1016/j.ceramint.2015.06.088>
- [7] S.S. Owøeye, G. Ofunke Matthew, E.O. Orienmhanda, S.O. Tunmilaya, „Preparation and Characterization of Foam Glass from Waste Container Glasses and Water Glass for Application in Thermal Insulation”, in Ceramic International, Elsevier, vol. 46, no. 8, Part 8, 2020, pp. 11770-11775. <https://doi.org/10.1016/j.ceramint.2020.01.211>
- [8] B.M. Goltsman, L. Yatsenko, N.S. Goltsman, „Study of the Water-Glass Role in the Foam Glass Synthesis Using Glycerol Foaming Agent”, in Solid State Phenomena, vol. 316, no. 5, 2021, pp. 153-158. <https://doi.org/10.4028/www.scientific.net/SSP.316.153>

- [9] *** „Glapor Cellular Glass Gravel, Technical Data SG 600 P”, Glapor Werk Mitterteich GmbH, Germany, 2023. <https://www.stboards.com/wp-content/uploads/2023/10/GlaporTechnicalData.pdf>
- [10] Felicia Cosmulescu, L. Paunescu, M.F. Dragoescu, S.M. Axinte, „Comparative Analysis of the Foam Glass Gravel Experimentally Produced by Microwave Irradiation”, in Journal of Engineering Studies and Research, vol. 26, no. 3, 2020, pp. 58-68.
- [11] L. Lakov, K. Toncheva, A. Staneva, T. Simionova, Z. Ilcheva, „Composition, Synthesis and Properties of Insulation Foam Glass Obtained from Packing Glass Waste”, in Journal of Chemical Technology and Metallurgy, vol. 48, no. 2, 2013, pp. 125-129.
- [12] P. Sooksan, N. Sudyod, N. Thongtha, R. Simsomphonphol, „Fabrication of Lightweight Foam Glasses for Thermal Insulation Applications”, in Materials Today: Proceedings, vol. 17, Part 4, 2019, pp. 1823-1830. <https://doi.org/10.1016/j.matpr.2019.06.219>
- [13] M.F. Dragoescu, L. Paunescu, S.M. Axinte, „Nonconventional Technique of Sintering/Foaming the Glass Waste Using a Liquid Carbonic Foaming Agent”, in Nonconventional Technologies Review, vol. 24, no. 3, 2020, pp. 4-12.
- [14] M.F. Dragoescu, L. Paunescu, S.M. Axinte, „High Porosity Glass Foam Made with a Liquid Foaming Agent by Microwave Irradiation”, in Academic Journal of Manufacturing Engineering, vol. 20, no. 1, 2022, pp. 56-63.
- [15] Natalia S. Karandashova, B.M. Goltsman, E.A. Yatsenko, „Analysis of Influence of Foaming Mixture Components on Structure and Properties of Foam Glass”, in IOP Conference Series: Materials Science and Engineering, IOP Publishing, vol. 262, 2017. <https://doi.org/10.1088/1757-899X/262/1/012020>
- [16] S.M. Axinte, L. Paunescu, M.F. Dragoescu, A.C. Sebe, „Manufacture of Glass Foam by Predominantly Direct Microwave Heating of Recycled Glass Waste”, Transaction on Networks and Communications, vol. 7, no. 4, 2019, pp. 37-45. <https://doi.org/10.14738/tnc.74.7214>
- [17] J.A. Jones, T.P. Lelyveld, S.D. Mavrofidis, S.W. Kingman, N.J. Miles, „Microwave Heating Applications in Environmental Engineering-A review”, in Resources, Conservation and Recycling, vol. 34, no. 2, 2002, pp. 75-90. [https://doi.org/10.1016/S0921-3449\(01\)00088-X](https://doi.org/10.1016/S0921-3449(01)00088-X)
- [18] Hellen J. Kitchen, S.R. Vallance, J.L. Kennedy, N. Tapia-Ruiz, L. Carassitti, „Modern Microwave Methods in Solid-State Inorganic Materials Chemistry: From Fundamentals to Manufacturing”, in Chemical Reviews, ACS Publications, vol. 114, no. 2, 2014, pp. 1170-1206. <https://pubs.acs.org/doi/10.1021/cr4002353>
- [19] Olga Kharissova, B.I. Kharissov, J.J. Ruiz Valdés, „Review: The Use of Microwave Irradiation in the Processing of Glasses and their Composites”, in Industrial & Engineering Chemistry Research, ACS Publications, vol. 49, no. 4, 2010, pp. 1457-1466. <https://pubs.acs.org/doi/10.1021/ie9014765>
- [20] M.F. Dragoescu, L. Paunescu, S.M. Axinte, A. Fiti, „Influence of the Color of Bottle Glass Waste on the Characteristics of Foam Glass Produced in Microwave Field”, in International Journal of Science and Engineering Investigations, vol. 7, no. 72, 2018, pp. 95-100, ISSN: 2251-8843.
- [21] *** „Glycerol: Versatile Renewable Chemical Properties” Kumar Metal Industries, 2023. <https://kumarmetal.com/glycerol-versatile-renewable-chemical-properties/>